CHARACTERIZATION OF TWO VERNIER TUNED DISTRIBUTED BRAGG REFLECTOR (VT-DBR) LASERS USED IN SWEPT SOURCE OPTICAL COHERENCE TOMOGRAPHY (SS-OCT)

A Thesis

presented to

the Faculty of California Polytechnic State University,

San Luis Obispo

In Partial Fulfillment

of the Requirements for the Degree

Master of Science in Electrical Engineering

by

Gregory M. Bergdoll

June 2015

COMMITTEE MEMBERSHIP

TITLE:	Characterization of two Vernier-Tuned Distributed Bragg Reflector (VT-DBR) Lasers used in Swept Source Optical Coherence Tomography (SS-OCT)
AUTHOR:	Gregory M. Bergdoll
DATE SUBMITTED:	June 2015
COMMITTEE CHAIR:	Dennis Derickson, Ph.D. Department Chair of Electrical Engineering
COMMITTEE MEMBER:	Jason Ensher, Ph.D. Engineering VP of Insight Photonic Solutions Inc.
COMMITTEE MEMBER:	Xiaomin Jin, Ph.D. Associate Professor of Electrical Engineering
COMMITTEE MEMBER:	Bridget Benson, Ph.D. Assistant Professor of Electrical Engineering

ABSTRACT

Characterization of two Vernier-Tuned Distributed Bragg Reflector (VT-DBR)

Lasers used in Swept Source Optical Coherence Tomography (SS-OCT)

Gregory M. Bergdoll

Insight Photonic Solutions Inc. has continued to develop their patented VT-DBR laser design; these wavelength tunable lasers promise marked image-quality and acquisition time improvements in SS-OCT applications.

To be well suited for SS-OCT, tunable lasers must be capable of producing a highly linear wavelength sweep across a tuning range well-matched to the medium being imaged; many different tunable lasers used in SS-OCT are compared to identify the optimal solution.

This work electrically and spectrally characterizes two completely new all-semiconductor VT-DBR designs to compare, as well. The Neptune VT-DBR, an O-band laser, operates around the 1310 nm range and is a robust solution for many OCT applications. The VTL-2 is the first 1060 nm VT-DBR laser to be demonstrated. It offers improved penetration through water over earlier designs which operate at longer wavelengths (e.g. - 1550 nm and 1310 nm), making it an optimal solution for the relatively deep imaging requirements of the human eye; the non-invasive nature of OCT makes it the ideal imaging technology for ophthalmology.

Each laser has five semiconductor P-N junction segments that collectively enable precise akinetic wavelength-tuning (i.e. - the tuning mechanism has no moving parts). In an SS-OCT system utilizing one of these laser packages, the segments are synchronously driven with high speed current signals that achieve the desired wavelength, power, and sweep pattern of the optical output.

To validate the laser's fast tuning response time necessary for its use in SS-OCT, a circuit model of each tuning section is created; each laser section is modeled as a diode with a significant lead inductance. The dynamic resistance, effective capacitance, and lead inductance of this model are measured as a function of bias current and the response time corresponding to each bias condition is determined.

Tuning maps, spectral linewidths, and side-mode suppression ratio (SMSR) measurements important to SS-OCT performance are also collected.

Measured response times vary from 700 ps to 2 ns for the Neptune and 1.2 to 2.3 ns for the VTL-2. Linewidth measurements range from 9 MHz to 124 MHz for the Neptune and 300 kHz to 2 MHz for the VTL-2. SMSR measurements greater than 38 dB and 40 dB were observed for the Neptune and VTL-2, respectively. Collectively, these results implicate the VT-DBR lasers as ideal tunable sources for use in SS-OCT applications.

Keywords: semiconductor laser, vernier, Bragg-reflector, optical coherence tomography, dynamic resistance, reflectometry, spectral linewidth, and SMSR.

ACKNOWLEDGMENTS

Thank you Insight Photonic Solutions for developing the VT-DBR lasers and making my thesis research possible. Dr. Jason Ensure, thank you for supporting my thesis work and taking time to answer all my questions. Dr. Dennis Derickson, thank you for giving me this research opportunity, guiding my exploration, and sharing your knowledge in photonics. It has been a pleasure to work with you all. Family, friends, and colleagues, thank you for your confidence in me; your support has made all my academic success possible.

TABLE OF CONTENTS

LIST OF TABLES

LIST OF FIGURES

1. INTRODUCTION

Tunable Lasers

A laser whose wavelength can be controlled across a useful range is considered tunable; although no laser is perfectly monochromatic and all have some environmentally-dependent variation in their output wavelength, only a small portion of laser types can be continuously tuned over a significant range.

The organic-dye tunable laser, discovered in 1966, is recognized as the first widely-tunable laser [1]. Illustrated in figure 1, it was found that broadband stimulated emission could be produced by sufficiently irradiating a phthalocyanine solution with a ruby laser beam [2]. Continuous tuning of this laser is typically achieved through the use of a Lyot filter in the lasing cavity which allows a narrow range of the output spectrum to be extracted for use, but other tuning schemes have been developed (e.g. - prisms, etalons, or diffraction gratings) [3]. Until its discovery, lasers were relatively monochromatic and unable to produce the broadband spectrum required for many of the laser applications in use today.

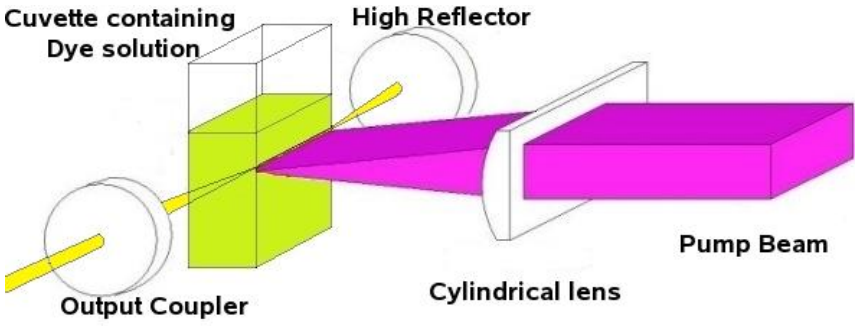

Figure 1 - Basic structure of a dye-laser. Dye solution is excited by the pump beam. Lasing is then achieved by resonating the subsequent stimulated emission between the reflective surfaces of the two mirrors surrounding the dye cuvette.

Vernier Tuned Distributed Bragg Reflector (VT-DBR) Lasers

VT-DBR lasers are a type of semiconductor tunable laser that achieve wavelength tuning by selecting the lasing cavity's oscillatory wavelength with two sampled grating distributed Bragg-reflector (SG-DBR) mirrors on either end of the cavity. An SG-DBR mirror is comprised of a set of evenly spaced distributed-Bragg reflectors (DBR); together they perform as a Fabry-Perot resonator, rejecting the transmission of a harmonically related set of wavelengths determined by the length of separation between its DBR structures; the rejected light is resonated in an electrically pumped active medium called the gain section. In this region of the cavity, a single mode commonly reflected by both DBR mirrors experiences significant amplification.

The distance light must travel between each mirror's repeated grating structure is controlled by pumping the semiconductor material it is comprised of with electric current; this changes the refractive index of the material which alters the reflective angle of incidence, changing the light-path distance between structures. Subsequently, the rejected wavelength common to both mirrors is oscillated through the gain medium where coherent amplification is achieved. Figure 2 illustrates the DBR structure of each mirror. It can be seen that each sampled grating mirror reflects a harmonically related set of wavelengths dependent on the incident light's wavelength, the effective index of refraction 'n', and the distance between the repeated grating structures 'L' [4].

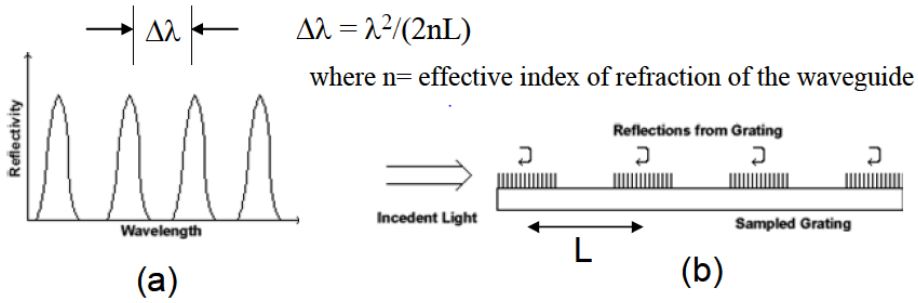

Figure 2 - Illustration of the sampled grating structure forming each laser mirror. The repeated grating structures spaced a distance 'L' in (b) produce a Fabry-Perot interferometer to produce the reflectivity spectrum found in (a).

By using slightly different spacing lengths between the grating structures in each mirror (i.e. - L_1 and L_2 where $L_1 \neq L_2$, but nearly equal), the resulting resonant wavelength between the mirrors is common to each mirror's reflectivity-profile and within the amplification range of the gain medium.

Figure 3 (a) illustrates this Vernier effect whereby the reflectivity peak common to both mirrors and within the amplification range of the gain medium is resonated to produce the laser's highly monochromatic output spectrum.

The peak wavelength in the spectrum of (b) corresponds to the reflected wavelength common to both mirrors; wavelengths from slightly misaligned reflectivity peaks between the two mirrors make up the remaining spectral-output peaks comprising significantly less of the total output power [4].

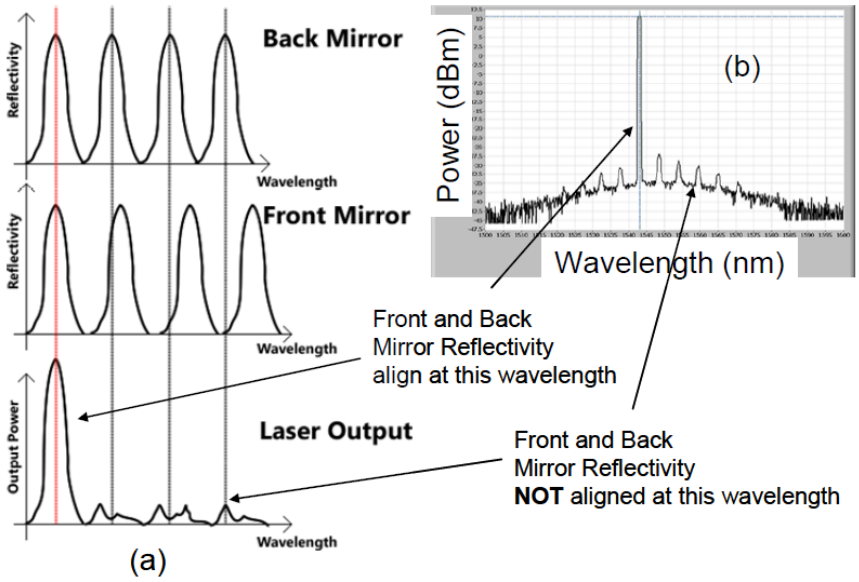

Figure 3 - Depiction of the reflectivity profiles of each VT-DBR laser mirror and the resulting resonant wavelength from the reflected peak that is common to both (a). The laser's output spectrum (b) shows the narrow output wavelength and the other, power suppressed, wavelengths corresponding to slightly misaligned reflectivity peaks.

In the VT-DBR laser, these DBR tuning sections forming the mirrors of the lasing cavity are called the front-mirror (FM) and back-mirror (BM) and together enable continuous tuning.

To achieve improved tuning precision and control, an additional tuning element called the phase section is placed intra-cavity; the phase section facilitates fine resonant wavelength adjustments by modulating the effective cavity length; the effective cavity length is changed by electrically pumping the phase section to alter the refractive index of the medium.

The output power of the laser is controlled by the semiconductor optical amplifier section of the laser. By electrically pumping this section, optical gain is achieved and, with the proper control, power leveling is possible across the tuning range of the device.

As with all lasers, environmental variables contribute to variations in the laser's wavelength. Temperature fluctuations that would otherwise cause the output wavelength to wander are prevented using a thermoelectric cooler (TEC). The TEC is incorporated into the laser package and electrically driven with a TEC controller to maintain a constant waveguide temperature.

The VT-DBR is well-suited for SS-OCT for many reasons. It exhibits a high signal to noise ratio (SNR) when compared to other tunable laser designs. Because the laser cavity is so small, relaxation oscillations are minimized and the laser can be quickly tuned to any wavelength in the tuning range of the device; Figure 4 illustrates the exceptionally small size of the VT-DBR laser chip [5].

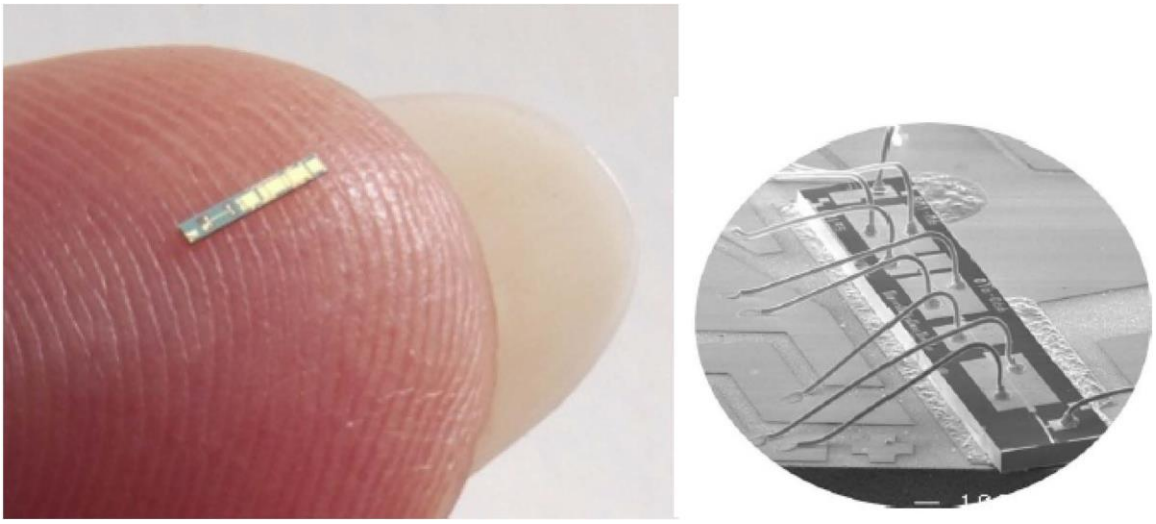

Figure 4 - VT-DBR laser chip (left) electrically connected to a chip-carrier (right) with 25 micron bond-wires using thermo-sonic bonding [5].

Earlier VT-DBR designs have been demonstrated in SS-OCT. A standard deviation of the phase linearity and repeatability were measured to be <160 pm. 2D and 3D OCT images measured ex-vivo and in-vivo were performed at sweep repetition rates up to 200 kHz [6].

Figure 5 depicts an example 3D image from a VT-DBR laser. The 1.5 GB data-set associated with this image was acquired in ~2.4 seconds. This high rate of data-acquisition makes the VT-DBR laser the most practical solution for in vivo OCT imaging.

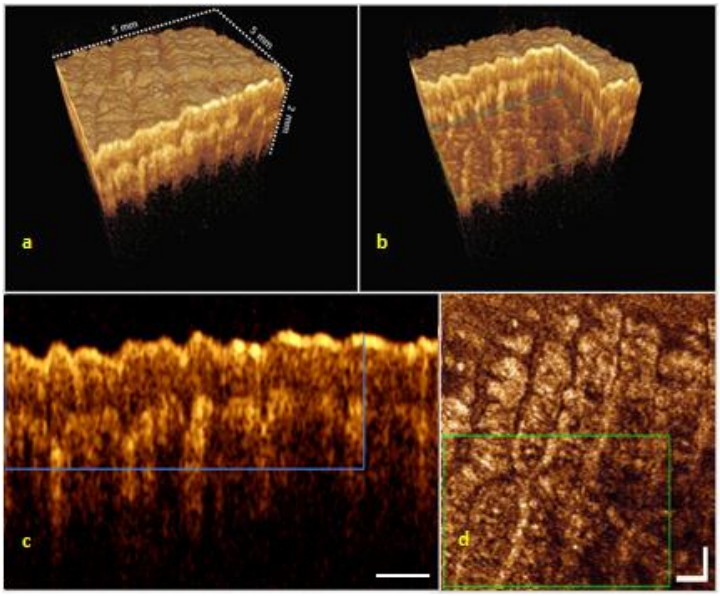

Figure 5 - In vivo SS-OCT image of the epidermis using a 1550 nm VT-DBR laser. The data is rendered in 3D (a) and cut-away (b) to reveal intra-sample morphology. Single b-scan (c) and en-face view (d) of the 3D data-set demonstrates versatility of OCT imaging.

The fast data acquisition and superior imaging-quality of VT-DBR lasers are made possible by the sweep efficiency and data rejection illustrated in Figure 6. The few non-linear regions of the OCT sweep are removed from the data-set and the resulting image resolution is improved.

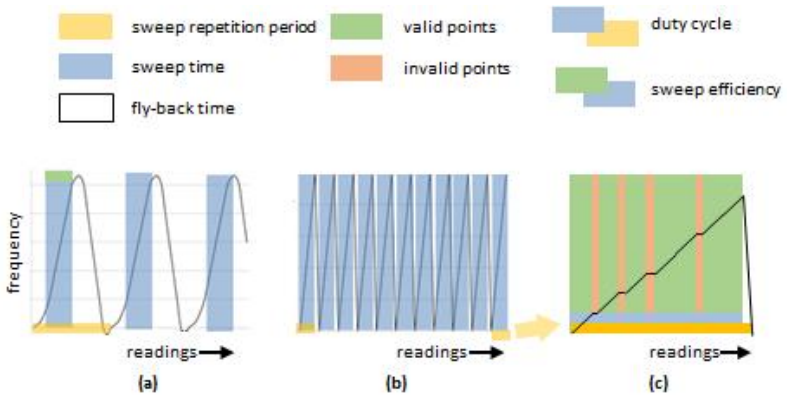

Figure 6 - Comparison of sweep-efficiency / duty-cycle in the VT-DBR (b) with mechanically tuned lasers (a). What few invalid data-points (c) exists in a VT-DBR data-set is easily removed in software.

The inertia of the tuning mechanism in mechanically tuned lasers prevents high sweep efficiencies and extends acquisition times beyond the required period of stability in many in-vivo measurement applications. For example, in ophthalmology, the patient is asked to limit eye movement during OCT image acquisition; unfortunately, the sweep efficiencies of alternative swept-source systems extend the required period of immobility beyond the capability of most humans.

In addition to all the other advantages that make the VT-DBR the clear choice for OCT systems, the VT-DBR laser can be manufactured at a fraction of the cost of alternative OCT lasers. The bulk of the complexity in a VT-DBR laser is in the conveniently small laser-chip itself and requires no bulky apparatus to achieve tuning functionality. These chips can be mass produced with as many as 2000 devices on a single silicon wafer.

A diagram illustrating the butterfly package's electrical pinout of the Neptune and VTL-2 lasers can be found in appendix A.

Swept Source Optical Coherence Tomography (SS-OCT)

SS-OCT is a type of frequency domain OCT imaging where the wavelength of a coherent light source is swept across its tuning range. OCT is made possible by the highly monochromatic and coherent light inherent in laser radiation; Figure 7 illustrates how laser light differs from other common sources of light [7].

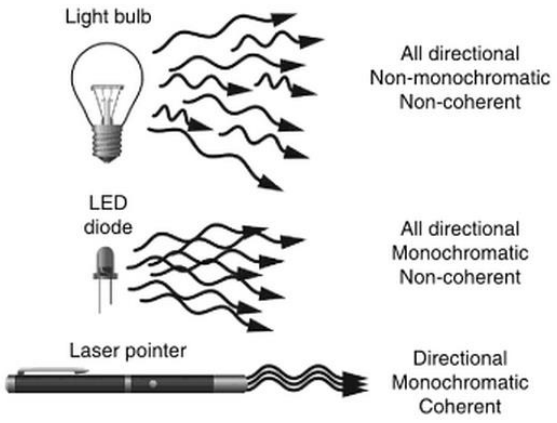

Figure 7 - Illustration of the output radiation properties of an incandescent lamp, LED, and laser pointer. Directional, monochromatic, and coherent light is unique to laser radiation.

Similar to ultrasound, an a-scan is resolved using the measured change in incident wave back-scattering versus sample depth, but using light instead of sound. By means of interferometry, an interference pattern is produced between the sample's reflected light (i.e. -reflections from the media being imaged) and the reference path's beam. The envelope of the interference pattern is captured with a photodiode and the resulting modulated electrical signal is Fast Fourier Transformed (FFT) using high speed digital signal processing (DSP) to produce a spectral plot where change in amplitude correspond to a refractive index change and image depth is resolved using the slope of the laser's linear

frequency sweep (i.e. - relative sample depth is correlated to a frequency difference in the FFT output).

Adjacent a-scans can be captured and concatenated in software to form a b-scan (i.e. - a cross-sectional slice of the medium being imaged); likewise, adjacent b-scans may be collected and appended together in software to render a 3D depiction of the light-scattering media being imaged. Figure 8 illustrates different rendering techniques used to study the morphology an eye's retinal tissue [8].

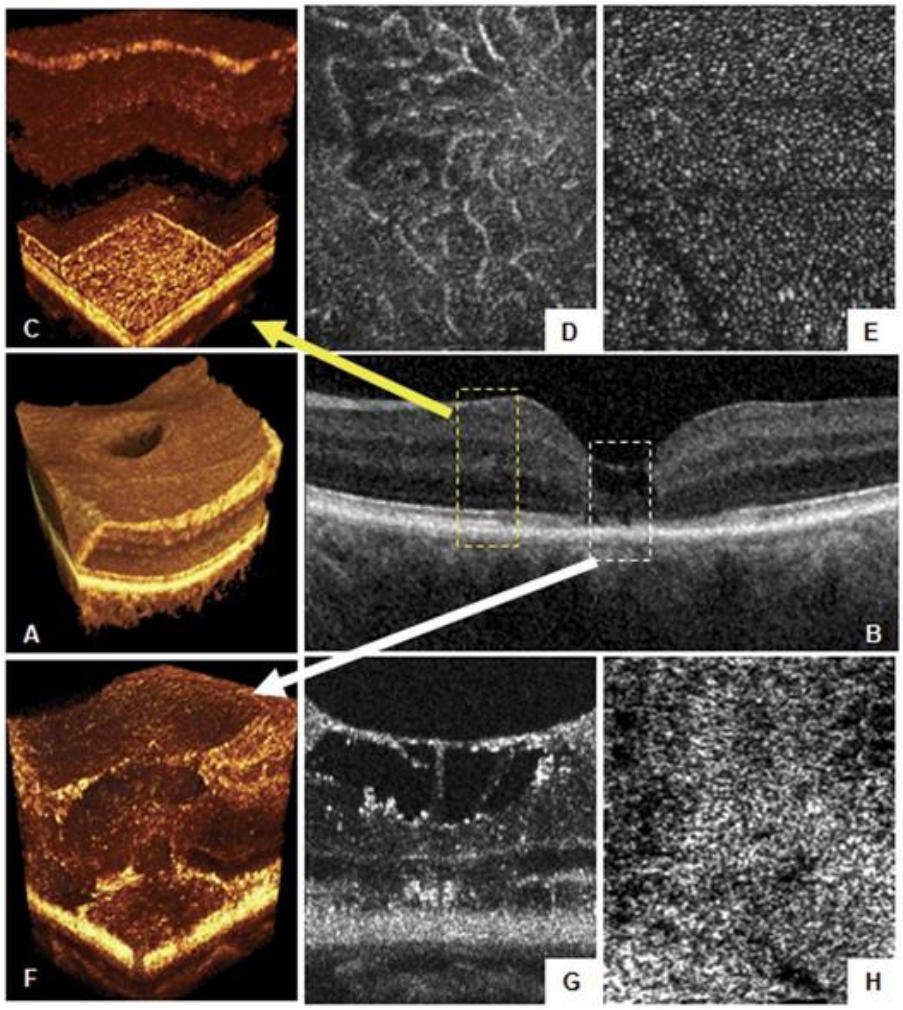

Figure 8 - OCT images of the retina. A three-dimensional data-set can be processed to produce enface images (d, e, and h), b-scans (b, g), and a 3D rendering of the eye-tissue's morphology.

In contrast to frequency domain OCT, time domain OCT uses a broadband source (e.g. – a super-luminescent diode) to illuminate the sample with its entire spectral output at once. The interference pattern at varied sample depths is measured by longitudinally modulating the interferometer's mirror position in the reference-path. As with mechanically tuned laser's, the requirement of movement in the measurement device limits its performance in OCT application. The finite inertia of the mirror limits the speed at which it can be modulated and results in relatively long image acquisition times in time-domain OCT schemes.

SS-OCT has been identified as the future of OCT because it offers better resolution with greatly reduced acquisition speeds, due to the superior signal to noise ratio (SNR) and high sweep repetition rates inherent to the VT-DBR laser. According to Professor Paulo Stanga, a consultant ophthalmologist for the Manchester Royal Eye Hospital, SS-OCT enables faster scanning speeds, increased penetration depth, and improved image resolution over other OCT measurement structures. In an interview, Dr. Stanga states that it will be important for ophthalmologists to move to swept source OCT systems because it allows for superior imaging of the vitreous, a location of the eye hard to image with other OCT technologies; additionally, most of the modern treatments for vision problems are administered by intro-vitreous injections in the vitreous region; so, it is imperative for doctors to have a clear image of this structure when determining the correct course of therapy [9].

In general, OCT imaging systems are ideal for ophthalmology because they are non-invasive and yield image resolutions down to a few micrometers which is sufficiently precise for the morphology used in diagnosis and treatment of retinal diseases. Figure 9, an OCT image of a human eye, demonstrates a SS-OCT b-scan produced for retinal diagnostics [10].

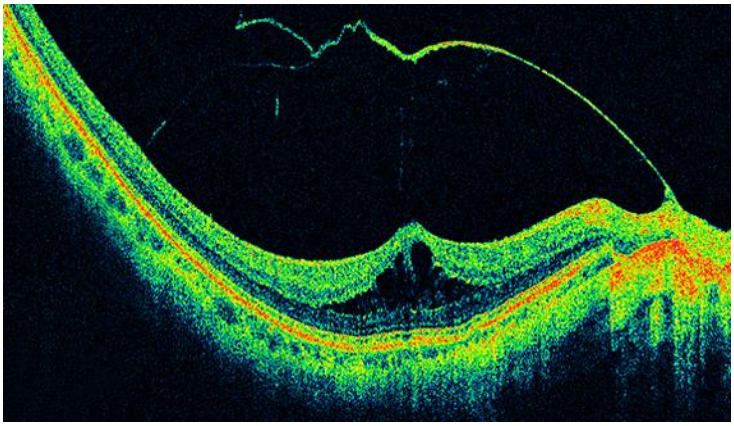

Figure 9 - Cross-sectional (i.e. - B-scan) image of an eye using frequency-domain optical coherence tomography (FD-OCT).

OCT has established its niche in biomedical imaging because it offers a far better image resolution than other medical imaging technologies used. Figure 10 illustrates a comparison of the penetration depth and resolution associated with common biomedical imaging systems.

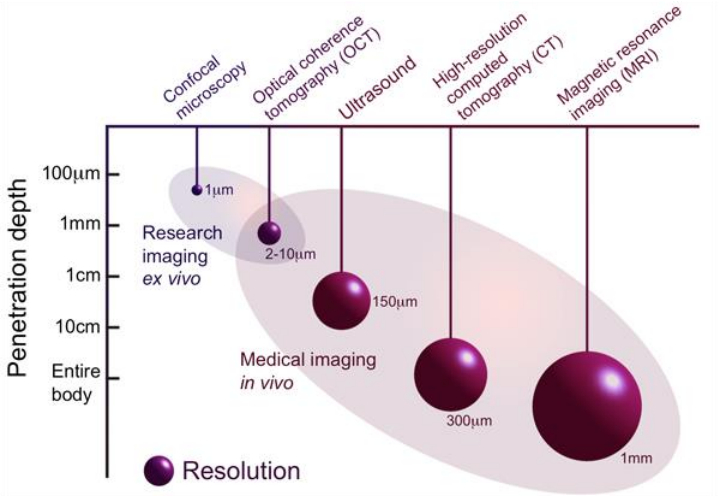

Figure 10 - Graph comparing the resolution and penetration depth of non-invasive imaging technologies used in bio-medical applications.

Despite its limited penetration depth of only a few millimeters, OCT offers the best in-vivo imaging resolution available. A few examples from a fast-growing list of OCT imaging applications include: dentistry, cardiovascular flow dynamics, nondestructive testing, material thickness, and pharmaceuticals.

Comparable Tunable Lasers for SS-OCT

The following table shows a comparison between the current swept-source solutions used in SS-OCT. The sweep-speed, sweep linearity, sweep flexibility, duty cycle, tuning range, coherence length, and side-mode suppression ratio (SMSR) of each are listed.

Table 1 - Comparison of performance parameters among various swept source lasers used in OCT.

Performance Parameter	VT-DBR	Polygon	MEMS-VCSEL	Desirable
Sweep speed	0-200+ kHz	3-50 kHz	100/200 kHz	200+ kHz
Duty cycle	>98%	~91%	<70%	100%
Sweep linearity	Standard deviations < 160 pm measured	Inherently non-linear (needs wavelength reference)	Inherently non-linear (needs wavelength reference)	Perfectly linear
Sweep flexibility	Any sweep pattern possible with akinetic-tuning	Linear only	Linear only	Novel sweep patterns for complex sensing schemes
Tuning range	30-50 nm per laser, >170 possible with output concatenation	20-170 nm	100+ nm	50+
Coherence length	20-1000 mm	3-30 mm	11-100 mm	>100 mm
SMSR	30-40 dBm	~30 dBm	40-55 dBm	>25 dBm

The VT-DBR specifications are based on previous demonstrations of this swept source technology [6] [5]. The performance specifications of the polygon tuned source are collected from a Santec SS-OCT system and two other designs characterized at Cal Tech University [11] [12]. The performance parameters of the micro-electromechanical mirror system (MEMS) vertical cavity surface

emitting laser (VCSEL) correspond to information from Santec and Thorlabs SS-OCT products [13] [14]. Desirable performance attributes are listed in the right column; these values resemble the performance limits that must be met to produce an OCT image at resolutions ranging from 3 - 20 µm.

Figure 11 and Figure 12 depict the two alternative SS-OCT systems described in Table 1.

Figure 11 - Thorlabs SS-OCT system utilizing the MEMS-VCSEL tuning scheme.

Figure 12 - Santec SS-OCT system utilizing the polygon mirror tuning scheme.

2. OBJECTIVES

The purpose of this work is to experimentally measure and characterize two VT-DBR lasers to validate their usability in SS-OCT in comparison to the alternative solutions listed in Table 1. The measured characteristics of each aid in the development of future designs and help facilitate application-specific performance prediction through the use of circuit modeling.

We understand that a potential limitation of the VT-DBR is the electrical response time of each tuning section. This work seeks to quantify that delay, as it relates directly to the optical tuning speed of the laser. The delay in a laser's optical response that is proportional to cavity length is minimized in the VT-DBR due to its relatively micro size.

Each section of the VT-DBR is a semiconductor diode and the response of each diode dictates the resulting optical response. The responses of each device are measured to estimate optical tuning speeds.

Figure 13 is the assumed circuit model for each section of the laser where the lead inductance, dynamic resistance, and effective capacitance are simplified into lumped components.

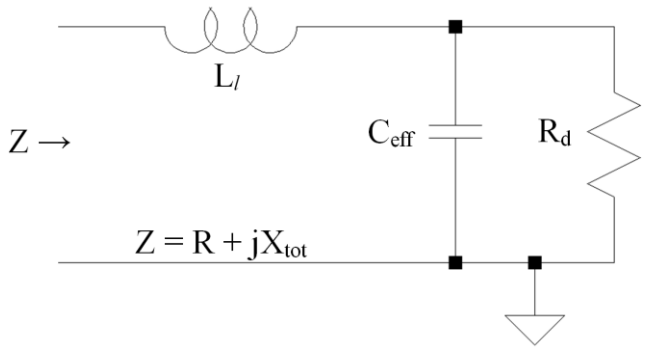

Figure 13 - Assumed circuit model of each laser section; lead inductance, effective capacitance, and dynamic resistance are all represented by lumped components.

In reality, these components are spatially distributed; for example, the lead inductance is the combined inductance formed by multiple bond-wire connections joining the outer package pin to the chip carrier to the laser chip itself.

Figure 14 shows the internal view of a VT-DBR laser package with the connections mentioned above clearly visible.

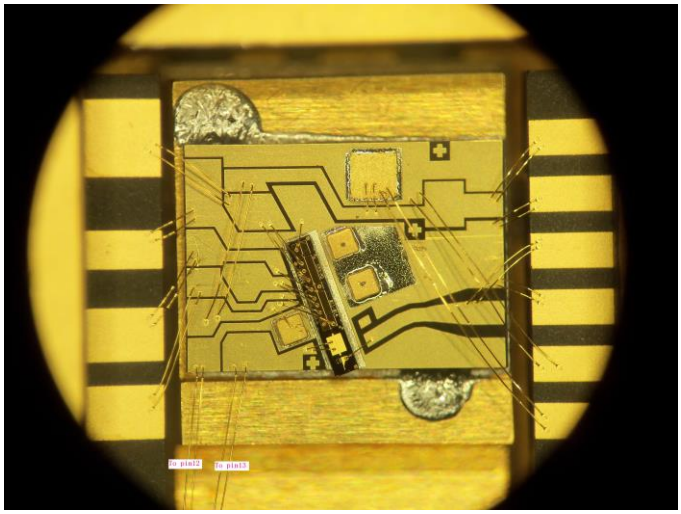

Figure 14 - Internal view of the VT-DBR laser package; 25 micron bond-wires connecting the laser's package to the chip carrier and chip carrier to the laser chip are made using thermosonic bonding.

Figure 15 shows a close-up view of the bond-wire connections between a VT-DBR laser chip and its carrier; it is assumed that these narrow conduction paths contribute the majority of the lead inductance in the circuit model.

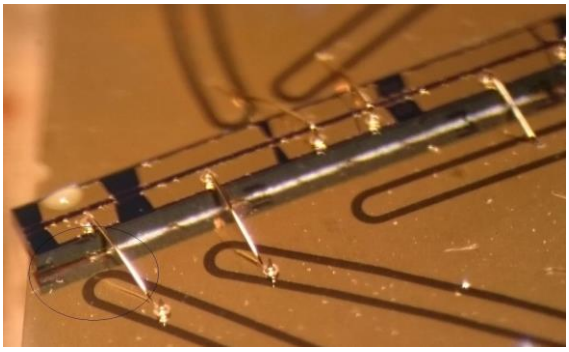

Figure 15 - Close-up view of the bond-wire connections between chip carrier and the laser chip in a VT-DBR laser package.

To make the electrical connection necessary to drive the laser and measure its performance, the laser package is soldered to a breakout board designed by Desmond Talkington in previous VT-DBR laser research [15]; it allows for easy electrical access to the package pins via the coaxial SMA connections at the perimeter of the PCB. Figure 16 depicts the breakout-board and identifies elements of interest.

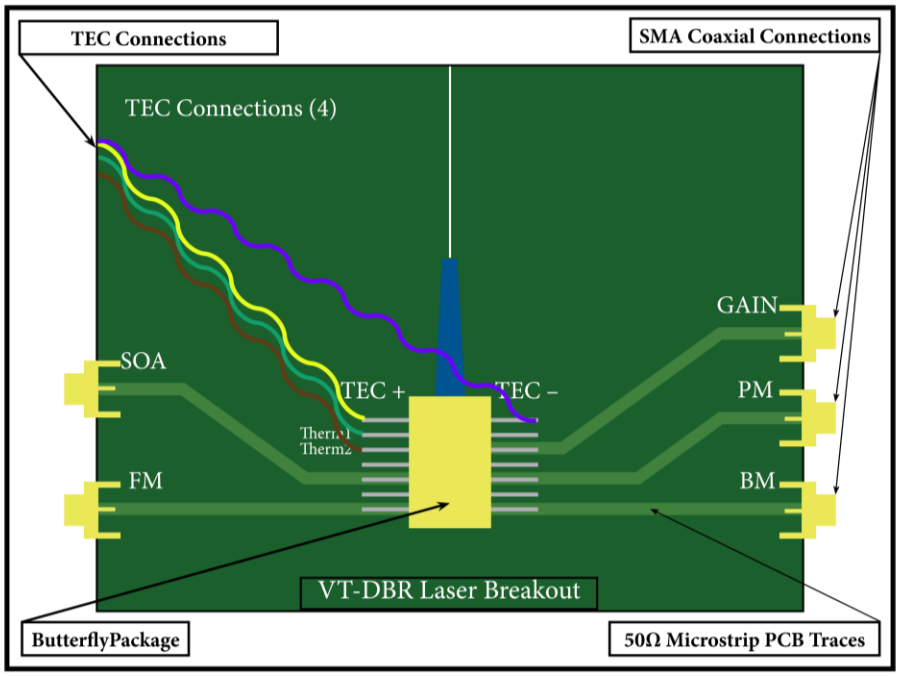

Figure 16 - VT-DBR laser break-out board for use in the characterization of VT-DBR lasers. All key components labeled including the Butterfly package, TEC connections, 50 Ω PCB traces, and SMA port connections.

I-V curves (i.e. - linear plots of the bias-current to port-voltage relation) are produced for each laser section by measuring the port voltage at current biases spanning the operating range of the section. This information is useful when designing the current sources and integrating circuitry that provides a driving signal to each section.

To determine their drive speed limitations, each section of the laser is injected with an electrical stimulus wave at current bias points within the section's operating range and the response is measured; this measurement is performed at many different current biases because the component values in the model corresponding to the diode segment (i.e. - dynamic resistance and effective capacitance) are heavily bias dependent.

The time and frequency domain responses versus current bias are collected using the time domain reflectometry (TDR) and frequency domain reflectometry (FDR) modes of an Anritsu MS4624B vector network analyzer (VNA); both are non-invasive sensing techniques that inform upon the electrical properties of the circuit of interest by transmitting an incident wave and measuring the resulting reflections. In this case, the circuits of interest are the tuning sections of the VT-DBR lasers (i.e. - the gain, SOA, phase, front-mirror, and back-mirror sections).

Using the TDR mode, a set of harmonically related DC-offset continuous wave (CW) sinusoids spanning 9 GHz are generated and the reflections of each are measured; the responses of the incident waves are combined by superposition to recover the effective response of the section to a step function

with a rise time of less than 112 ps. This series of signals is generated by the VNA and transmitted to the laser port under test (PUT) via a 50 Ω SMA coaxial cable. The dynamic resistance corresponding to the initial DC offset bias is determined by measuring the reflection coefficient, rho (ρ), in the TDR plot's steady-state response.

Using the FDR mode, the complex impedance of each laser section, from package pin to ground, is measured as a function of current bias (i.e. - the DC offset). The VNA generates a smith chart impedance locus by measuring the reflections of a swept sinusoidal stimulus signal and generating a continuous plot of impedance versus stimulus frequency. The impedance corresponding to an input stimulus of 10 MHz is recorded, as this represents the worst case scenario and upper bound of section drive signals that might be used.

For each section, the lead inductance is estimated using the largest positive-reactance in the series of impedance measurements made for that PUT. Effective capacitance is estimated by subtracting the inductive reactance from the total measured reactance, calculating the susceptance (B), and solving for the effective capacitance that would produce a susceptance of B in the circuit model.

In addition to fast sweep speeds and flexibility. The optical output of the laser requires narrow linewidth, wide spectral tuning, and good SMSR characteristics to perform well in SS-OCT applications. Table 1 lists the desired spectral characteristics necessary for SS-OCT. The spectral characteristics presented in this work include high-resolution tuning maps produced using

computer automation, SMSR measurements, and spectral linewidths at tuning section bias points of interest.

MatLab, a computer program, is used to achieve the automated wavelength tuning and measurement; the function “LaserMeasurement()” presented in appendix E commands two precision current sources connected to the FM and BM tuning ports of the VT-DBR break-out board through a series of bias conditions. The range and resolution of the bias currents in the data-set are defined by the user in the argument of the function. The output of the laser is measured with an optical spectrum analyzer (OSA) to determine the wavelength and peak power of the dominant signal.

The bias condition, wavelength, and power measurement data are then used by the function “TuningMapper()” to generate power and wavelength tuning-maps useful for identifying the tuning path and operating points of interest.

A novel way of presenting the tuning-map in a video format is also presented; using the “TuningMapVid()” function, a video showing a birds-eye view of the tuning map structure is generated. This tool further aids the visualization of the tuning map structure and offers a quick way to explore the tunable spectrum of the laser.

Aided by the tuning-maps, linewidth measurement points are selected by identifying operating points with stable single mode operation. Full width half maximum (FWHM) linewidth measurements are made using the self-homodyne method. This measurement technique makes use of an interferometer, DC-

biased photodiode, and spectrum analyzer to make accurate spectral linewidth measurements.

The SMSR is also collected at bias points of interest to estimate the signal to noise ratio (SNR) of the laser.

Before lasing, the TEC is always energized to prevent damage to the device from overheating. A constant waveguide temperature of 25 +/- 0.05 degrees is always maintained when lasing to eliminate performance variations due to temperature fluctuations.

3. ELECTRICAL CHARACTERIZATION

I-V Curves

The following figure depicts the test configuration used to collect the I-V curves associated with each laser segment. An LDC-3744B laser diode controller (LDC) is used to fix the waveguide temperature and supply a precise current bias to the PUT. A 34401A Agilent voltmeter is used to measure the resulting voltage that develops at the PUT, given a current bias from the LDC.

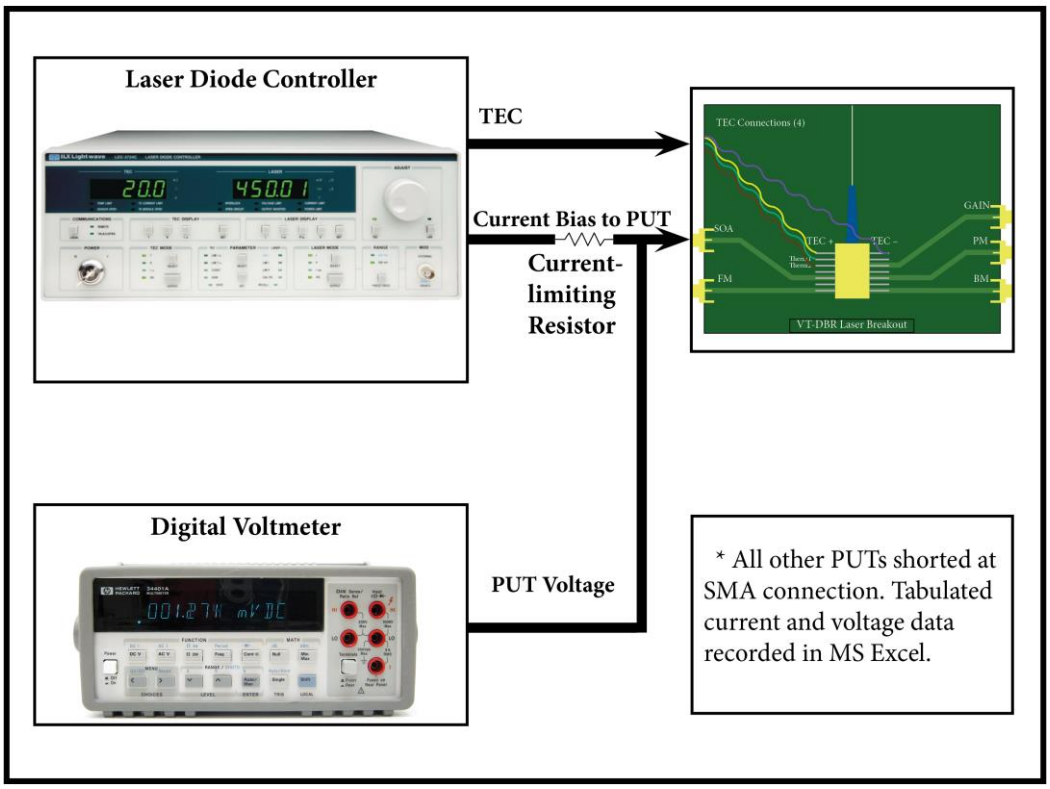

Figure 17 - IV curve collection instrument-setup. A laser-diode controller (i.e. - LDC-3744B) is used to drive the on-chip TEC and provide the current bias to the PUT. A current-limiting resistor is used to protect the PUT from transient voltage/current spikes and provide a point to measure the PUT voltage. An HP 34401A voltmeter is used to measure the PUT voltage.

The current to voltage relation is measured by stepping the input current of the PUT through incremental bias points within its operating range and the resulting port voltage is recorded; all bias and subsequent PUT voltages are tabulated in an excel document.

The current-limiting resistor protects each section from transient current spikes that might otherwise damage the device; this resistor also gives access to the coaxial center-conductor so the port voltage can be easily measured.

The measured I-V curves inform upon the current and voltage range requirements necessary to drive each laser section. A key element in the assumed circuit model of each section, the dynamic resistance, is also embodied by the inverse slop of a line tangent to the curve at a particular voltage.

All other break-out board ports are short-circuited to prevent deviations in the measurement results due to electrical interference between the adjacent signal paths.

Figure 18 shows an example I-V measurement point of the Neptune laser's gain section where the laser current driver is delivering ~1.9 mA of current and an 881 mV port voltage is measured using the Agilent voltmeter.

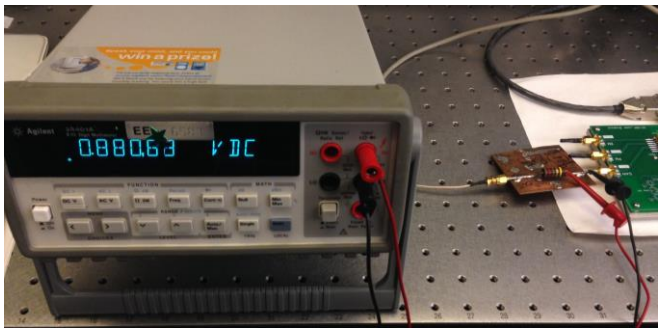

Figure 18 - Gain port voltage measurement of the Neptune laser with a 1.9 mA current bias being delivered from the laser-diode controller. An 881 mV port voltage is observed.

FDR and TDR Response

Each PUT is interrogated with a 9 GHz Anritsu VNA to capture its frequency and time domain reflectometry responses at a sequence of bias points within the current range of each PUT. The instrument configuration used to collect this data is illustrated in Figure 19 below.

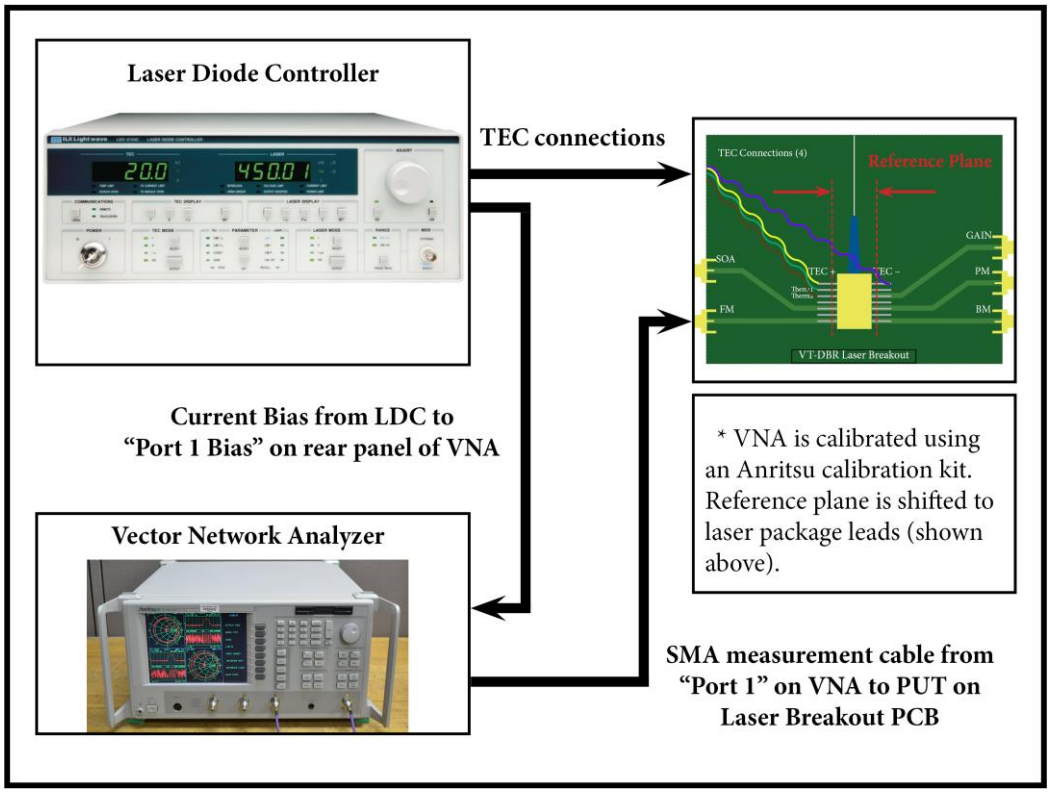

Figure 19 - VNA instrument configuration used to collect the TDR and FCR responses of each PUT. An LDC-3744B is used to drive the onchip TEC and deliver bias current through the "Port 1 Bias" connection on the back panel of the VNA. The VNA is first calibrated and reference plane shifted to the beginning of the package leads. The measurement reference plane is identified by the dashed red lines on the breakout board PCB.

The PUT current bias is accomplished using the "Port 1 Bias" connection on the back of the VNA. All electrical connections are secured and maintained while current is being delivered to any section of the laser; if a connection is broken while current flows, the corresponding section could be damaged.

Dynamic Resistance Extraction from TDR

The Dynamic resistance is measured by analyzing the steady-state response of the TDR measurement. The VNA is first calibrated to remove measurement error introduced by the measurement system itself. Once calibrated, the VNA's reference plane is shifted to the input of the PUT; the spatial reference shift and windowing features of the VNA allow for the accurate measurement of the S_{11} scattering parameter, limited only by its 112 ps rise-time.

Figure 20 shows the Neptune laser package soldered to the break-out board used in my characterization research; the measurement reference plane for all VNA measurements is identified by the dashed-red lines dissecting the laser package leads [15].

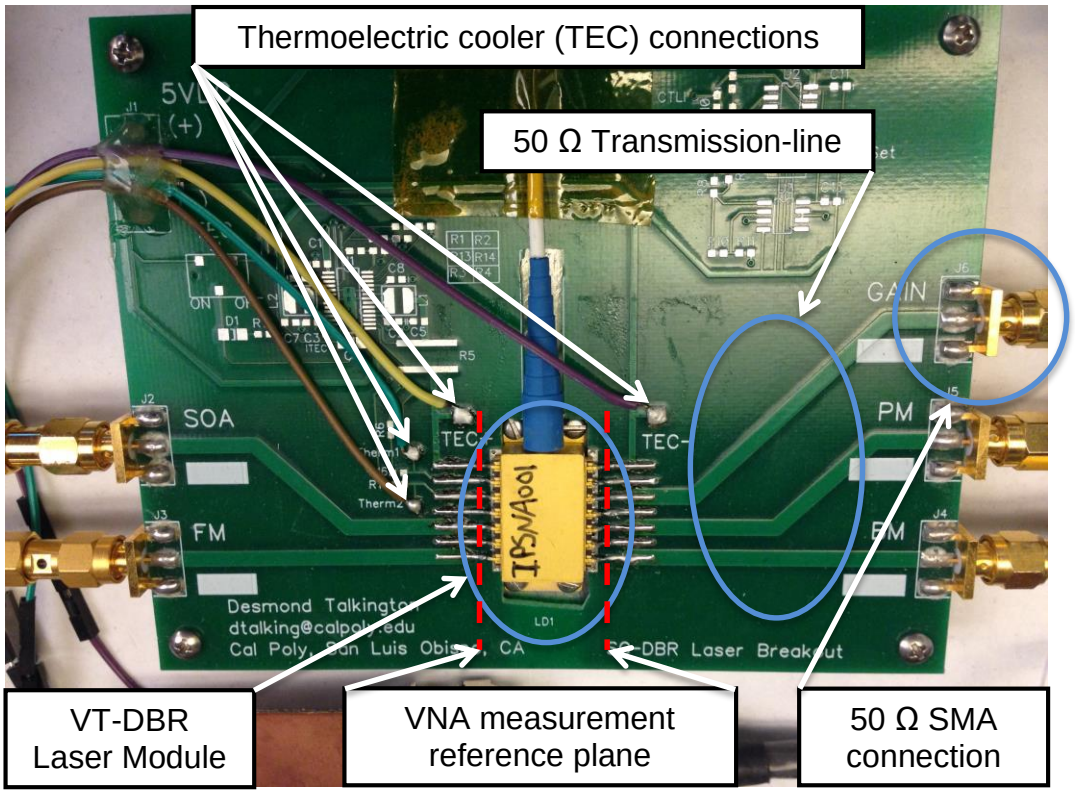

Figure 20 - Butterfly package break-out board designed by Desmond Talkington for experimental research of the packaged VT-DBR lasers; a 50 Ω electrical system is used to

reduce source signal reflection and achieve an accurate measurement of the lumped component values in the PUT.

Next, the TDR response of each PUT is measured at a sequence of bias points and the dynamic resistance is calculated at each using the steady-state reflected voltage waveform. Additionally, the response time (τ_r) can be visually estimated by measuring the elapsed time between the incident signal's arrival to the reference plane and the 63.2% point of the section's voltage transition.

The VNA is put into TDR mode and the step input response plot is displayed. Figure 21 illustrates the measurement points of interest on the response plot, including the response time and reflection coefficient (ρ).

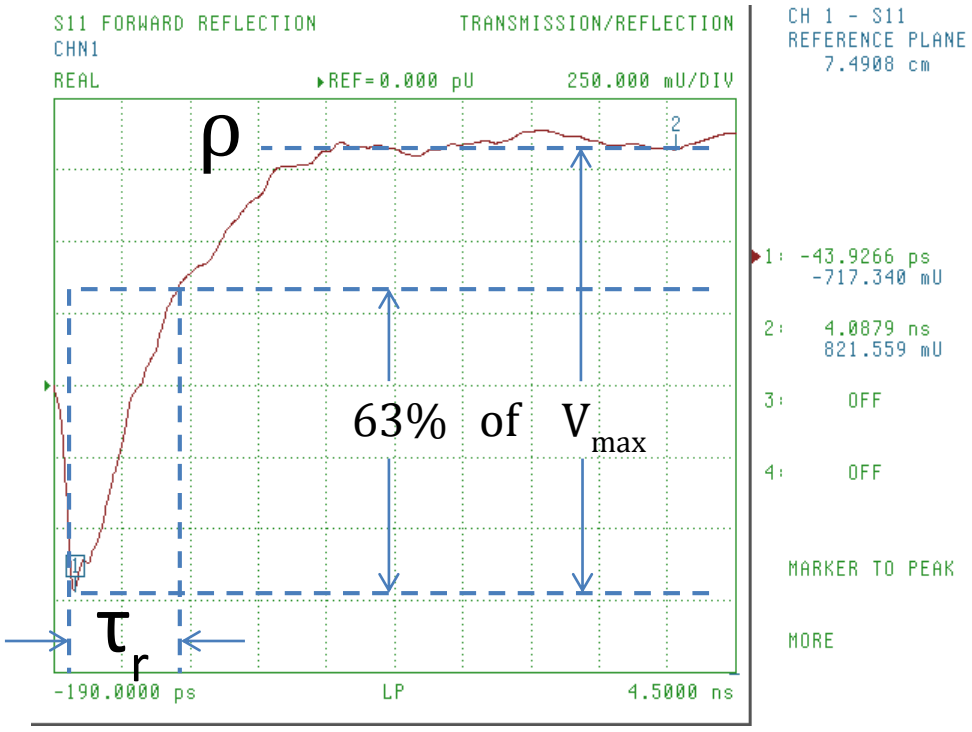

Figure 21 - Example TDR response with measurement points of interest identified. The rise time (τ_r) and the steady state reflection coefficient (ρ) corresponding to the dynamic resistance are recorded for each bias condition.

Equation (1) relates the reflection coefficient measured at V_{max} to the dynamic resistance of the PUT at the particular bias. Z_o represents the 50 Ω characteristic impedance of the transmission lines used to connect the VNA to the laser's package leads. Every TDR measurement for the Neptune and VTL-2 lasers can be found in the corresponding '.zip' files in appendix K and L, respectively.

$$R_d = Z_o \frac{(1+\rho)}{(1-\rho)} \tag{1}$$

Figure 22 illustrates the relation between the dynamic resistance and an I-V curve of a typical diode. At a particular bias point, the dynamic resistance of a diode is defined by the inverse-slope of the tangent line at that point. From the illustration, it is clear that this dynamic resistance of a diode changes dramatically across its operating range.

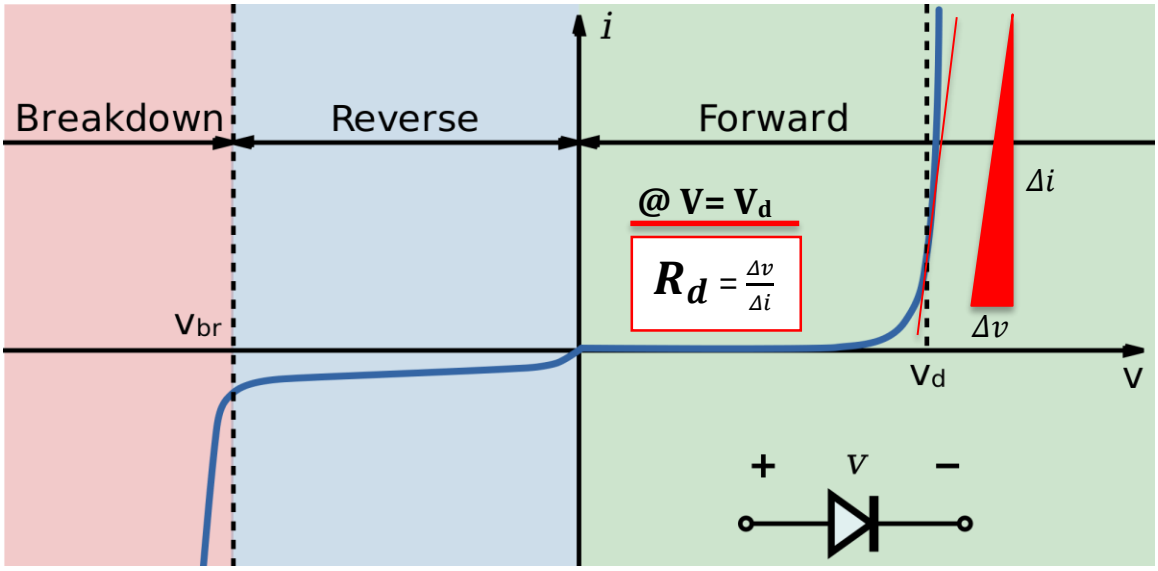

Figure 22 - Typical I-V curve of a diode across the breakdown, reverse-bias, and forward-bias regions of operation.

Response Time Extraction from FDR

The complex impedance of each PUT is also measured at the same bias points used for the TDR measurements. The VNA mode is changed to display the FDR response in the form of a smith chart. A marker is placed on the impedance locus point corresponding to a 10 MHz stimulus.

As in the TDR measurements, the plot data is taken at each bias point and the complex impedance is recorded in an excel spreadsheet. This data is then used to estimate the fixed lead-inductance and bias dependent effective-capacitance.

Figure 23 identifies the pertinent information in an example FDR measurement. As with the TDR data, every FDR measurement for the Neptune and VTL-2 lasers can be found in the corresponding '.zip' files in appendix K and L, respectively.

The largest reactance measured for each PUT is rounded up to the nearest tenth of an ohm to account for the finite reactance contribution of the effective capacitance. The inductive reactance is then used to estimate the fixed lead inductance using equation (2).

$$\boldsymbol{L_{lead} = \frac{X_L}{2\pi f}} \tag{2}$$

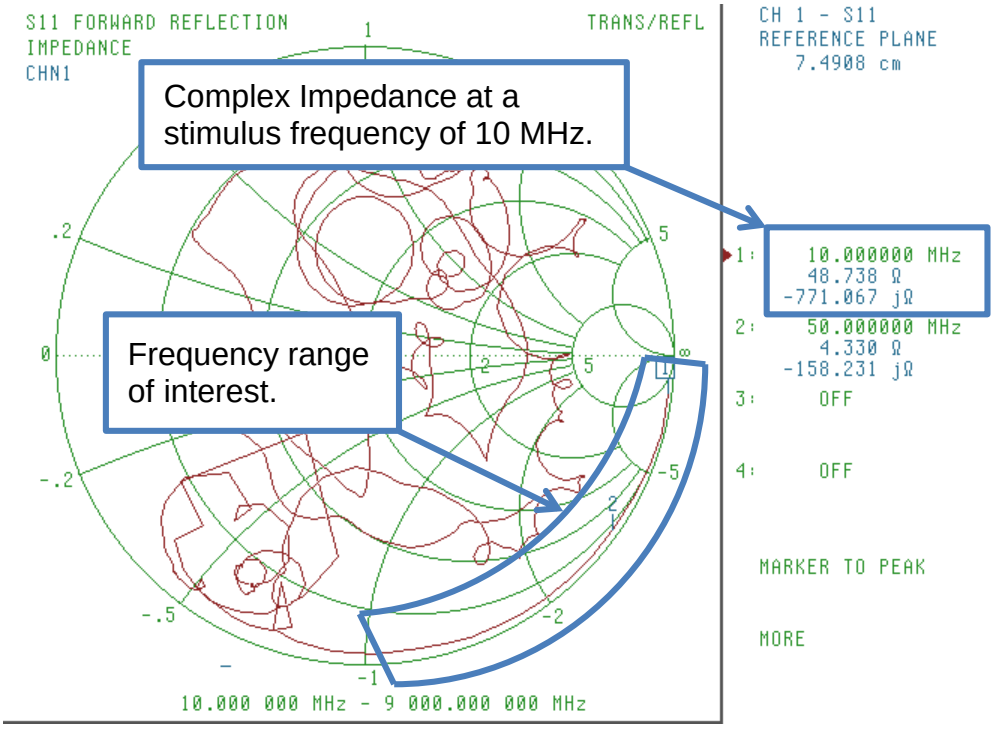

Figure 23 - Frequency domain reflectometry measurement of the Neptune laser's front-mirror section with zero current bias.

The capacitive reactance is then estimated by subtracting the inductive reactance from the total measured reactance. Equation (3) illustrates this relation.

$$\boldsymbol{X_C = X_{tot} - X_L} \tag{3}$$

The capacitive susceptance 'B' is then calculated using equation (4), below. X_C is the capacitive reactance calculated in equation (3) above and R is the resistance from the complex impedance measurement shown in Figure 23.

$$\boldsymbol{B = \frac{X_C}{|Z|^{-2}} = \frac{X_C}{R^{-2} + {X_C}^{-2}}} \tag{4}$$

From the susceptance, the effective lumped capacitance in the circuit model is estimated using equation (5).

$$C_{eff} = \frac{B}{2\pi f} \tag{5}$$

Finally, the response time of each section is estimated for the given bias condition using the RC-circuit charging time constant equation below. R is the resistance “seen” by the capacitor (i.e. - the parallel combination of the resistance in the complex impedance measurement with the 50 Ω characteristic impedance of the transmission line providing the PUT connection.)

$$\tau_r = RC_{eff} \tag{6}$$

TDR Measurement Validation

To ensure the accuracy of the TDR measurements taken from both lasers with the 9 GHz Anritsu MS4624B VNA, TDR measurements are repeated for the BM section of the VTL-2 laser on a second TDR instrument. Response time values derived from the frequency domain measurements on the Anritsu are also compared to those measured in the time domain of the second measurement setup; an HP 54754A TDR module in an Agilent mainframe is used to make the comparable measurements.

Unlike the Anritsu VNA, the HP TDR module produces an actual step-input and measures its reflection versus measuring the reflections of a harmonically related set of sinusoids and using the superposition principle. This configuration has a rise-time of approximately 49 ps which will allows the measurement of lower response times than the Anritsu VNA.

Figure 24 is a photo of the measurement setup used. As always, the TEC controller is energized first to maintain the waveguide temperature while lasing. The TDR module is calibrated using the automated calibration process built into the mainframe's user interface to remove measurement inaccuracies introduced by the coaxial cable and the instrument itself. The same calibration-kit loads used in the Anritsu VNA's calibration are used here as well.

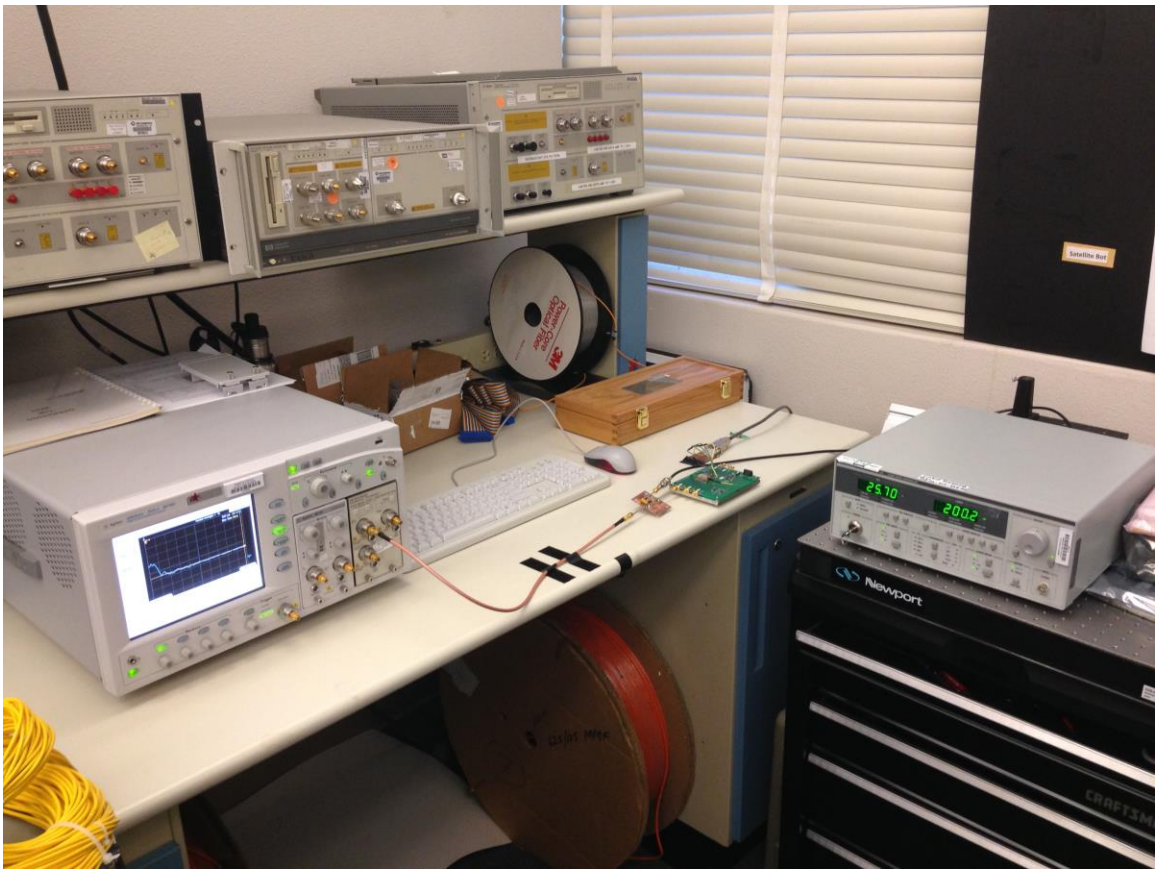

Figure 24 - TDR validation instrument configuration. HP 54754A TDR module is connected to the PUT through a bias-T; the PUT is biased with the LDC current source.

It was necessary to produce a custom bias-T so non-zero bias measurements could be made because this measurement instrument is not capable of supplying a current bias to the PUT.

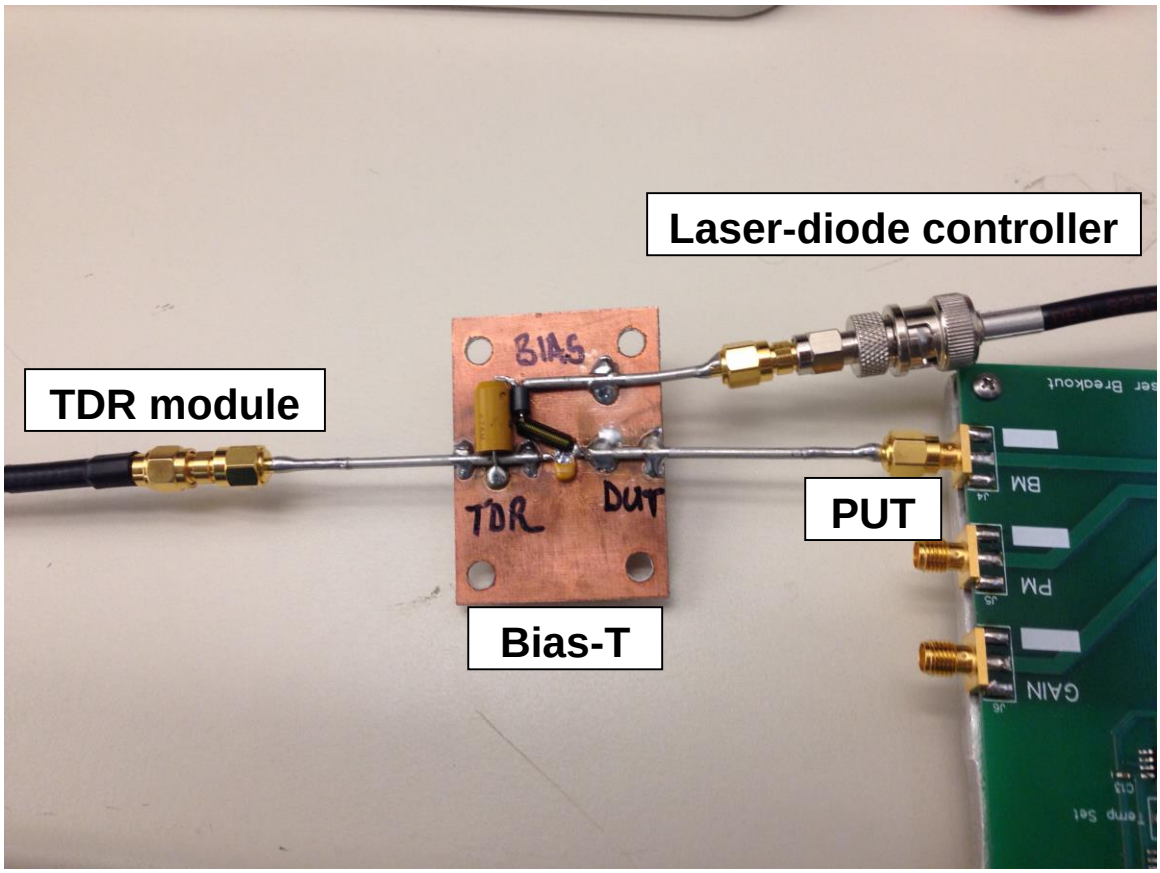

Figure 25 - Custom bias-T enabling non-zero current measurements with an HP 54754A TDR module. The bias connection forms a low-pass filter to prevent TDR stimuli from reaching the bias source. The stimulus signal is transferred to the PUT via an AC coupling capacitor.

Figure 25 is a picture of the bias-T made for this measurement. The bias path leaving the 'T' forms a low-pass filter with a C-L-C π-configuration; the filter prevents high frequency content from reaching the bias source.

The TDR connection is AC shorted to the PUT connection via a small AC coupling capacitor, allowing the PUT to have a non-zero voltage and receive a step input from the TDR module without lifting the TDR port's center-conductor from ground. Figure 26 illustrates the filtering circuit components that collectively form the bias-t.

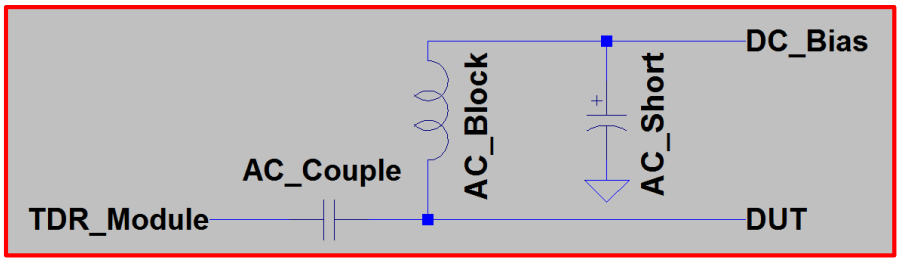

Figure 26 - Bias-T circuit schematic.

Figure 27 is an example TDR measurement of the VTL-2 laser's BM port with a 10.1 mA bias. The response time is measured to be approximately 0.3 ns. A dynamic resistance of 6.2 Ω is displayed explicitly on the TDR plot; Unlike the TDR mode of the Anritsu VNA, this instrument configuration makes the conversion from reflection coefficient to resistance automatically.

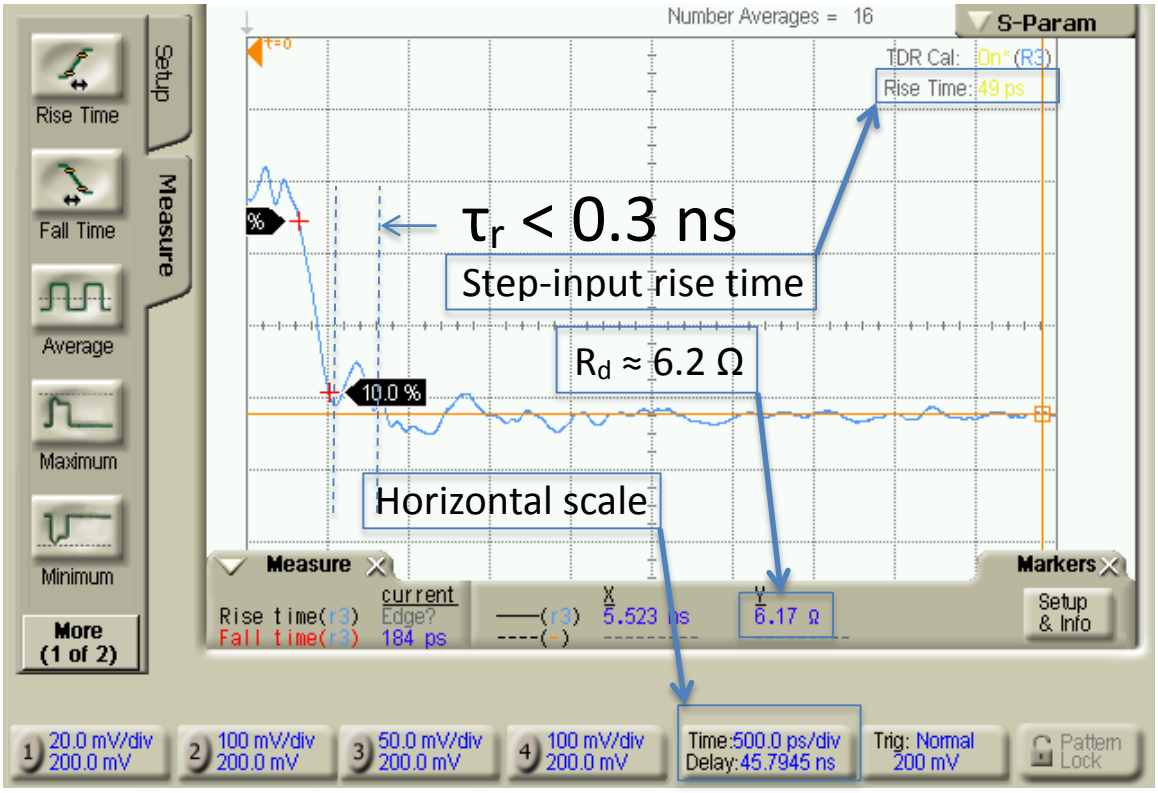

Figure 27 - TDR measurement of the VTL-2 laser's BM section at a 200 mA bias using the HP 54754A TDR module with a step-input rise time of 49 ps. A PUT response time of 0.3 ns is observed which deviates from the Anritsu VNA measurement by only 60 ps.

The response-time curves of the VTL-2 laser's BM port using the two collection methods are compared in Figure 28. The plot shows the response times corresponding to the FDR measurements using the Anritsu VNA in red and the TDR measurements using the HP 54754A TDR module in blue.

From the high degree of correlation in the response time curves, we can assume with a fairly high level of confidence that both measurement instruments and methods yield precise reflectometry measurements.

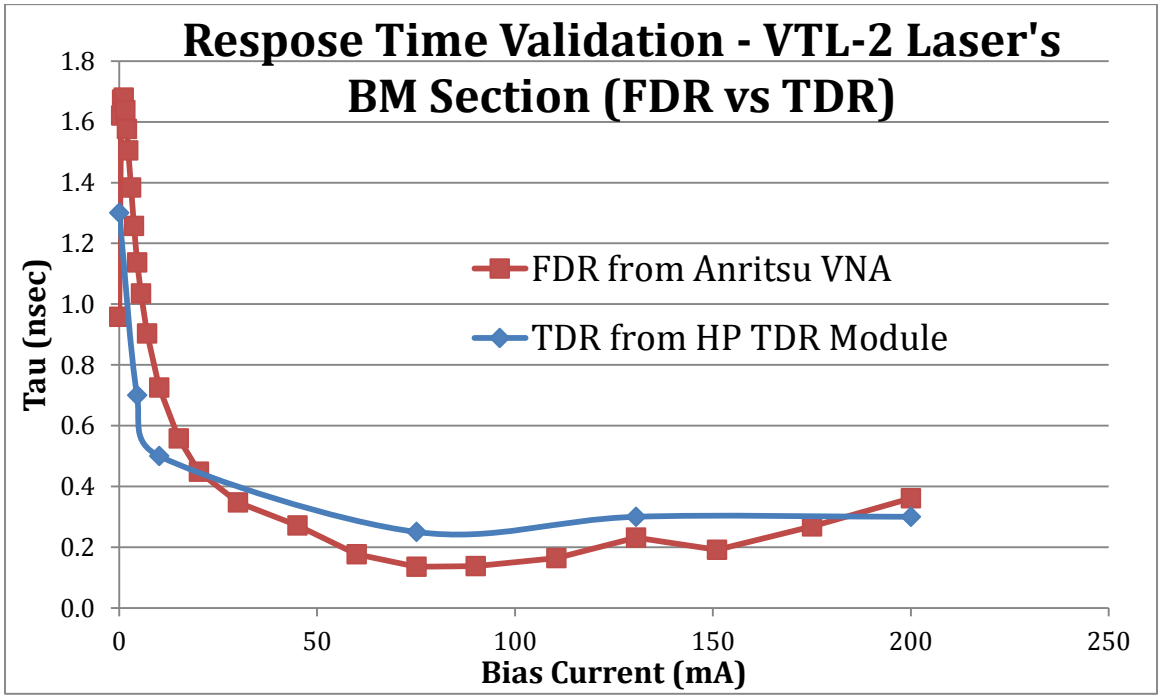

Figure 28 - Comparison of the VTL-2 laser's BM section response-times between the two collection instruments and methods. A very high correlation is observed.

Deviations between the two interpolated curves are limited to 250 ps across the measurement range of the BM section. TDR plot screen captures on the HP TDR module can be found in appendix D.

4. SPECTRAL CHARACTERIZATION

Tuning Maps

A wavelength-tuning map provides a visual representation of the laser's primary longitudinal mode as a function of the FM and BM bias currents. This allows for the optimal tuning path for the desired linear wavelength sweep to be identified. With the 3D surface plot of this data, anomalies that might cause non-linearity in the wavelength sweep of the laser can be identified and avoided.

Similarly, a power-tuning map is a visual representation of the peak power in the dominant mode of the laser's output spectrum as a function of FM and BM bias. With the power-tuning map, supplemental gain required by the SOA can be easily calculated and used to realize any power profile.

Together, these tuning maps serve as a tool for identifying appropriate spectral linewidth measurements points by illustrating bias regions that exhibit stable single-mode operation.

The instrument configuration used to collect the tuning maps is shown in Figure 29, below. As always, the TEC controller in the LDC is used to maintain the waveguide temperature. The SOA and Gain sections of the laser are biased to 100 mA each to achieve stable lasing. The FM and BM ports are connected to precision current drivers that are computer controlled through a GPIB interface.

With the MatLab function "LaserMeasurement()" I wrote for tuning map data collection, the user defines the desired tuning map current boundaries and resolution with the start, stop, and step arguments of the function. The output of the laser is coupled into an Agilent 86140B OSA, also controlled by the

computer, to measure the power and wavelength of the dominant signal in the laser's output spectrum at each bias point. The function records the data collected in an excel file called "TuningMap.xls" which is generated in the MatLab working director when the function is run. Each time a new data collection process is started, a new sheet is created in the excel document and titled with the current date and time so that the dataset can be easily referenced.

In addition to the measurement of the dominant mode's power and wavelength at each bias point, an OSA screen capture of the laser's output spectrum is saved to a folder in the working directory with the same name as the corresponding data-sheet.

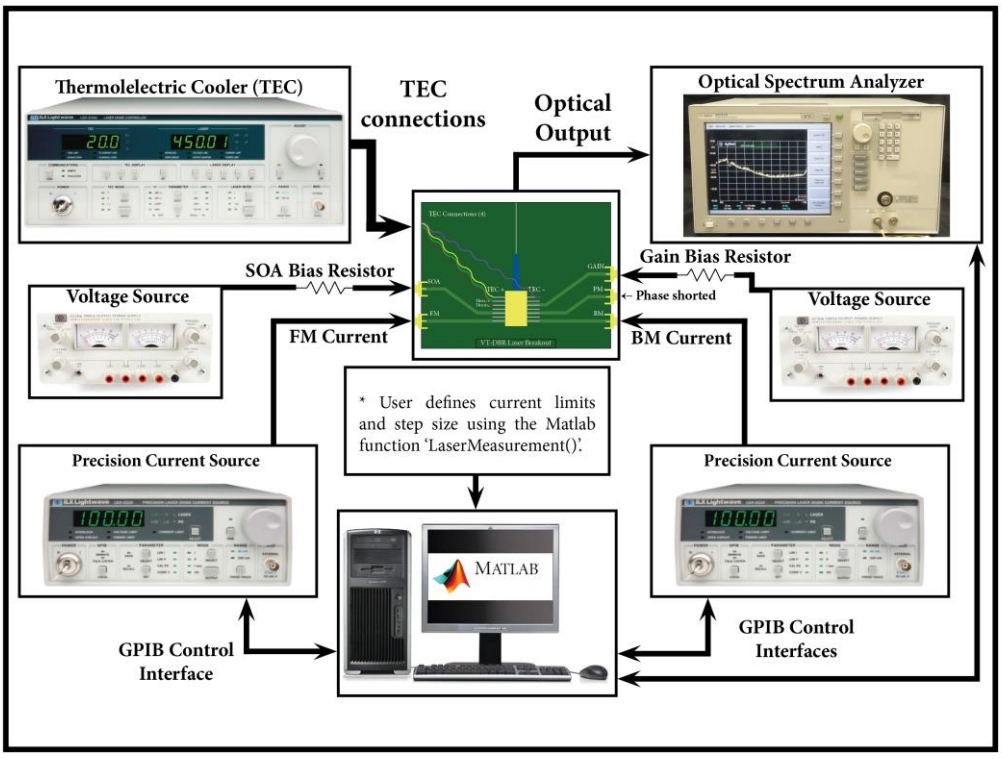

Figure 29 - Instrument configuration used for tuning map collection. The user runs the MatLab function 'LaserMeasurement()' with the bias current start, stop, and step/resolution values for the FM and BM precision current sources passed in the function's argument.

Once a data-set is collected, the MatLab function “TuningMapper()” is used to plot the 3D wavelength and/or power tuning surfaces for analysis. The user is prompted with a series of questions to arrive at the desired tuning map; the selected data-set is plotted into a 3D tuning surface by linearly interpolating between the measured data-point vertices.

Upon execution of the function, the user is asked which excel sheet to extract a data-set from and what tuning maps to generate; wavelength, power, or both are the available selections. Using the cursor, the tuning surface view can be manipulated, zoomed, and probed to analyze the laser’s tuning characteristics within the data-set’s measurement range.

Using the MatLab function “TuningMapVid()”, a video of the tuning surfaces can be produced in a file-type specified by the user on line 17 of the function code. In the execution of the function, a video is created by appending a sequence of figure images together. The view-angle is incrementally advanced through a circular path surrounding the surface’s centroid while the view-point elevation and field of view is decreased; this video rendering of the tuning surface provides a novel view of the tuning surface from many angles, elevations, and fields of view.

As with the “TuningMapper()” function, when the function is executed, the user is prompted to select the desired data-set sheet in the “TuningMap.xls” file to process. The user is also asked to enter the number of frames or “viewpoint angles” to comprise the video sequence of; a number less than 500 is recommended for larger file formats.

Side-Mode Suppression Ratio

The SMSR is measured at bias points of interest to investigate whether amplified spontaneous emission (ASE) is being back-coupled from the SOA and degrading the SMSR. Being a relative measurement of the peak-power difference between the dominant mode and the most powerful side-mode, the SMSR informs on the laser's performance in applications requiring high spectral discrimination. SS-OCT is only one such application.

In Figure 30, an example SMSR measurement is illustrated to identify the power peak of the dominant mode, the most powerful side-mode, and the difference between the two (i.e. - the SMSR itself).

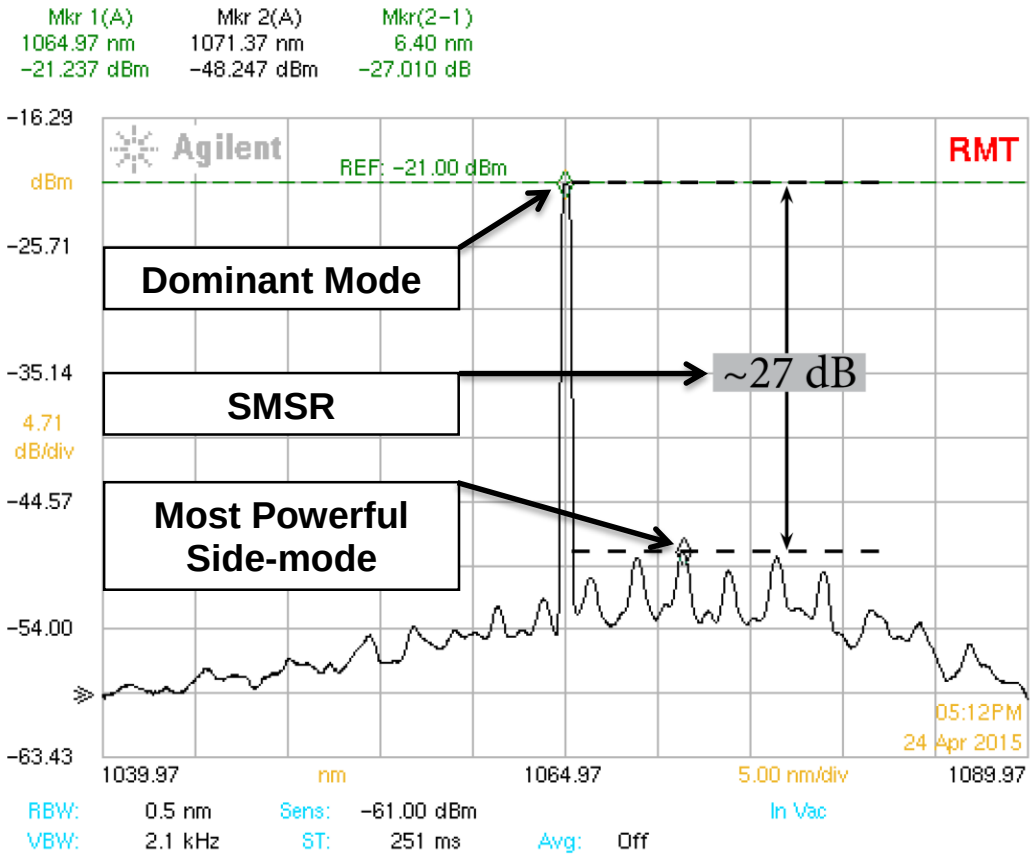

Figure 30 - SMSR measurement example. An SMSR of greater than 27 dB is observed between the power of the dominant mode and the most powerful side-mode.

Spectral Linewidth

The spectral linewidth of each device is measured at stable tuning-bias points of interest; these points are selected using the tuning maps of each device. Figure 31 illustrates the instrument configuration used to make linewidth measurements; the self-homodyne measurement method presented in the book “Fiber Optics Test and Measurement” is used [16].

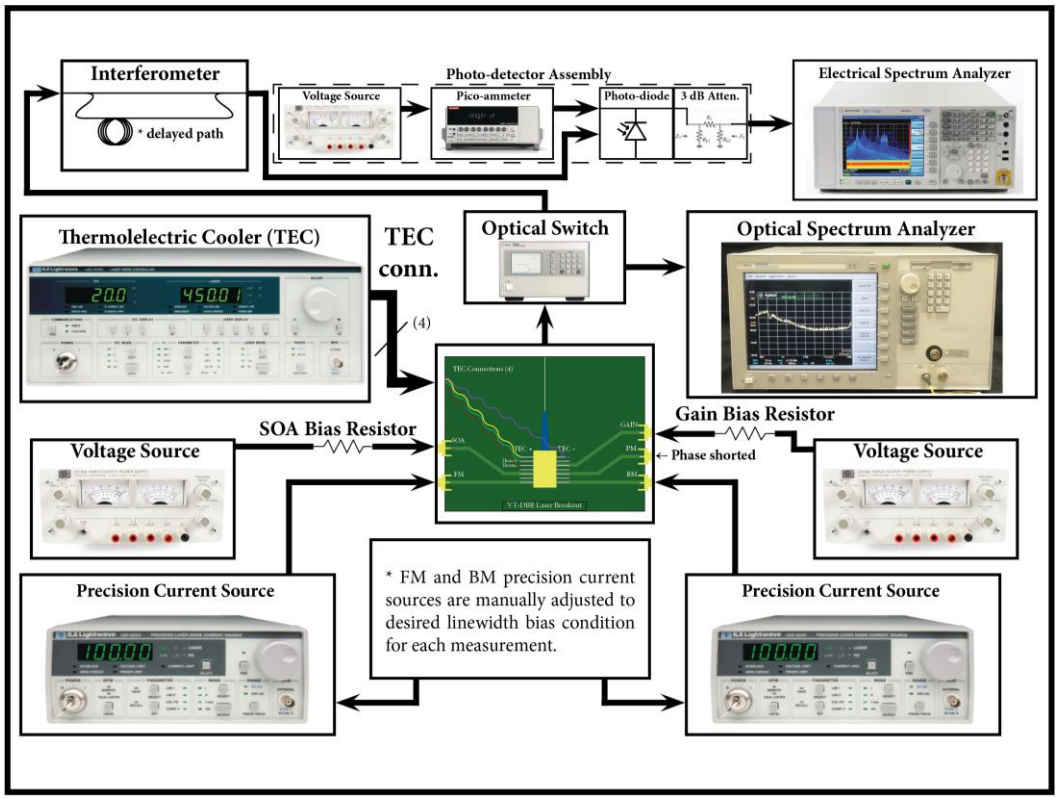

Figure 31 - Instrument configuration for spectral linewidth measurements. SOA and Gain sections are biased at 100 mA. FM and BM sections are manually tuned using precision current sources. The laser's output is directed using an Agilent optical switch. The signal path includes an interferometer, reverse-biased photodiode, 3 dB attenuator, and electrical spectrum analyzer (ESA). This setup facilitates the self-homodyne measurements method.

The self-homodyne measurement technique allows high frequency signal spectrums (e.g. - the optical spectrum) to be measured with high precision; these

spectrums are generally too high in the frequency to be accurately measured by traditional OSAs due to their inadequate bandwidth resolutions.

The optical signal from the laser is coupled with a delayed version of itself using the interferometer. A suitable path delay is used to ensure a valid autocorrelation measurement can be made for the wavelengths being measured (i.e. - 3.5 μs in this case). The autocorrelation signal is coupled to the photo-detector assembly and the resulting modulated spectrum envelope is measured at its full-width half maximum (FWHM) using the ESA; the modulation process doubles the spectral width, allowing the FWHM optical spectrum to be measured at HWHM in the electrical spectrum.

Before reliable measurements can be made, the noise floor of the Agilent CXA signal analyzer is established as a reference. An example noise floor measurement is presented in Figure 32.

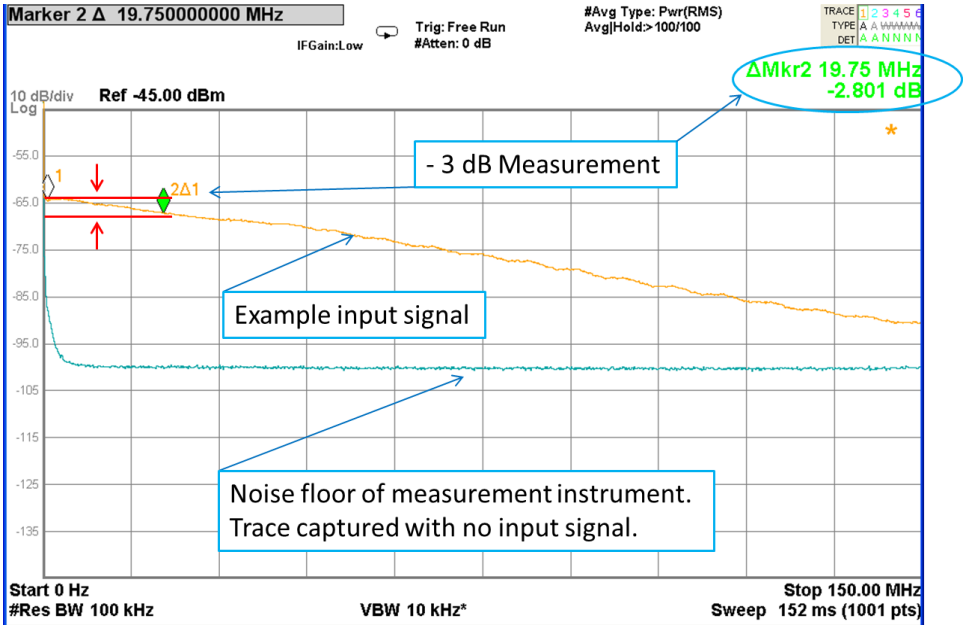

Figure 32 - Noise floor of Agilent CXA signal analyzer used for measuring spectral linewidth and an example FWHM linewidth measurement of the Neptune laser.

5. NEPTUNE VT-DBR LASER CHARACTERIZATION

The following I-V graphs were collected from the Neptune laser. To improve accuracy of the interpolated curves, more data points were taken around the knee-in current region of operation where the current to voltage relation becomes far less linear.

All sections have knee-in current voltages just under 1V. The dramatic transition from high to low dynamic resistance is seen to occur over a very small change in voltage bias. The linear segments of the curve on either side of the knee-in current threshold indicates very large and small dynamic resistances at negative-low and high PUT voltages respectively.

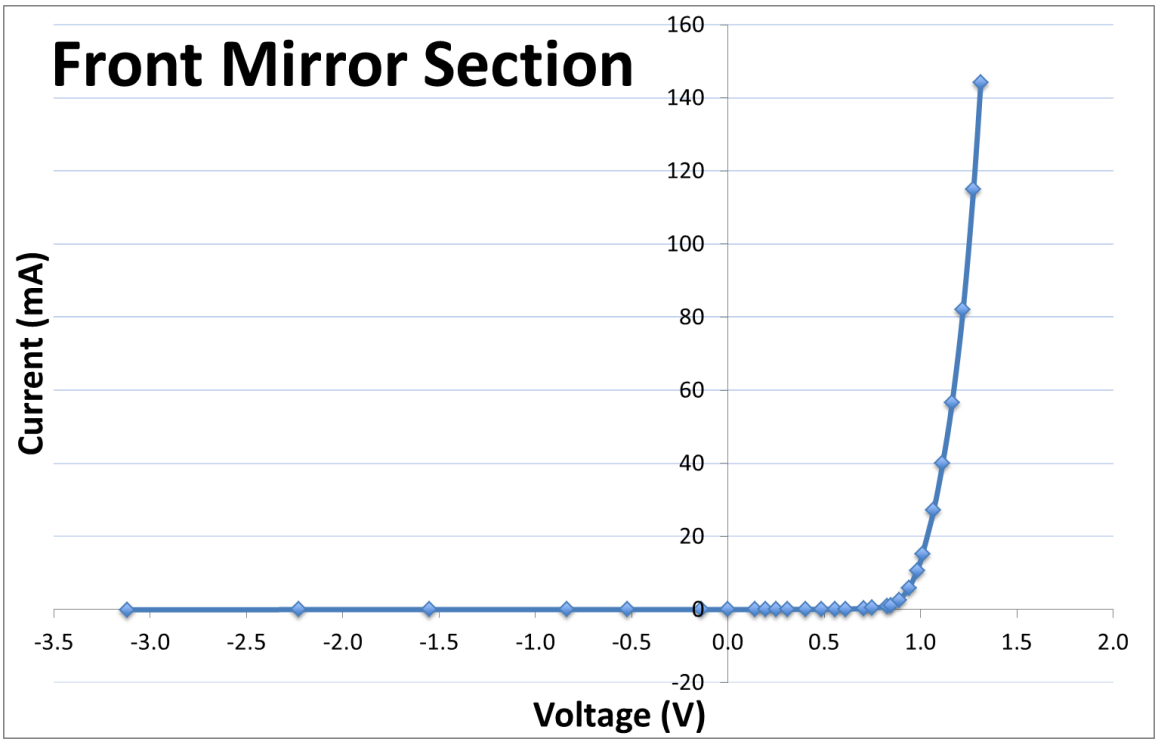

Figure 33 - I-V curve of the Neptune VT-DBR laser's front-mirror section.

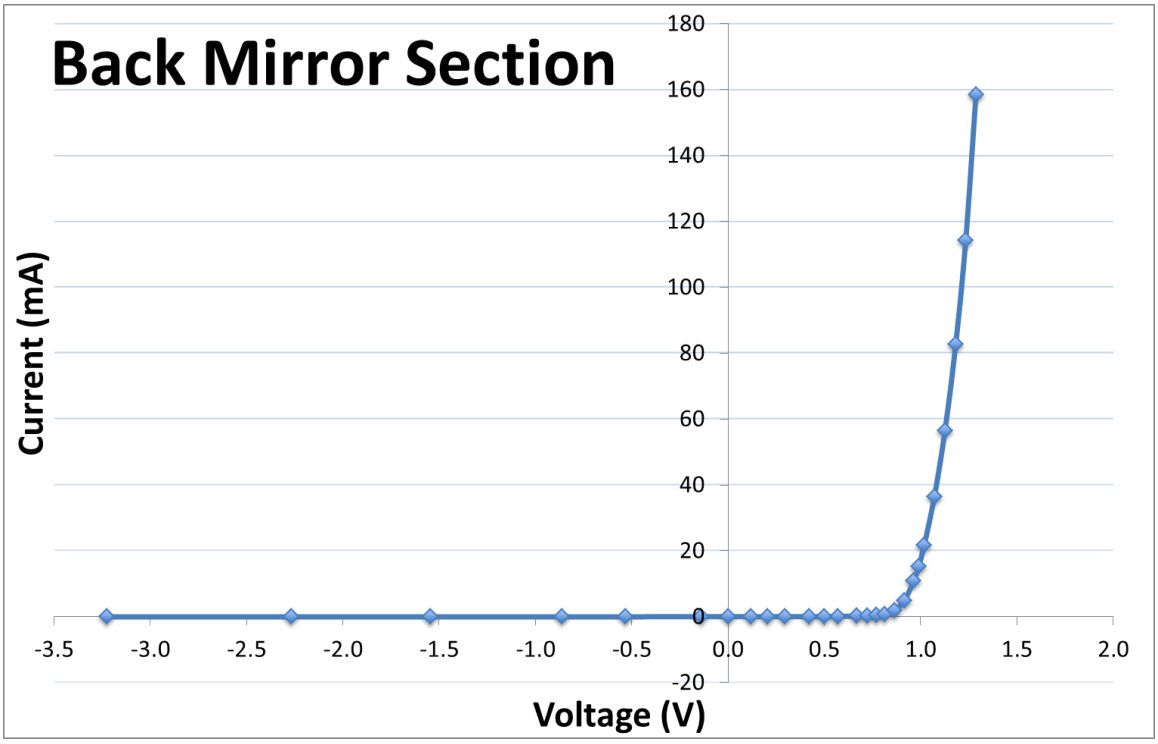

Figure 34 - I-V curve of the Neptune VT-DBR laser's back-mirror section.

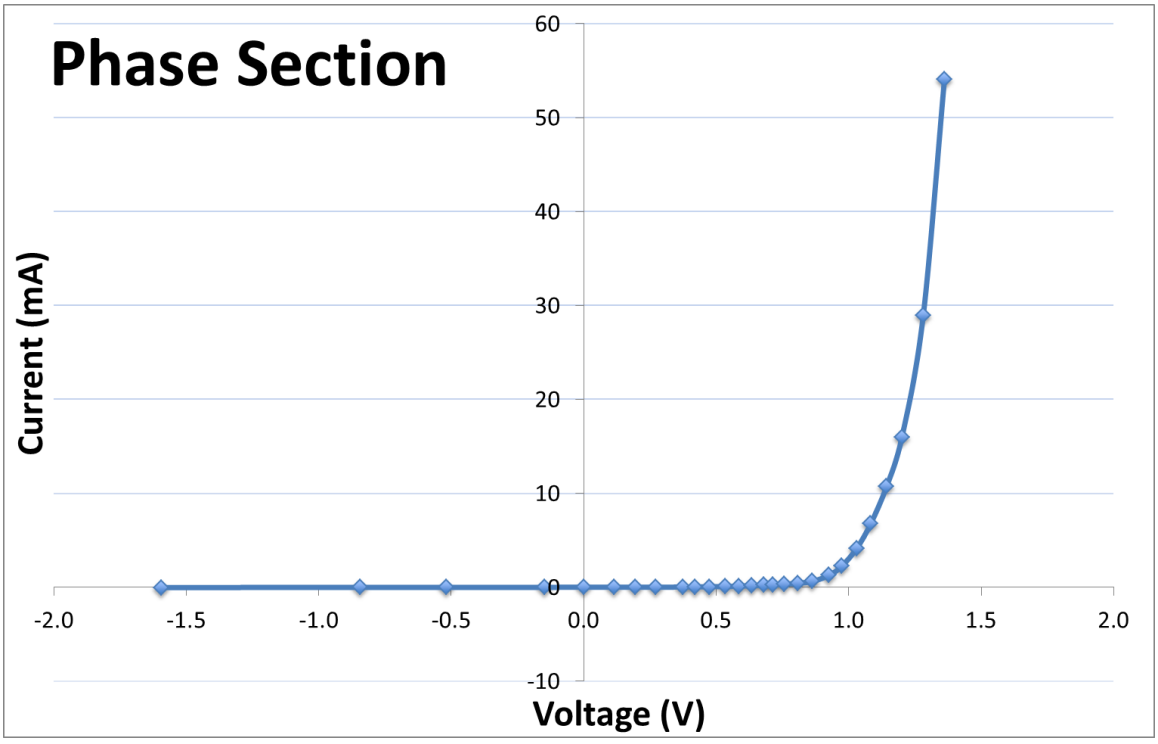

Figure 35 - I-V curve of the Neptune VT-DBR laser's phase section.

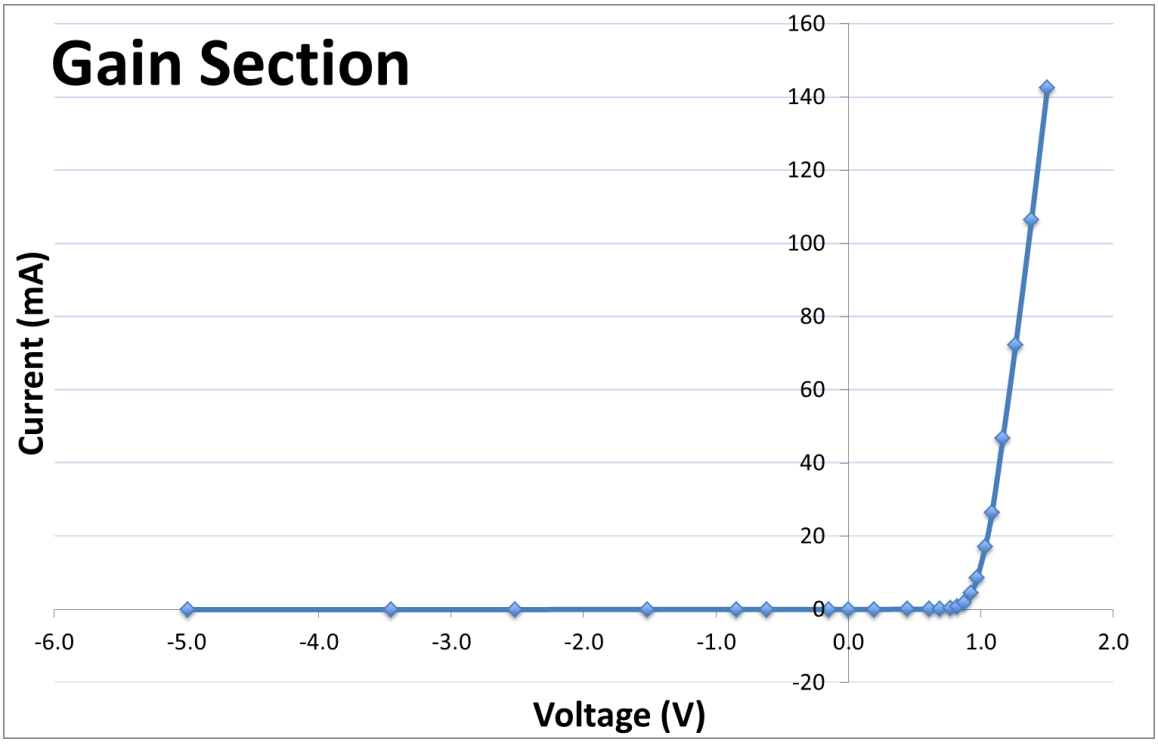

Figure 36 - I-V curve of the Neptune VT-DBR laser's gain section.

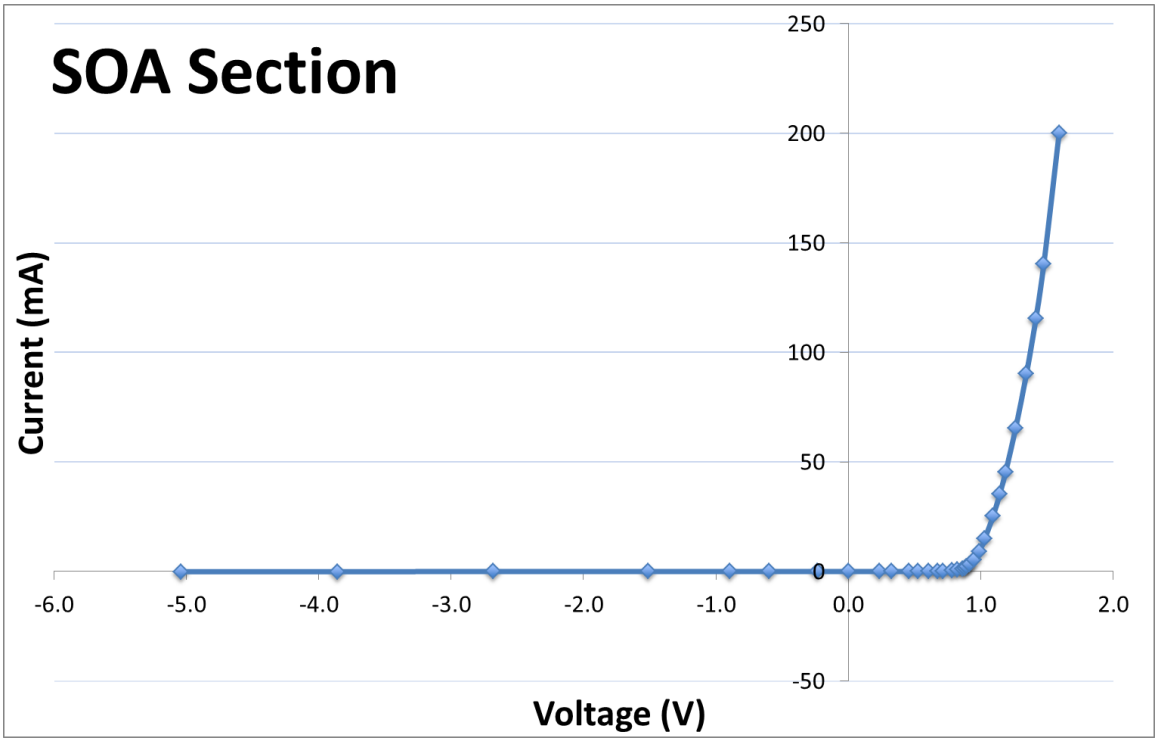

Figure 37 - I-V curve of the Neptune VT-DBR laser's SOA section.

The dynamic resistance calculations from the TDR measurements of the Neptune laser ranged from 2.9 kΩ down to 0 Ω, but the zero calculations are not accurate and a product of the result of slight measurement system inaccuracies; however, I believe the actual dynamic resistance is very close to 0 Ω in the aforementioned cases.

Figure 38 is an example TDR measurement of the Neptune laser's FM port with a 10.1 mA bias. The response time is measured to be approximately 0.45 ns. The dynamic resistance calculation for the rho value of -0.8149 measured is approximately 2.9 Ω and shown following the figure.

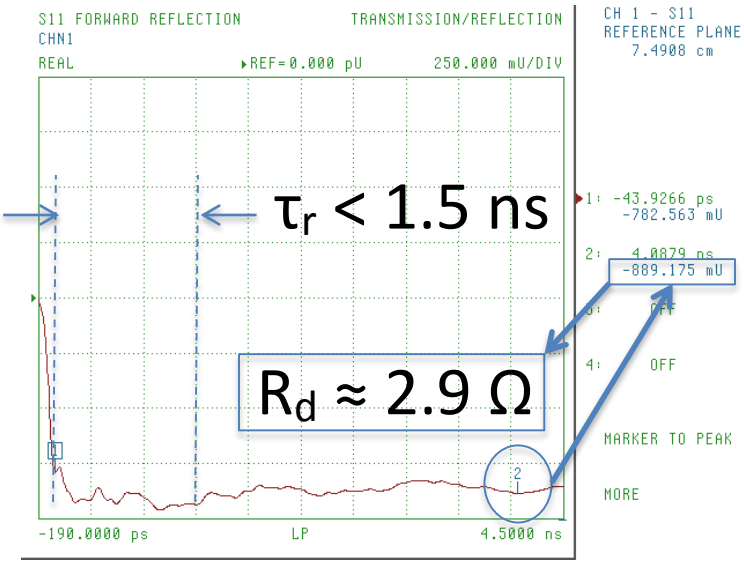

Figure 38 - TDR measurement of the Neptune laser's FM section with a 10.1 mA current bias.

$$R_d = 50\frac{(1+(-0.8892)}{(1-(-0.8892))} \approx 2.9\ \Omega$$

An example FDR measurement of the Neptune laser's FM section at a 100 mA bias is shown in Figure 39 below; this bias condition yielded the largest

positive reactance measurement (i.e. - 0.063 Ω) for this PUT. The lead inductance is then estimated using equation (2) with f = 10 MHz.

$$\boldsymbol{L_{lead} = \frac{0.1}{2\pi(10,000,000)} \approx 1.6\,nH}$$

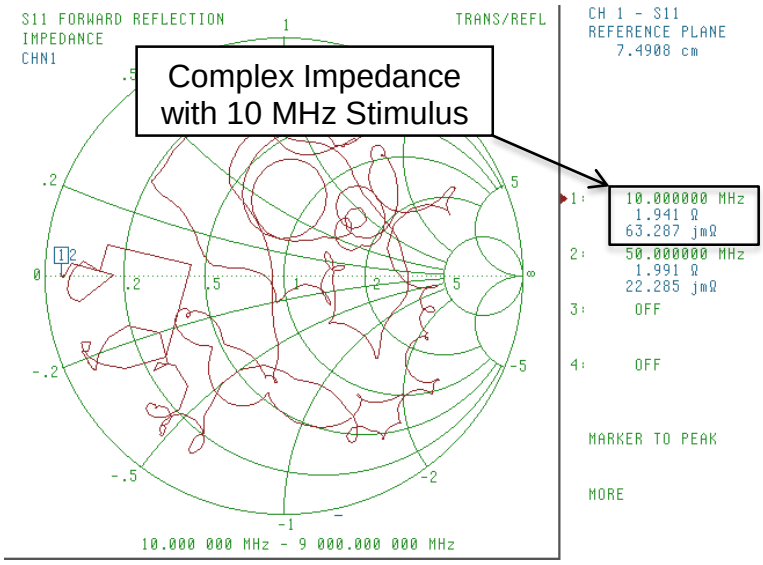

Figure 39 - FDR measurement of the Neptune laser's FM with a 100 mA current bias. A complex impedance of 1.941 + 0.0633j is observed.

The capacitive reactance is estimated using equation (3).

$$\boldsymbol{X_C = 0.06329 - 0.1 \approx\ -0.037\,\Omega}$$

Next, the susceptance of the effective capacitance is estimated with equation (4).

$$\boldsymbol{B = \frac{-X_C}{|Z|^{-2}} = \frac{-(-0.037)}{1.941^{-2} + 0.037^{-2}} \approx 0.009817\,\Omega^{-1}}$$

Then, the effective capacitance is calculated with equation (5).

$$C_{eff} = \frac{0.009817}{2\pi(10,000,000)} \approx 156\,pF$$

Finally, the response time for this bias condition is calculated using equation (6).

$$\tau_s = RC_{eff} \approx 1.87 * 156E^{-12} \approx 0.29\,ns$$

The above RLC calculations are performed for every bias condition of each PUT and presented in appendix B. Figure 40 plots the bias dependent response times of each Neptune laser section.

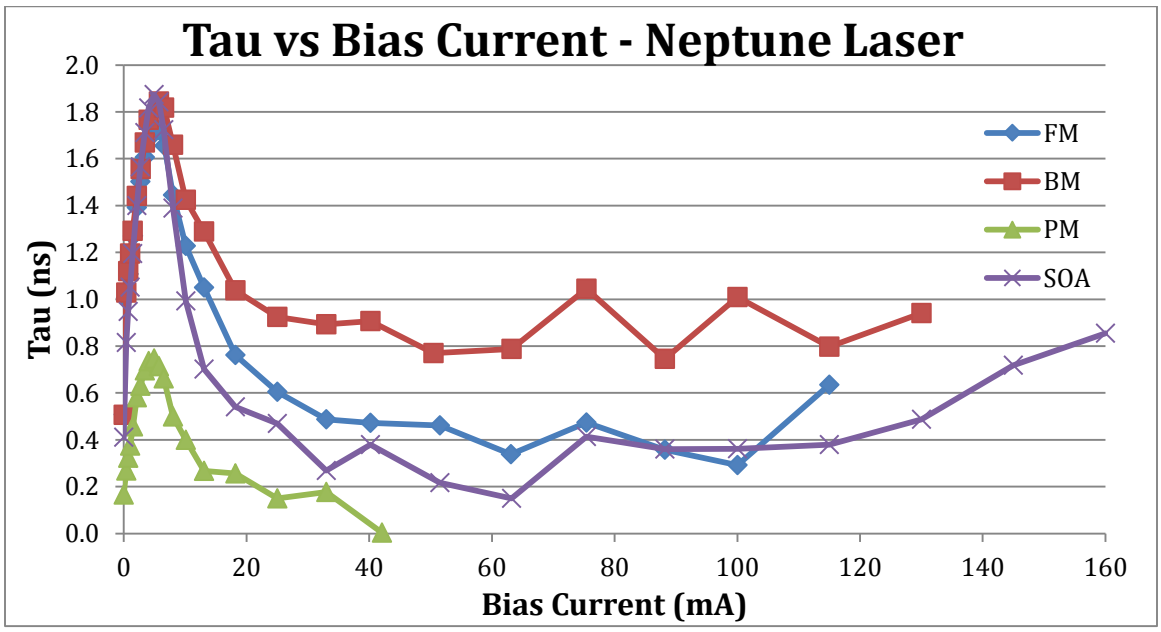

Figure 40 - Neptune laser's response times versus bias current for each PUT.

Figure 41 is a picture of the Neptune laser's wavelength tuning map with FM and BM currents ranging from 0 to 100 mA at an increment of 1 mA along each

tuning axis. A tunable range of 37 nm is observed, from 1272 nm to 1309 nm. This data-set represents the largest tuning map area measured from the Neptune laser and contains 10,201 data-points collected over a week period. The image is produced by taking a screen capture of the surface-plot figure generated by the "TuningMapper()" function after the desired viewpoint is set. The view of the surface is manipulated by simultaneously clicking and dragging the plot surface and using the zoom tool to achieve the desired view.

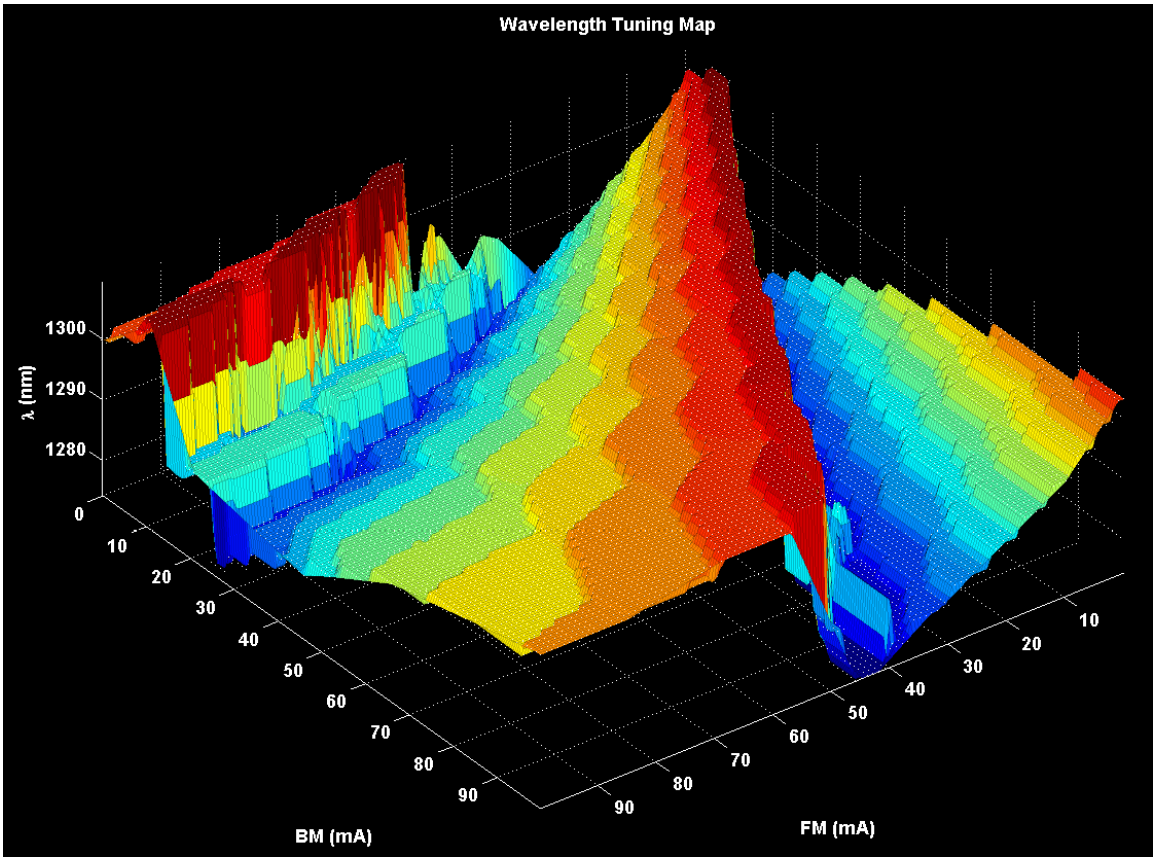

Figure 41 - Wavelength tuning map of the Neptune laser. This data-set represents the largest tuning area measured from the Neptune laser; BM and FM are biased from 0 to 100 mA at an increment of 1 mA along each tuning axis. Wavelengths range from 1272 nm (blue) to 1309 nm (red) in a tuning range of ~37 nm.

The FM current, BM current, and dominant mode wavelength respectively define the X, Y, and Z position on the tuning map. The surface is also color coded to reflect the wavelength at a given point.

Figure 42 presents the power tuning map corresponding to the same data-set as Figure 41 above. Again, the color of the surface corresponds to the magnitude of the power making surface gradients more pronounced.

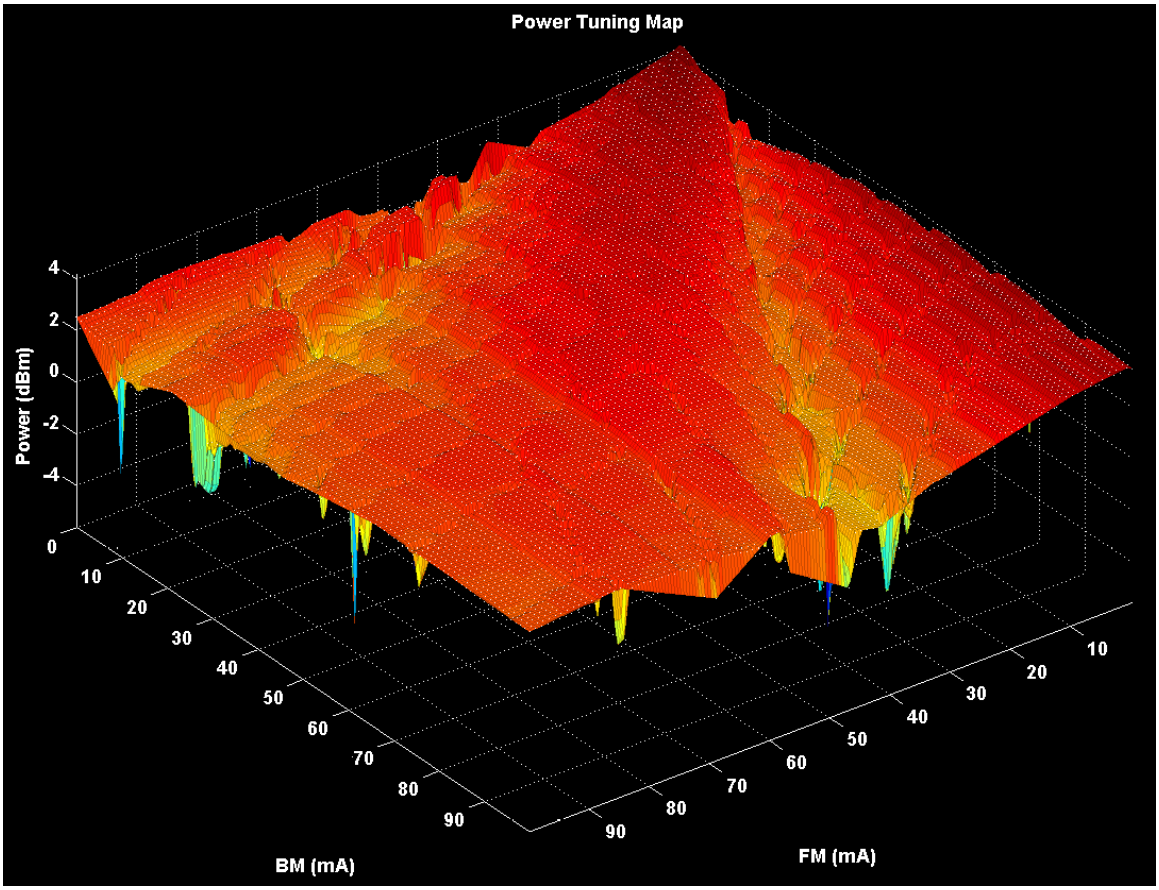

Figure 42 - Power tuning map of the Neptune laser. Data measurement points correspond to the same points used to generate the wavelength tuning map (i.e. - identical tuning current start, stop, and step values as the wavelength tuning-map data). Measured powers at stable operating points range from 1.2-4.0 dBm.

Next, a small area from the large tuning map above is measured a second time at a higher resolution to capture more detail in the tuning surface. This data-

set is collected in the range of 45 to 55 mA in both FM and BM sections at a resolution of 200 µA along each tuning axis.

With the improved surface detail, a small wavelength variation on an otherwise flat tuning surface was identified around the data-point corresponding to a 51.786 mA bias in the FM and a 50.386 mA bias in the BM. Figure 43 shows a picture of the anomaly marked with a data-cursor.

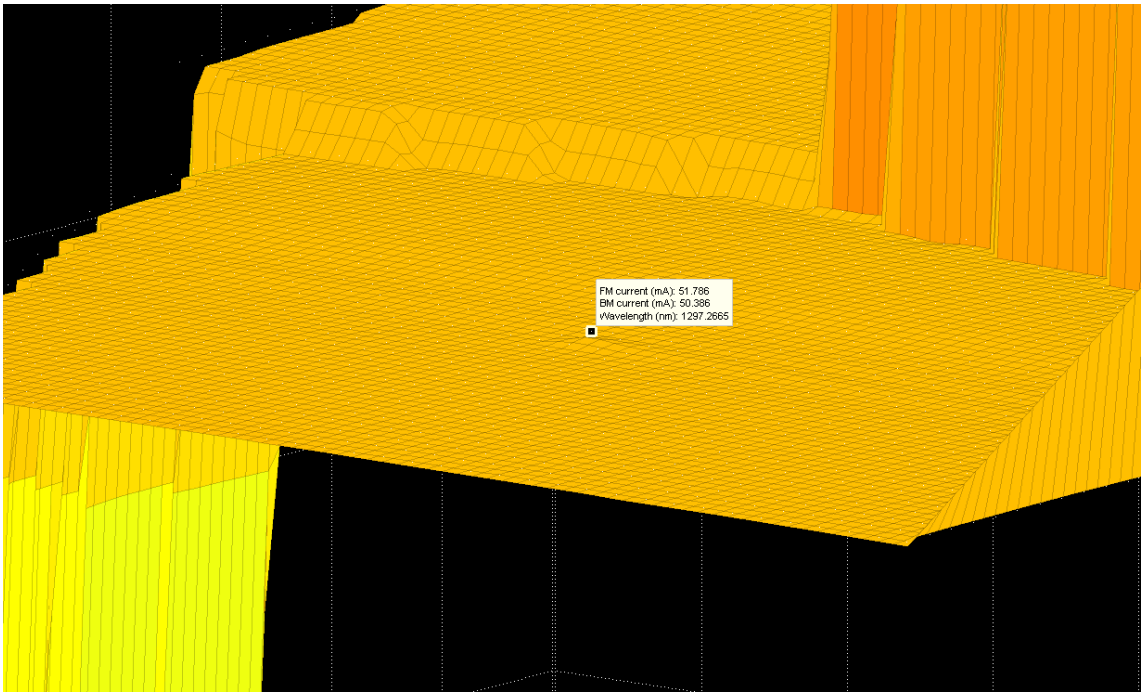

Figure 43 - Wavelength tuning map anomaly marked with a data-cursor. The anomaly is positioned at an FM bias of 51.786 mA and a BM bias of 50.386 mA with a peak output wavelength of 1297.3 nm.

In Figure 44, the anomaly is further investigated by collecting another data-set with even greater detail; this is achieved by reducing the surface spanned in the measurement and increasing the resolution to 50 µV between data-points along each tuning axis.

Significantly more detail is captured in this plot; the surface appears very rippled, but these small deviations are all less than 3 pm and might be caused by performance limitations (i.e. - temperature fluctuations up to +/- 0.05 degrees Celsius) in the TEC controller or measurement device itself.

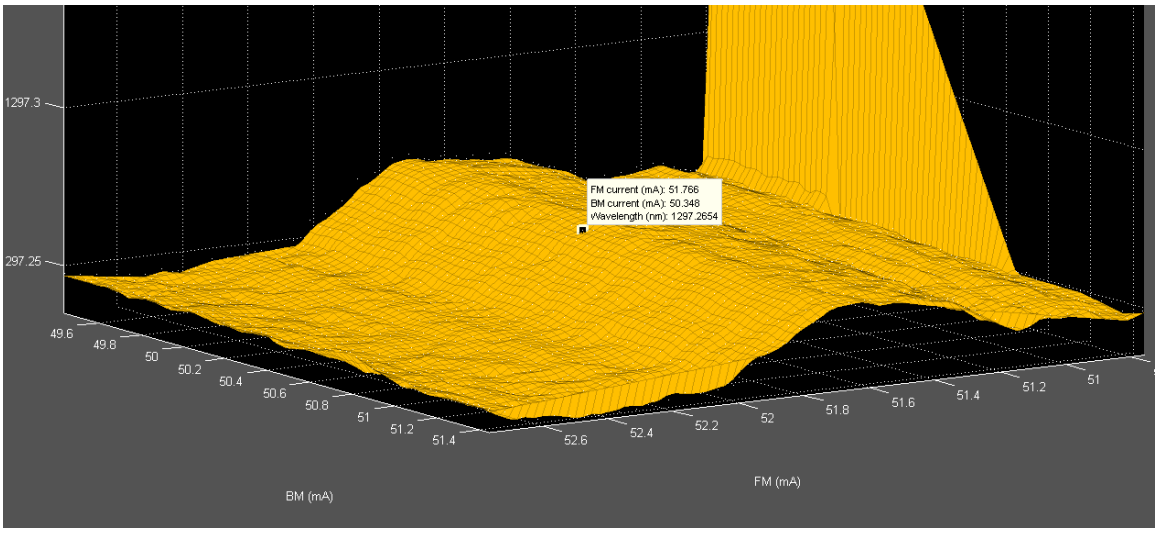

Figure 44 - Improved image of wavelength tuning map anomaly. Tuning map span is reduced to less than 2 mA along each tuning axis and the resolution is improved to 50 µA between data-points.

The larger ripple running parallel to the BM axis introduces a measured wavelength deviation of >15 pm; one might suspect its cause to be temperature fluctuations in the waveguide, but the fact it appears in two data-sets collected at different times makes that hypothesis far less likely. Anomalies of this size must be avoided to reduce points of non-linearity in a SS-OCT wavelength sweep.

I wrote the MatLab data-collection function such that data-points are gathered along the BM axis and sequenced along the entire BM range specified before iterating to the next FM current; therefore, I suspect fluctuations in environmental variables that affect the output wavelength (e.g. - cavity

stress/strain) will manifest similar anomalies that run along BM axis. However, I do not believe it to be the cause here.

A measure of the Neptune laser's SMSR is presented in Figure 45. The Gain and SOA sections are biased at 100 mA to initial lasing. The FM, BM, and phase sections are zero biased and an SMSR of greater than 43 dB is observed.

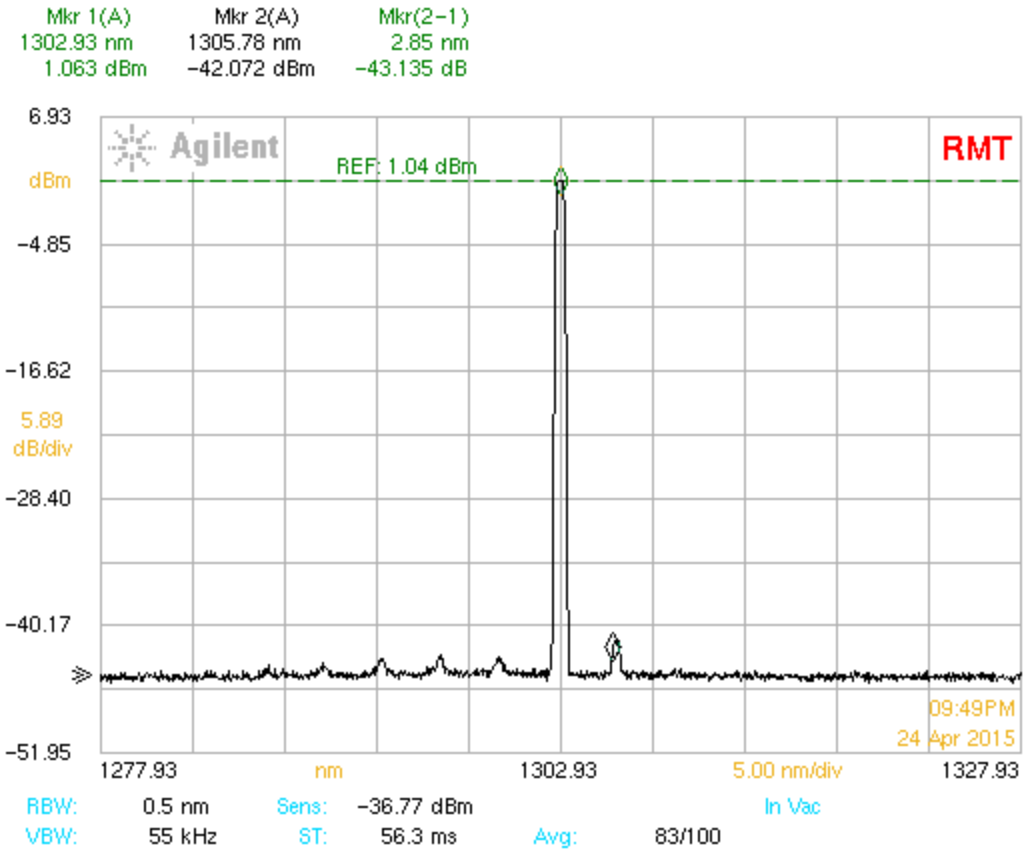

Figure 45 - Neptune laser's side mode suppression ratio (SMSR) measured with 100 mA bias in the Gain and SOA sections. FM, BM, and Phase sections are zero-biased for this measurement. An SMSR greater than 43 dB is observed.

In Table 2, all the SMSR measurements of the Neptune are presented. The spectrum of Figure 45 corresponds to measurement 1 below.

Table 2 - SMSR measurements of the Neptune laser. Gain and SOA sections are biased at 100 mA. Phase section is shorted.

Measurement	FM Bias (mA)	BM Bias (mA)	Wavelength (nm)	SMSR (dB)
1	0	0	1302.93	43.1
2	0	41.72	1291.13	42.2
3	38.42	41.72	1300.73	40.6
4	68.71	0	1306.03	38.7

OSA screen captures of all SMSR measurements can be found in appendix G.

Using the power and wavelength tuning maps, suitable measurement points are chosen from the middle of the wavelength tuning path and away from steep gradients on the power tuning map; this selection method ensures the stable, single-mode operation necessary accurate linewidth measurements.

Data cursors identified on the wavelength tuning map found in Figure 46 illustrate suitable measurement points; these bias conditions also represent plateaued regions on the power tuning map of the laser.

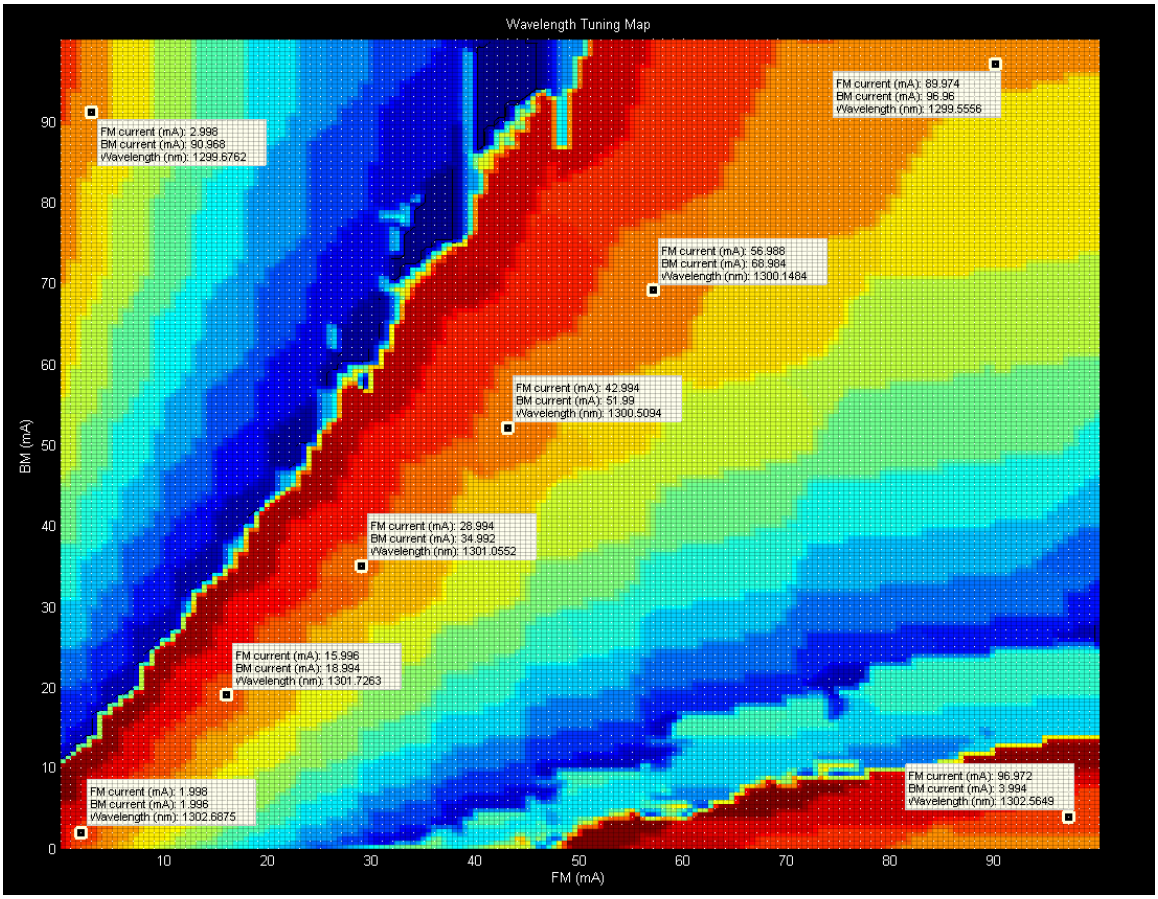

Figure 46 - Stable linewidth measurement points identifies by data-cursors on the Neptune's wavelength tuning map.

Figure 47 shows the Neptune's output spectrum and a corresponding linewidth measurement at a particular bias. For this measurement, the Gain and SOA sections are biased at 100 mA, FM and BM sections are biased at 2 mA, and phase section is shorted. Additional screen capture pairs of the Neptune's optical spectrum and linewidth are presented in appendix H.

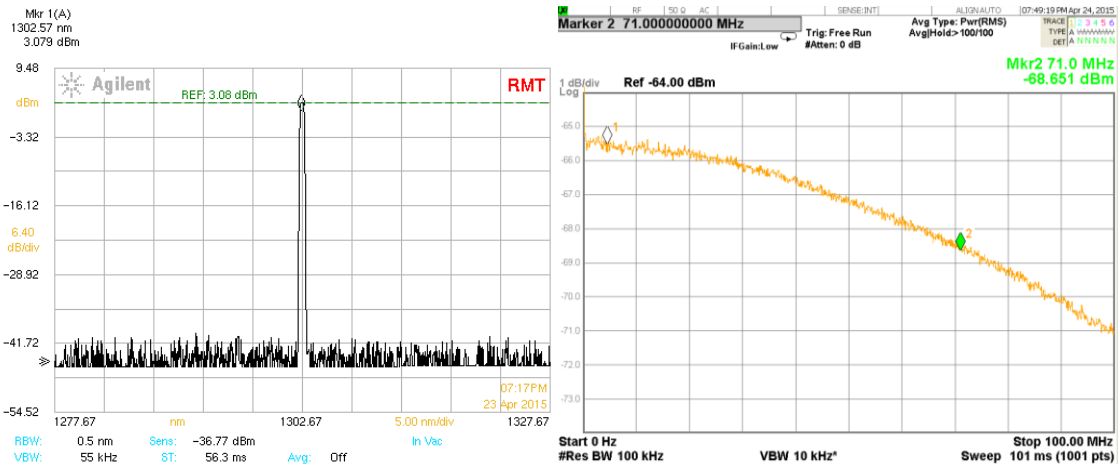

Figure 47 - Example of the Neptune laser spectrum (left) and linewidth (right). Gain and SOA biased at 100 mA, FM and BM biased at 2 mA, and phase section shorted.

The linewidth measurements corresponding to the points identified in Figure 46 are shown in **Table** 3. Linewidths from 40 to 108 MHz are observed.

Table 3 - Neptune laser linewidth measurements. Gain and SOA sections are biased at 100 mA. The phase section is shorted.

FM bias (mA)	BM bias (mA)	Wavelength (nm)	Δ*v* (MHz)
89.97	96.96	1299.56	48.7
76.98	85.01	1299.78	43.5
64.64	74.92	1299.98	67.3
56.99	68.98	1300.15	70.8
50.01	60.01	1300.33	86.4
42.99	51.99	1300.16	39.2
36.97	44.05	1300.78	78.0
28.94	34.99	1301.06	91.2
23.03	28.03	1301.33	101.9
16.00	18.99	1301.73	107.6
9.06	10.00	1302.03	49.9
2.00	2.00	1302.69	71.0
0.00	0.00	1305.01	9.1

Additional linewidth measurements of the Neptune laser are presented in Table 4 and Table 5. Measurements in Table 4 are made with the FM section zero-biased. Linewidths range from 4 to 28 MHz.

Table 4 - Neptune laser linewidth measurements. Gain and SOA sections are biased at 100 mA. The phase and FM sections are shorted.

BM bias (mA)	Wavelength (nm)	Δ*v* (MHz)
99.98	1302.88	7.3
89.98	1299.88	27.2
80.46	1299.98	11.9
70.00	1296.93	25.5
60.05	1296.98	4.8
50.13	1294.08	8.4
40.07	1291.18	6.8
30.59	1288.28	3.6
20.00	1282.53	16.8
10.20	1276.93	25.3
5.02	1308.88	27.7

Measurements in Table 5 are made with the BM section zero-biased. Linewidths range from 6 to 130 MHz. From the results, the FM current bias appears to be more influential on the spectral linewidth of the Neptune laser.

Table 5 - Neptune laser linewidth measurements. Gain and SOA sections are biased at 100 mA. The phase and BM sections are shorted.

FM bias (mA)	Wavelength (nm)	Δ*v* (MHz)
99.96	1299.66	18.6
90.05	1299.61	5.5
80.00	1302.76	39.9
68.04	1305.96	57.4
59.22	1306.06	40.6
51.21	1309.26	45.4
37.51	1282.96	79.3
31.85	1277.66	134.2
19.71	1286.71	104.6
10.11	1293.16	120.7
6.02	1296.41	130.0

6. VTL-2 VT-DBR LASER CHARACTERIZATION

The following I-V graphs were collected from the VTL-2 laser. As with the Neptune's I-V curve data, accuracy is improved by collecting more data points in the non-linear region of operation.

When compared to those of the Neptune laser, the I-V curves of the VTL-2 have dramatically smaller slopes at biases above the knee-in current. The subsequent difference in dynamic resistance is confirmed by comparing the TDR measurements of each in appendices B and C. These results further validate the TDR measurements taken from each laser. I suspect the physical difference in the structures and material systems of each laser section are the dominant cause for these discrepancies.

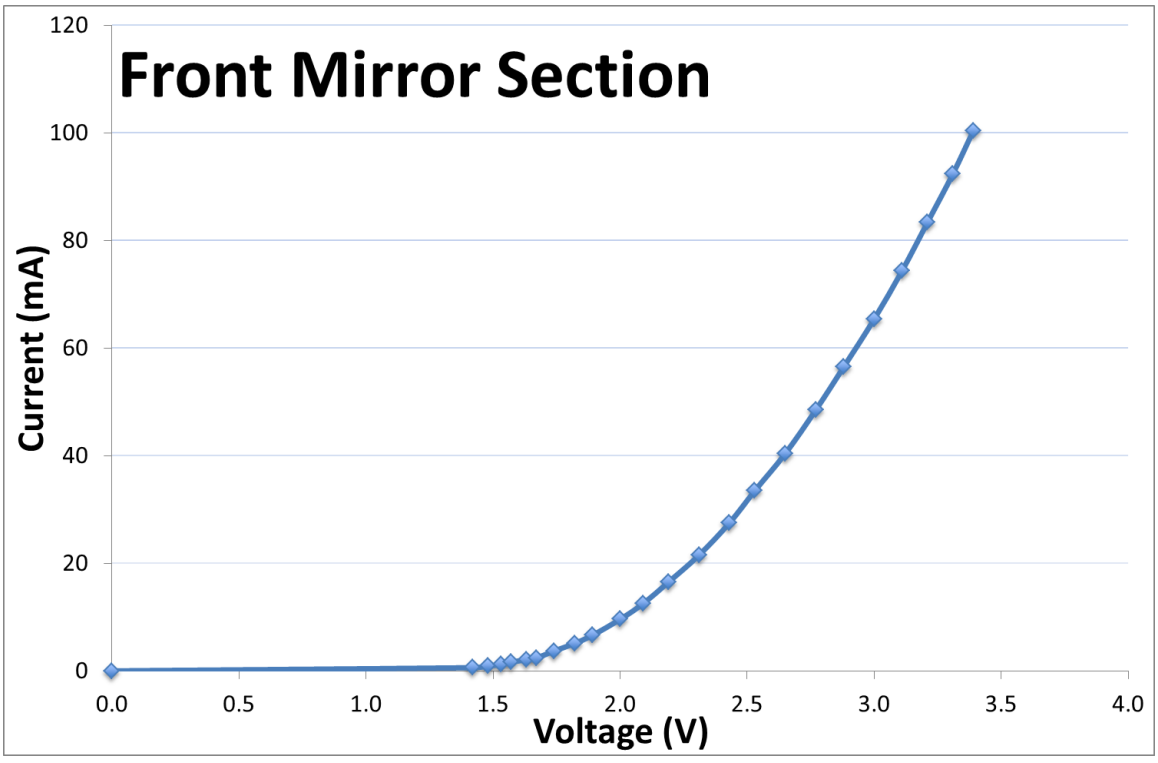

Figure 48 - I-V curve of the VTL-2 VT-DBR laser's front-mirror section.

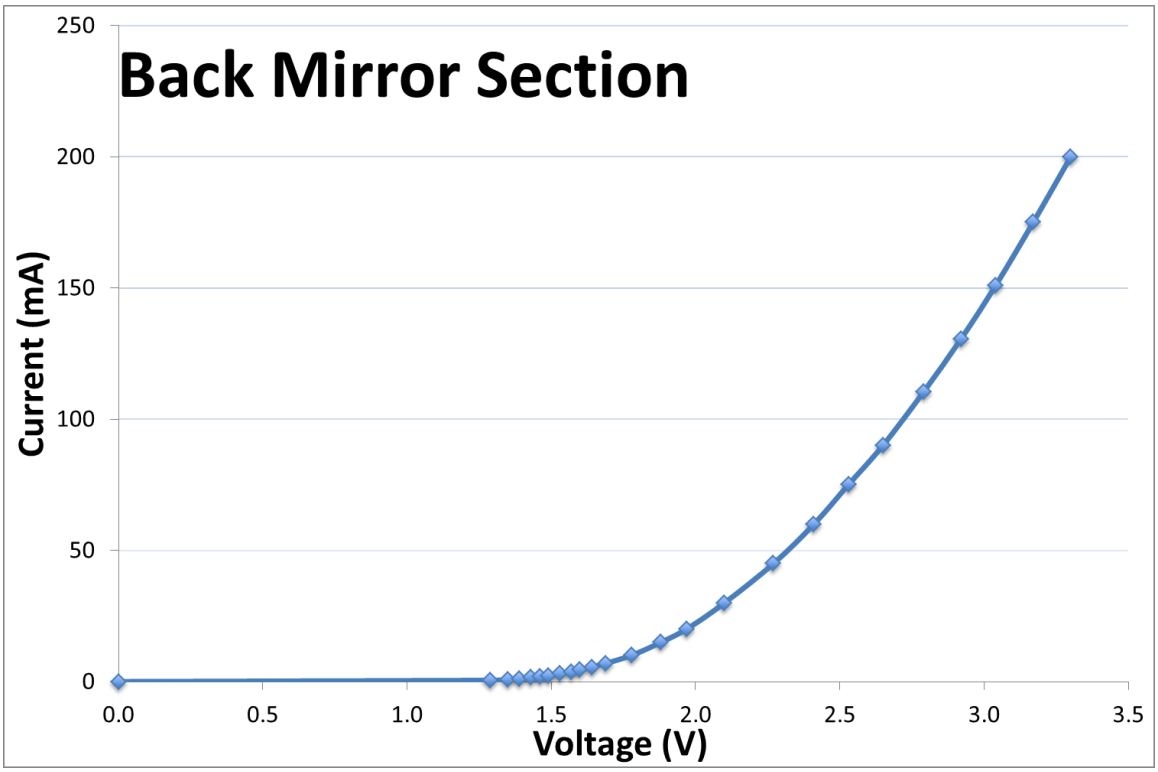

Figure 49 - I-V curve of the VTL-2 VT-DBR laser's back-mirror section.

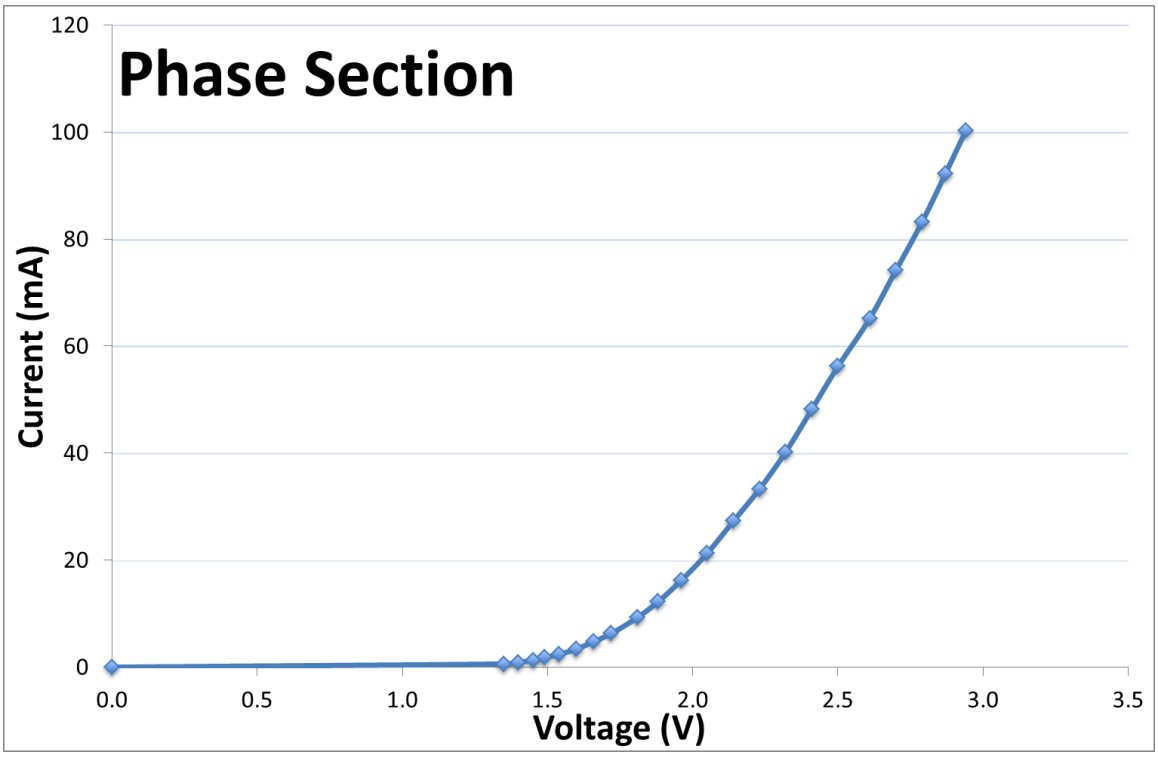

Figure 50 - I-V curve of the VTL-2 VT-DBR laser's phase section.

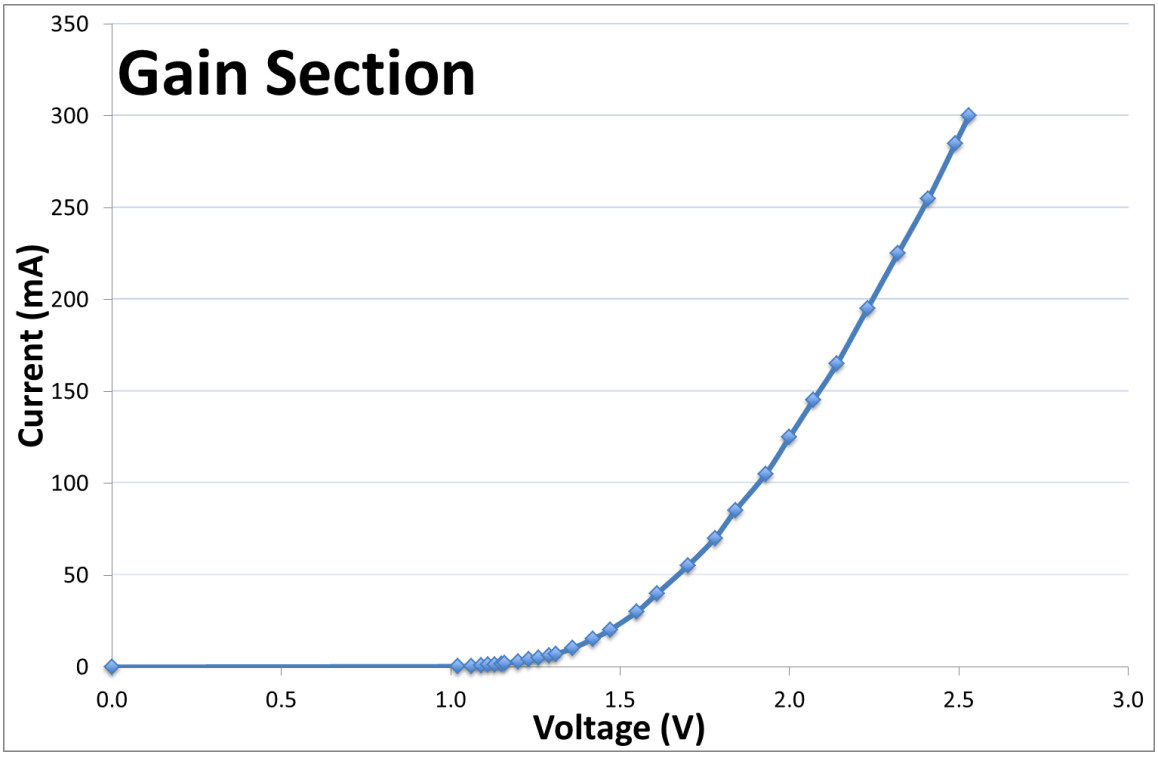

Figure 51 - I-V curve of the VTL-2 VT-DBR laser's gain section.

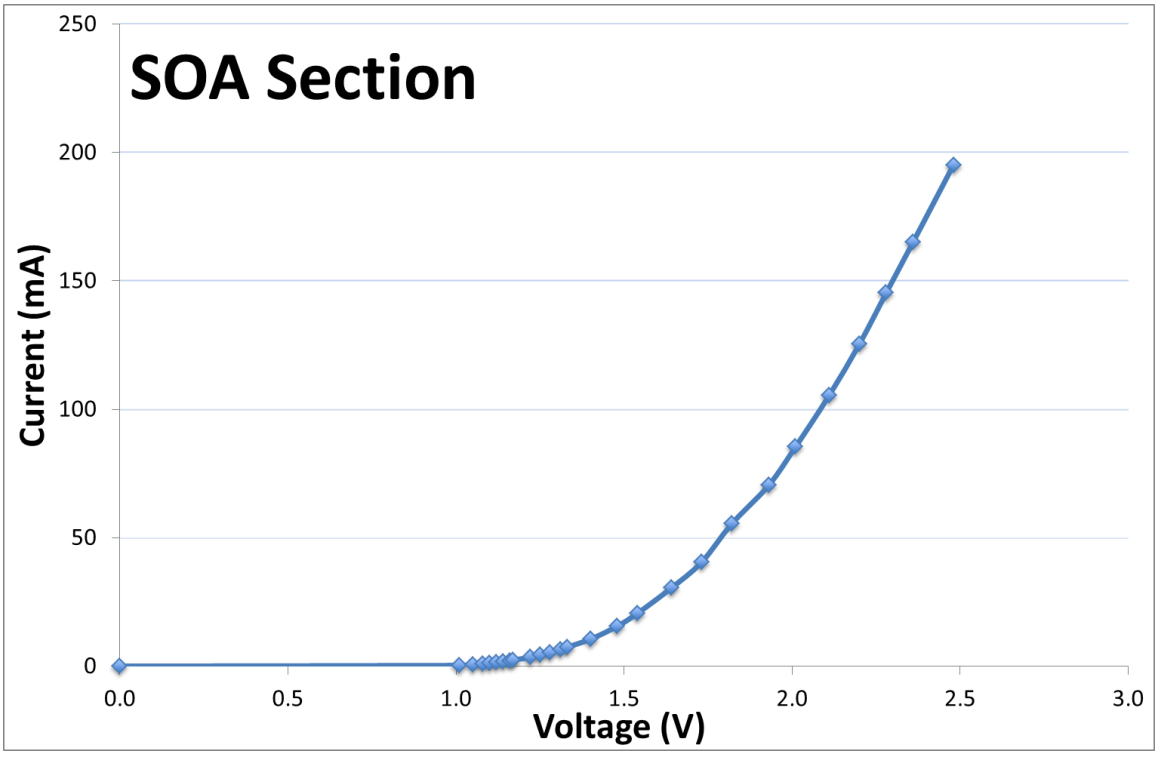

Figure 52 - I-V curve of the VTL-2 VT-DBR laser's SOA section.

Figure 53 is an example TDR measurement of the VTL-2 laser's BM port with a 10.1 mA bias. The response time is measured to be approximately 0.7 ns. The dynamic resistance calculation for the rho value of -0.3220 measured is approximately 25.6 Ω and shown following the figure.

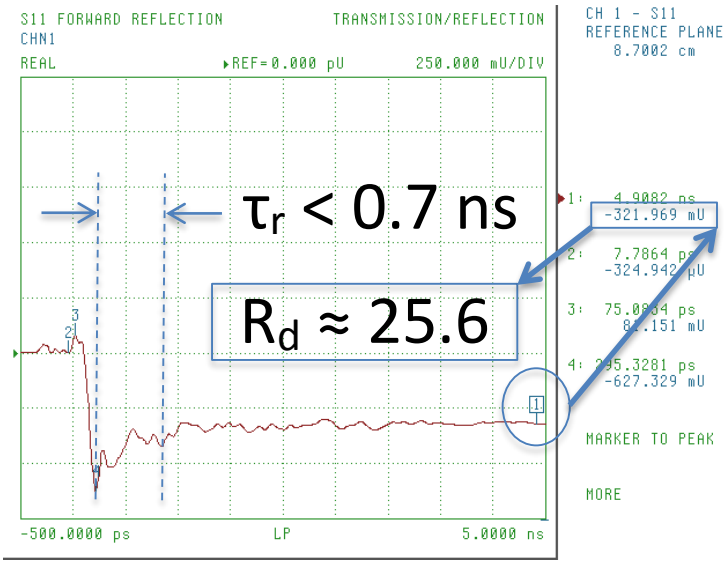

Figure 53 - TDR measurement of the VTL-2 laser's BM section with a 10.1 mA current bias.

$$R_d = 50\,\frac{(1+(-0.3220)}{(1-(-0.3220))} \approx 25.6\,\Omega$$

An example FDR measurement of the VTL-2 laser's BM section at a 90.1 mA bias is shown in Figure 54 below; this bias condition yields the largest positive reactance (i.e. - 0.063 Ω) for this PUT. The lead inductance is then estimated using equation (2) where f = 10 MHz.

$$L_{lead} = \frac{1.0}{2\pi(10,000,000)} \approx 16\,nH$$

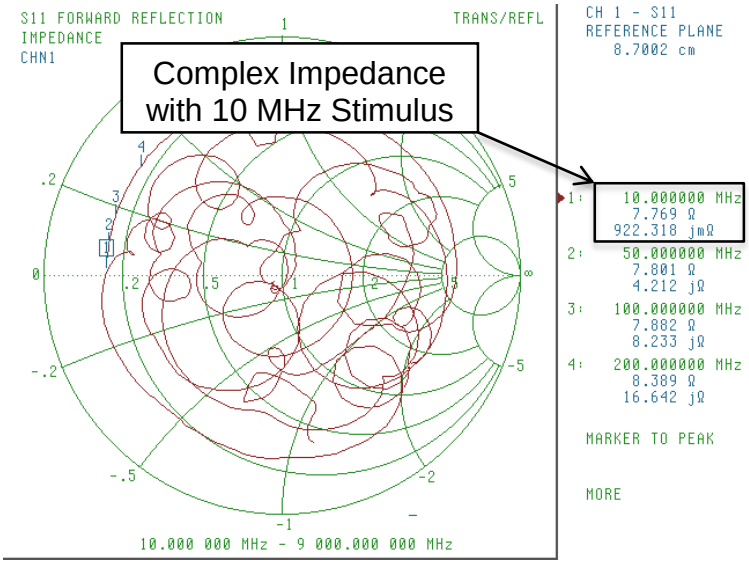

Figure 54 - FDR measurement of the VTL-2 laser's BM with a 90.1 mA current bias. A complex impedance of 7.769 + 0.9223j is observed.

The capacitive reactance is estimated using equation (3).

$$\boldsymbol{X_C = 0.922 - 1 \approx \ -0.078\ \Omega}$$

Next, the susceptance of the effective capacitance is estimated with equation (4).

$$\boldsymbol{B = \frac{-X_C}{|Z|^{-2}} = \frac{-(-0.078)}{7.769^{-2} + 0.078^{-2}} \approx 0.001292\ \Omega^{-1}}$$

Then, the effective capacitance is calculated with equation (5).

$$\boldsymbol{C_{eff} = \frac{0.001292}{2\pi(10,000,000)} \approx 20.6\ pF}$$

Finally, the response time for this bias condition is calculated using equation (6).

$$\tau_s = RC_{eff} \approx 6.72 * 20.6E^{-12} \approx 0.14\,ns$$

The above RLC calculations are performed for every bias condition of each PUT and presented in appendix C.

A measure of the VTL-2 laser's SMSR is presented in Figure 45. The Gain and SOA sections are biased at 100 mA to initial lasing. The FM, BM, and phase sections are zero biased and an SMSR of greater than 33 dB is observed.

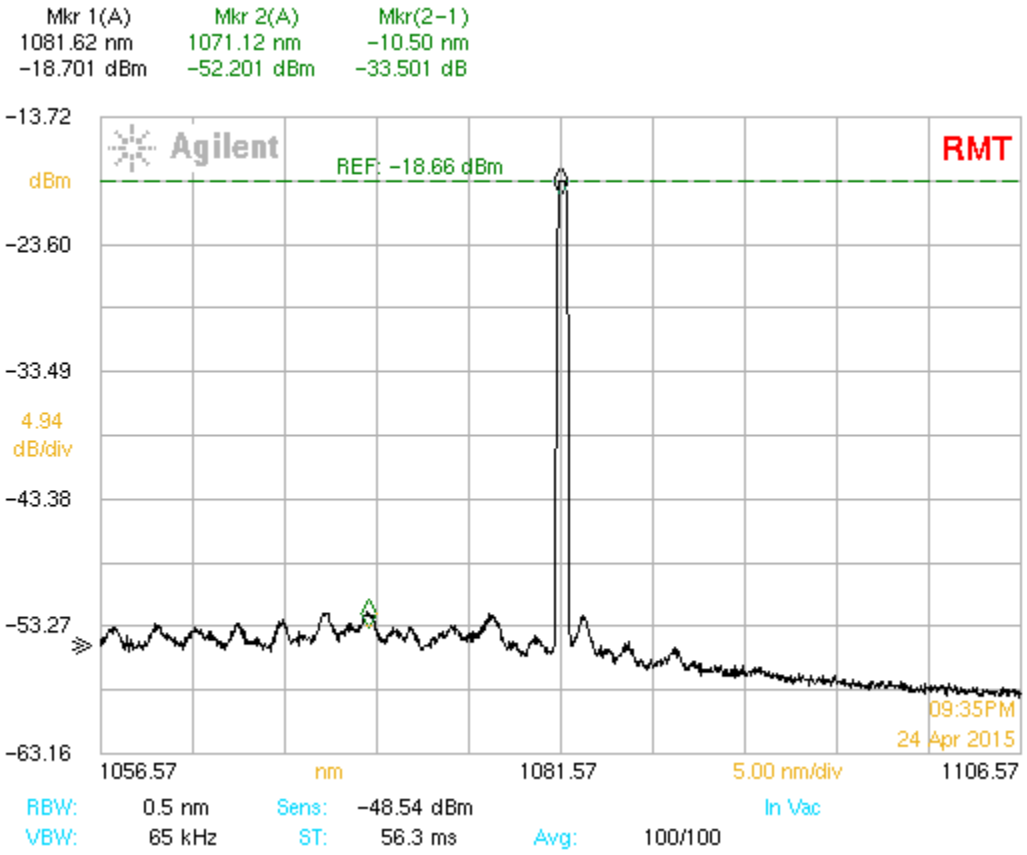

Figure 55 - VTL-2 laser's side mode suppression ratio (SMSR) measured with 100 mA bias in the Gain and SOA sections. FM is biased at 40.4 mA, BM is zero biased, and the phase section is shorted. A SMSR greater than 43 dB is observed.

In Table 6, all the SMSR measurements for the VTL-2 are presented. The spectrum of Figure 55 corresponds to measurement 3 below.

Table 6 - SMSR measurements of the VTL-2 laser. Gain and SOA sections are biased at 100 mA. Phase section is shorted.

Measurement	FM Bias (mA)	BM Bias (mA)	Wavelength (nm)	SMSR (dB)
1	0	40.95	1067.17	32.9
2	40.39	94.68	1074.57	30.3
3	40.38	0	1081.57	33.5

OSA screen captures for each SMSR measurement can be found in appendix I.

Figure 56 shows the VTL-2's output spectrum and a corresponding linewidth measurement at a particular bias. For this measurement, the Gain and SOA sections are biased at 100 mA, the FM and BM sections are biased at 79 mA, and the phase section is shorted. Additional OSA and linewidth measurement screen capture pairs are presented in appendix J.

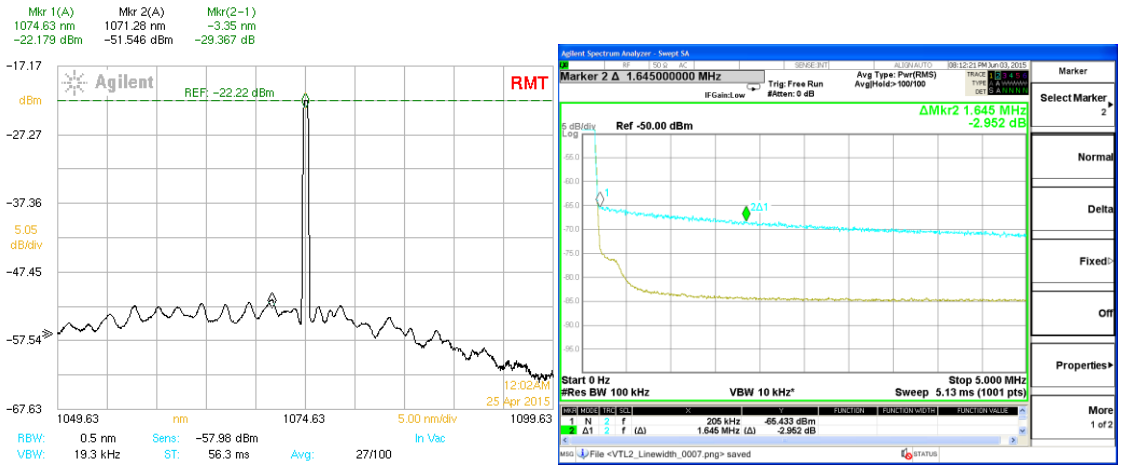

Figure 56 - Example of the VTL-2 laser spectrum (left) and linewidth (right). Gain and SOA biased at 100 mA, FM and BM biased at 79 mA, and phase section shorted.

In Table 7 below, VTL-2 linewidth measurements ranging from 300 kHz to 2 MHz are shown.

Table 7 - VTL-2 laser linewidth measurements. Gain and SOA sections are biased at 100 mA. The phase section is shorted.

FM bias (mA)	BM bias (mA)	Wavelength (nm)	Δ*v* (MHz)
0	0	1079.60	0.5
21.91	0	1084.18	0.7
40.05	0	1081.68	1.9
80.04	0	1081.63	0.9
0	26.30	1064.88	0.5
0	40.21	1067.13	0.4
0	81.29	1069.53	0.3
79.18	79.06	1074.63	1.9

The VTL-2 laser achieves dramatically better linewidths than the Neptune laser. Again, I suspect this is inherent to the internal cavity structure and material system that comprises its sections.

7. SUMMARY OF RESULTS

In summary, the Neptune and VTL-2 both display electrical and spectral performance that exceeds the SS-OCT requirements listed in Table 1. The dynamic resistance, effective capacitance, and lead inductance that make up the circuit modeling each section permit extremely fast transitions times that facilitate the VT-DBR's performance advantage over alternative swept-sources.

Maximum response times for each section of the Neptune laser are presented in Table 8.

Table 8 - Maximum response time for each section of the Neptune VT-DBR laser.

Section	Bias (mA)	L_{lead} (nH)	R_d (Ω)	C_{eff} (pF)	τ_{RC} (ns)
FM	4.92	1.6	35	85	1.7
BM	5.74	0.2	26	109	1.8
Phase	4.93	1.6	40	33	0.7
Gain	4.9	16	31	102	2.0
SOA	4.92	4.8	32	96	1.9

Maximum response times for each section of the VTL-2 laser are presented in Table 9.

Table 9 - Maximum response time for each section of the VTL-2 VT-DBR laser.

Section	Bias (mA)	L_{lead} (nH)	R_d (Ω)	C_{eff} (pF)	τ_{RC} (ns)
FM	0.6	30	247	28	1.2
BM	1.1	16	138	46	1.7
Phase	0.9	29	159	42	1.6
Gain	1.5	32	105	68	2.3
SOA	1.2	30	122	61	2.2

The Neptune's maximum response-time is lower, on average; however, the VTL-2 is notably faster when comparing the two across their tuning ranges.

Measured I-V curves of each device helped to validate the dynamic resistance calculations from the TDR response data and report the section voltage of each section under bias so the drive circuitry can be designed according to these specifications.

The tuning maps collected from the Neptune helped identify the optimal tuning path of the laser and revealed anomalies in the tuning surface that should be avoided to minimize the invalid data-points associated with a SS-OCT sweep. Additionally, the maps aided the selection of relevant linewidth measurement points by showing where stable modes of operation in the tuning path could be achieved.

The side mode suppression ratio of the Neptune is typical of tunable DBR lasers with an average SMSR > 41 dB. The SMSR of the VTL-2 is significantly less than that of the Neptune at an average SMSR just above 32 dB. The SMSRs of both lasers are well above the 25 dB value listed in Table 1. This additional spectral discrimination results in improved OCT image quality.

The Neptune laser's measured linewidth did not exceed 130 MHz and its average measure was 51.6 MHz which corresponds to an average coherence length of 1.85 meters. The VTL-2 linewidths were substantially lower, with a maximum of 1.9 MHz and an average of only 900 kHz; this ridiculously low linewidth, comparable to those found in mode-locked lasers, affords the VTL-2 an average coherence length of 106 meters. The linewidths of both lasers make them great swept-sources for OCT, but the exceptionally long coherence length of the VTL-2 make it an ideal solution for a number of other applications that

require a longer coherence length (e.g. - remote sensing, seismology, and topography contour mapping).

In conclusion, both lasers exhibit superb performance characteristics that validate them as excellent light sources for use in SS-OCT. Their superior performance, robust set of applications, and predictably low cost at increased economies of scale make VT-DBR lasers the tunable light sources of the future.

8. FUTURE WORK

In following my work, a future scholar might use the TDR, FDR, and RLC data I have collected to develop an improved circuit model of each laser section. The bias dependent circuit models I have used to estimate the VT-DBR laser's response times are valid at discrete bias points; by attempting to produce a mathematical model that describes the electrical characteristics of each laser section continuously with respect to their bias current, the tuning limitations of the VT-DBR lasers can be better understood and analyzed; from this, design changes that improve tuning response time and accuracy may become evident.

The development of an automated linewidth/SMSR collection system would also be a great contribution to the advancement of these lasers; because their values dramatically impact OCT image quality and fluctuate across the tuning range of the device, it is desirable to have a more continuous understanding of these performance parameters.

A measure of the amplitude deviation in the output wavelength or relative intensity noise (RIN) is also desirable.

Another useful measurement involves lasing at a stable mode and driving the gain/SOA section of the laser with a swept sinusoid; at some increased frequency, the optical output power of the laser is reduced by half due to the bandwidth limitations of the section; this important -3 dB measurement identifies the speed at which the laser's power can be modulated.

Similar to the amplitude modulations measurement above, frequency modulation limitations of the laser's output are also very important. By applying a

swept sinusoid to each tuning section of the laser and measuring the reduction on the tuning span as a function of tuning signal frequency, the bandwidth of each tuning port can be calculated and used to estimate sweep speed limits.

Practical demonstrations of these lasers, like those performed with earlier VT-DBR designs, are huge steps towards validating the niche of each and bringing them to market. Given the promising future of the VT-DBR design, even a crude demonstration would be a significant contribution toward the advancement of photonics.

Relative intensity noise (RIN) measurements of the optical output are also very important. Although difficult to measure over the finite noise in the driving source, this measure is particularly important to fiber-optic communications and remote-sensing.

I hope my MatLab functions will be used by future graduate students to aid their research and inspire their curiosity in these fascinating devices. The tuning maps they produce aid the development of a fundamental knowledge in the operation of VT-DBRs and present a useful tool to better understanding them.

BIBLIOGRAPHY

[1] P.P. Sorokin and J.R. Lankard, "Stimulated Emission Observed from an Organic Dye, Chloro-aluminum Phthalocyanine," *IBM Journal of Research and Development*, vol. 10, no. 2, pp. 162-163, March 1966.

[2] Leslie Wright. (2015, May) www.fineartradiography.com. [Online]. http://www.fineartradiography.com/hobbies/lasers/dye/

[3] F.J. Duarte and L.W. Hillman, "Narrow-linewidth Pulsed Dye Laser Oscillators," in *Dye Laser Principles: With Applications*. San Diego, United States: Academic Press, Inc., 1990, ch. 4, pp. 134-170.

[4] Dennis Derickson et al., "SGDBR single-chip wavelength tunable lasers for swept source OCT," in *SPIE Digital Library*, San Jose, 2008.

[5] Michael P Minneman, Jason Ensher, Michael Crawford, and Dennis Derickson, "All-Semiconductor High-Speed Akinetic Swept-Source for OCT," *SPIE-OSA-IEEE Asia Communications and Photonics*, vol. 8311, 2011.

[6] M. Bonesi et al., "Akenetic all-semiconductor programmable swept-source at 1550 nm and 1310 nm with centimeter coherence length," *OSA - Optics Express*, vol. 22, no. 3, Jan 2014.

[7] Helena Jelinkova, *Lasers for Medical Applications: Diagnostics, Therapy and Surgery*, 1st ed., Helena Jelinkova, Ed. Philadelphia, USA: Woodhead , 2013.

[8] Wolfgang Drexler, "Where is retinal optical coherence tomography

heading?," *SPIE Newsroom*, vol. 10.1117/2.1200903.1584, 2009.

[9] Paulo Stanga. (2015, April) YouTube.com. [Online]. https://www.youtube.com/watch?v=r-PerZ7Vg6I

[10] James Strong. (2015, April) Ophthalmic Photographers' Society - Eye Imaging Experts. [Online]. http://www.opsweb.org/?page=RetinalOCT

[11] S.M.R. Motaghian Nezam, "High-speed polygon-scanner-based wavelength-swept laser source in the telescope-less configuration with applications in optical coherence tomography," *Optics Letters*, vol. 33, no. 15, August 2008.

[12] Santec Inc. (2015, May) Santec.com. [Online]. http://www.santec.com/en/products/oct/hsl-11002100

[13] Santec Inc. (2015, May) Santec.com. [Online]. http://www.santec.com/en/products/oct/hsl-1020

[14] Thorlabs Inc.. (2015, May) Thorlabs.com. [Online]. http://www.thorlabs.us/newgrouppage9.cfm?objectgroup_id=6473

[15] Desmond Talkington, "Characterization and Modeling of an O-Band 1310 nm Sampled-Grating Distributed Bragg Reflector (SG-DBR) Laser for Optical Coherence Tomography (OCT) Applications," California Polytechnic State University, San Luis Obispo, Thesis 2013.

[16] Dennis Derickson, *Fiber Optic Test and Measurement*, 1st ed., Dennis Derickson, Ed. Upper Saddle River, United States of America: Printice-Hall Inc., 1998.

APPENDICES

Appendix A: Butterfly Laser Package Pinout Diagram

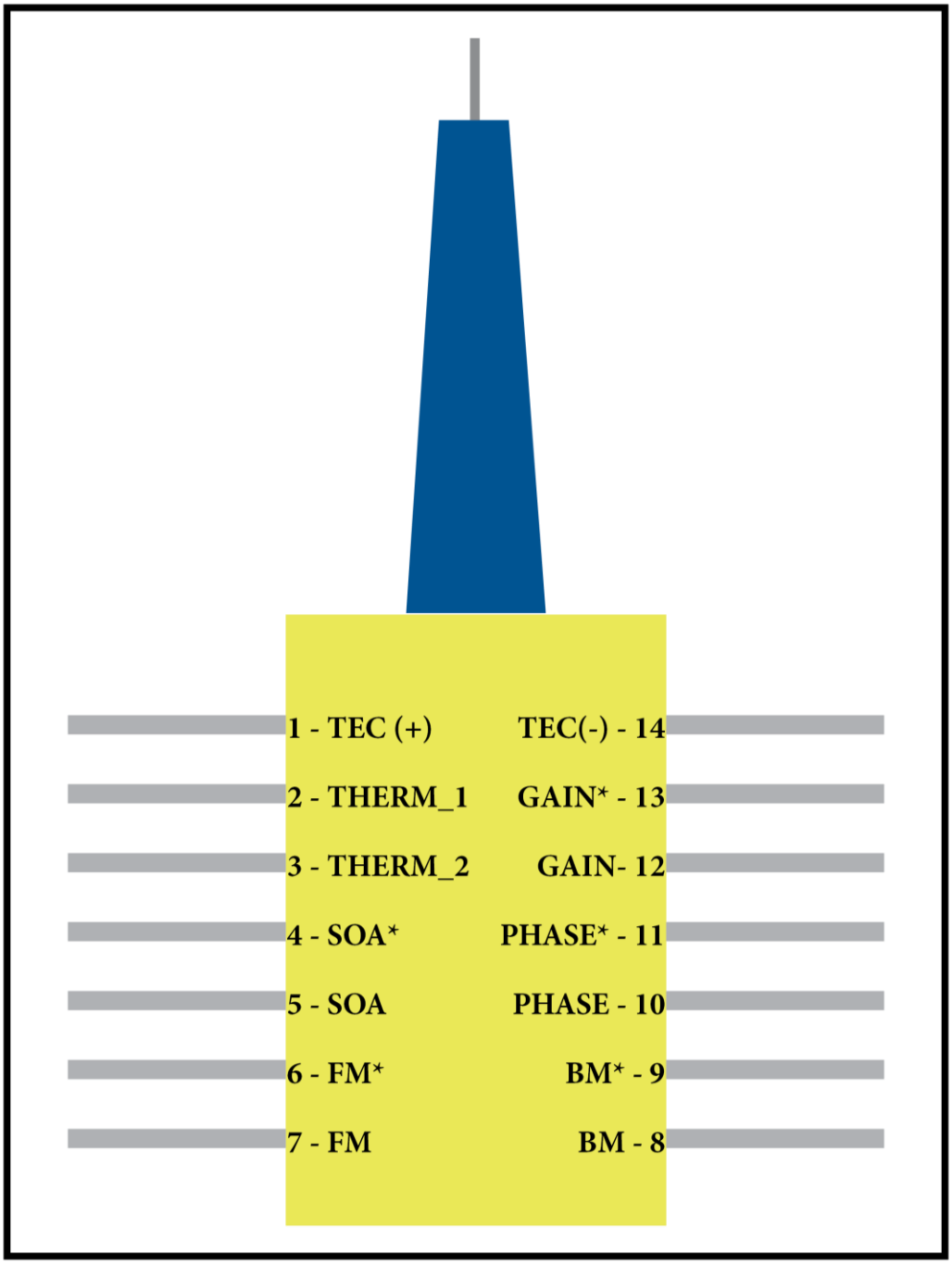

Appendix B: Tabulated RLC Data for the 1310nm Neptune Laser

FM - Forward Bias	Time Domain Data		Frequency Domain Data		* Lead inductance estimated to be **1.6 nH** based on highest reactance measurement from this PUT.					
DC_Bias (mA)	**Gamma (V/V)**	**Dyn_R (Ω)**	**Resistance (Ω)**	**Reactance (Ω)**	**Xc (Ω)**	**Magnitude (Ω)**	**Phase (Degrees)**	**Susceptance (1/Ω)**	**Capacitance (pF)**	**Tau (ns)**
0.00	0.8216	**510.5**	48.738	-771.100	-771.200	772.739	-86.384	0.00129152	20.56	0.507
0.37	0.6597	**243.9**	335.196	-423.900	-424.000	540.493	-51.672	0.00145140	23.10	1.005
0.76	0.5190	**157.9**	285.288	-195.700	-195.800	346.016	-34.463	0.00163539	26.03	1.107
1.00	0.4310	**125.7**	239.371	-131.800	-131.900	273.306	-28.856	0.00176582	28.10	1.162
1.49	0.2806	**89.0**	172.409	-71.760	-71.860	186.785	-22.626	0.00205969	32.78	1.271
2.12	0.1075	**62.0**	118.441	-38.470	-38.570	124.563	-18.038	0.00248583	39.56	1.391
2.71	-0.0387	**46.3**	87.623	-24.450	-24.550	90.997	-15.652	0.00296480	47.19	1.502
3.41	-0.1906	**34.0**	63.737	-15.390	-15.490	65.592	-13.660	0.00360036	57.30	1.606
4.11	-0.3242	**25.5**	47.490	-10.170	-10.270	48.588	-12.203	0.00435027	69.24	1.686
4.92	-0.4600	**18.5**	34.509	-6.478	-6.578	35.130	-10.792	0.00533002	84.83	1.732
5.73	-0.5811	**13.2**	25.448	-4.173	-4.273	25.804	-9.532	0.00641727	102.13	1.722
6.60	-0.6874	**9.3**	18.684	-2.627	-2.727	18.882	-8.304	0.00764876	121.73	1.656
8.03	-0.8077	**5.3**	12.173	-1.292	-1.392	12.252	-6.524	0.00927261	147.58	1.445
10.10	-0.8892	**2.9**	8.608	-0.685	-0.785	8.644	-5.211	0.01050675	167.22	1.228
13.10	-0.9401	**1.5**	6.774	-0.410	-0.510	6.793	-4.306	0.01105160	175.89	1.049
18.20	-0.9818	**0.5**	5.395	-0.187	-0.287	5.403	-3.045	0.00983268	156.49	0.762
25.00	-1.0000	**0.0**	4.527	-0.088	-0.188	4.531	-2.378	0.00915774	145.75	0.605
33.00	-1.0000	**0.0**	3.875	-0.028	-0.128	3.877	-1.892	0.00851516	135.52	0.487
40.20	-1.0000	**0.0**	3.461	-0.010	-0.110	3.463	-1.820	0.00917384	146.01	0.473
51.50	-1.0000	**0.0**	2.996	0.008	-0.092	2.997	-1.759	0.01023988	162.97	0.461
63.10	-1.0000	**0.0**	2.681	0.040	-0.060	2.682	-1.282	0.00834334	132.79	0.338
75.40	-1.0000	**0.0**	2.339	0.027	-0.073	2.340	-1.788	0.01333029	212.16	0.474
88.20	-1.0000	**0.0**	2.053	0.052	-0.048	2.054	-1.339	0.01138219	181.15	0.357
100.00	-1.0000	**0.0**	1.941	0.063	-0.037	1.941	-1.092	0.00981732	156.25	0.292
115.00	-1.0000	**0.0**	1.718	0.029	-0.071	1.719	-2.367	0.02401435	382.20	0.635

FM - Reverse Bias	Time Domain Data		Frequency Domain Data							
DC_Bias (µA)	Gamma (V/V)	Dyn_R (Ω)	Resistance (Ω)	Reactance (Ω)	Xc (Ω)	Magnitude (Ω)	Phase (Degrees)	Susceptance (1/Ω)	Capacitance (pF)	Tau (ns)
-5	0.8239	**517.9**	17.574	-799.2	-799.3	799.493	-88.740	0.00125049	19.90	0.259
-10	0.8241	**518.5**	16.026	-809.9	-810.0	810.159	-88.867	0.00123408	19.64	0.238
-15	0.8240	**518.2**	13.456	-818.7	-818.8	818.911	-89.058	0.00122097	19.43	0.206
-20	0.8242	**518.8**	3.985	-827.6	-827.7	827.710	-89.724	0.00120814	19.23	0.071
-25	0.8244	**519.5**	10.559	-828.3	-828.4	828.467	-89.270	0.00120695	19.21	0.167
-30	0.8247	**520.5**	10.958	-832.3	-832.4	832.472	-89.246	0.00120114	19.12	0.172
-35	0.8248	**520.8**	15.954	-830.3	-830.4	830.553	-88.899	0.00120379	19.16	0.232
-45	0.8246	**520.1**	8.932	-841.2	-841.3	841.347	-89.392	0.00118850	18.92	0.143
-55	0.8249	**521.1**	15.056	-844.6	-844.7	844.834	-88.979	0.00118348	18.84	0.218
-65	0.8252	**522.1**	9.138	-851.6	-851.7	851.749	-89.385	0.00117399	18.68	0.144
										Max Tau (ns)
										1.73

BM - Forward Bias	Time Domain Data		Frequency Domain Data		* Lead inductance estimated to be **0.16 nH** based on highest reactance measurement from this PUT.					
DC_Bias (mA)	Gamma (V/V)	Dyn_R (Ω)	Resistance (Ω)	Reactance (Ω)	Xc (Ω)	Magnitude (Ω)	Phase (Degrees)	Susceptance (1/Ω)	Capacitance (pF)	Tau (ns)
0.00	0.8909	**866.6**	45.457	-745.600	-745.610	746.994	-86.511	0.00133622	21.27	0.506
0.39	0.7137	**299.3**	322.487	-425.400	-425.410	533.827	-52.836	0.00149282	23.76	1.028
0.72	0.6000	**200.0**	293.048	-224.600	-224.610	369.225	-37.469	0.00164759	26.22	1.120
1.02	0.4889	**145.7**	237.659	-136.400	-136.410	274.025	-29.855	0.00181663	28.91	1.194
1.44	0.3592	**106.1**	180.583	-81.240	-81.250	198.020	-24.224	0.00207208	32.98	1.291
2.13	0.1600	**69.0**	119.754	-41.120	-41.130	126.620	-18.955	0.00256538	40.83	1.440
2.73	0.0136	**51.4**	88.637	-26.090	-26.100	92.400	-16.408	0.00305702	48.65	1.555
3.43	-0.1441	**37.4**	64.502	-16.500	-16.510	66.581	-14.357	0.00372427	59.27	1.670
4.04	-0.2755	**28.4**	49.427	-11.490	-11.500	50.747	-13.098	0.00446554	71.07	1.767
5.74	-0.5494	**14.5**	25.500	-4.595	-4.605	25.912	-10.237	0.00685823	109.15	1.843
6.54	-0.6500	**10.6**	18.962	-3.056	-3.066	19.208	-9.185	0.00830989	132.26	1.818
8.04	-0.7859	**6.0**	11.593	-1.504	-1.514	11.691	-7.440	0.01107617	176.28	1.659
10.10	-0.8732	**3.4**	7.891	-0.817	-0.827	7.934	-5.983	0.01313703	209.08	1.425
13.10	-0.9234	**2.0**	6.083	-0.547	-0.557	6.108	-5.232	0.01492772	237.58	1.288
18.20	-0.9639	**0.9**	4.801	-0.335	-0.345	4.813	-4.110	0.01489083	236.99	1.038
25.00	-0.9914	**0.2**	3.970	-0.240	-0.250	3.978	-3.603	0.01579939	251.46	0.925
33.00	-1.0000	**0.0**	3.407	-0.195	-0.205	3.413	-3.443	0.01759706	280.07	0.893
40.20	-1.0000	**0.0**	3.065	-0.176	-0.186	3.071	-3.473	0.01972675	313.96	0.907
50.50	-1.0000	**0.0**	2.753	-0.131	-0.141	2.757	-2.932	0.01855534	295.32	0.771
63.20	-1.0000	**0.0**	2.386	-0.114	-0.124	2.389	-2.975	0.02172248	345.72	0.787
75.40	-1.0000	**0.0**	2.194	-0.141	-0.151	2.199	-3.937	0.03122133	496.90	1.044
88.20	-1.0000	**0.0**	1.967	-0.086	-0.096	1.969	-2.794	0.02475308	393.96	0.746
100.00	-1.0000	**0.0**	1.804	-0.109	-0.119	1.808	-3.774	0.03640728	579.44	1.009
115.00	-1.0000	**0.0**	1.620	-0.074	-0.084	1.622	-2.968	0.03192149	508.05	0.797
130.00	-1.0000	**0.0**	1.570	-0.086	-0.096	1.573	-3.499	0.03880174	617.55	0.940

BM - Reverse Bias	Time Domain Data		Frequency Domain Data							
DC_Bias (μA)	Gamma (V/V)	Dyn_R (Ω)	Resistance (Ω)	Reactance (Ω)	Xc (Ω)	Magnitude (Ω)	Phase (Degrees)	Susceptance (1/Ω)	Capacitance (pF)	Tau (ns)
-5	0.8528	**629.3**	20.362	-760.3	-760.3	760.583	-88.466	0.00131431	20.92	0.303
-10	0.8530	**630.3**	15.846	-781.3	-781.3	781.471	-88.838	0.00127938	20.36	0.245
-15	0.8533	**631.7**	21.213	-780.7	-780.7	780.998	-88.444	0.00127994	20.37	0.303
-20	0.8532	**631.2**	11.400	-792.6	-792.6	792.692	-89.176	0.00126139	20.08	0.186
-25	0.8532	**631.2**	21.531	-798.9	-798.9	799.200	-88.456	0.00125080	19.91	0.300
-30	0.8527	**628.9**	14.256	-801.9	-801.9	802.037	-88.982	0.00124663	19.84	0.220
-35	0.8528	**629.3**	8.112	-811.3	-811.3	811.351	-89.427	0.00123245	19.62	0.137
-45	0.8532	**631.2**	17.657	-813.5	-813.5	813.702	-88.757	0.00122866	19.55	0.255
-55	0.8529	**629.8**	18.830	-833.9	-833.9	834.123	-88.706	0.00119856	19.08	0.261
										Max Tau (ns)
										1.84

PM - Forward Bias	Time Domain Data		Frequency Domain Data		* Lead inductance estimated to be **1.6 nH** based on highest reactance measurement from this PUT.					
DC_Bias (mA)	Gamma (V/V)	Dyn_R (Ω)	Resistance (Ω)	Reactance (Ω)	Xc (Ω)	Magnitude (Ω)	Phase (Degrees)	Susceptance (1/Ω)	Capacitance (pF)	Tau (ns)
0.00	0.9056	**1009.3**	484.169	-4291.000	-4291.100	4318.328	-83.562	0.00023011	3.66	0.166
0.39	0.7125	**297.8**	768.578	-231.900	-232.000	802.830	-16.797	0.00035995	5.73	0.269
0.72	0.5894	**193.5**	438.021	-90.420	-90.520	447.276	-11.676	0.00045247	7.20	0.323
1.02	0.4835	**143.6**	309.940	-54.030	-54.130	314.631	-9.907	0.00054681	8.70	0.375
1.50	0.3433	**102.3**	203.920	-30.300	-30.400	206.174	-8.479	0.00071517	11.38	0.457
2.13	0.1887	**73.3**	134.975	-18.470	-18.570	136.246	-7.834	0.00100037	15.92	0.581
2.72	0.0681	**57.3**	98.594	-11.670	-11.770	99.294	-6.808	0.00119380	19.00	0.630
3.42	-0.0602	**44.3**	71.497	-7.587	-7.687	71.909	-6.137	0.00148659	23.66	0.696
4.04	-0.1614	**36.1**	55.632	-5.386	-5.486	55.902	-5.632	0.00175551	27.94	0.736
4.93	-0.2830	**27.9**	40.301	-3.338	-3.438	40.447	-4.876	0.00210148	33.45	0.746
5.73	-0.3787	**22.5**	31.008	-2.165	-2.265	31.091	-4.178	0.00234320	37.29	0.714
6.53	-0.4594	**18.5**	24.816	-1.452	-1.552	24.864	-3.579	0.00251034	39.95	0.663
8.03	-0.5630	**14.0**	18.578	-0.701	-0.801	18.595	-2.469	0.00231648	36.87	0.499
10.10	-0.6428	**10.9**	14.808	-0.383	-0.483	14.816	-1.868	0.00220035	35.02	0.400
13.10	-0.7175	**8.2**	11.759	-0.144	-0.244	11.762	-1.189	0.00176385	28.07	0.267
18.20	-0.8046	**5.4**	8.578	-0.062	-0.162	8.580	-1.082	0.00220084	35.03	0.256
25.00	-0.8794	**3.2**	6.152	0.035	-0.065	6.152	-0.605	0.00171724	27.33	0.150
33.00	-0.9271	**1.9**	4.700	0.043	-0.057	4.700	-0.695	0.00257997	41.06	0.176
42.10	-0.9568	**1.1**	3.845	0.099	-0.001	3.845	-0.015	0.00006764	1.08	0.004

PM - Reverse Bias	Time Domain Data		Frequency Domain Data							
DC_Bias (μA)	Gamma (V/V)	Dyn_R (Ω)	Resistance (Ω)	Reactance (Ω)	Xc (Ω)	Magnitude (Ω)	Phase (Degrees)	Susceptance (1/Ω)	Capacitance (pF)	Tau (ns)
-5	0.9063	**1017.2**	293.642	-3654.0	-3654.1	3665.879	-85.406	0.00027191	4.33	0.185
-10	0.9064	**1018.4**	420.030	-3671.0	-3671.1	3695.051	-83.473	0.00026888	4.28	0.191
-15	0.9065	**1019.5**	254.702	-3693.0	-3693.1	3701.873	-86.055	0.00026949	4.29	0.179
-20	0.9064	**1018.4**	166.839	-3707.0	-3707.1	3710.852	-87.423	0.00026921	4.28	0.165
-25	0.9062	**1016.1**	351.470	-3816.0	-3816.1	3832.251	-84.738	0.00025984	4.14	0.181
-30	0.9063	**1017.2**	409.722	-3808.0	-3808.1	3830.078	-83.859	0.00025959	4.13	0.184
										Max Tau (ns)
										0.75

Gain - Forward Bias	Time Domain Data		Frequency Domain Data		* Lead inductance estimated to be **4.8 nH** based on highest reactance measurement from this PUT.					
DC_Bias (mA)	Gamma (V/V)	Dyn_R (Ω)	Resistance (Ω)	Reactance (Ω)	Xc (Ω)	Magnitude (Ω)	Phase (Degrees)	Susceptance (1/Ω)	Capacitance (pF)	Tau (ns)
0.00	0.9662	**2908.6**	80.297	-1000.000	-1000.300	1003.518	-85.411	0.00099330	15.81	0.487
0.39	0.7296	**319.8**	347.914	-330.500	-330.800	480.076	-43.556	0.00143531	22.84	0.999
0.72	0.58	**188.4**	280.550	-184.700	-185.000	336.056	-33.402	0.00163814	26.07	1.106
1.02	0.4729	**139.7**	219.594	-116.300	-116.600	248.630	-27.967	0.00188621	30.02	1.223
1.49	0.3259	**98.3**	156.600	-65.600	-65.900	169.901	-22.822	0.00228293	36.33	1.377
2.11	0.1604	**69.1**	108.213	-37.100	-37.400	114.494	-19.066	0.00285304	45.41	1.553
2.70	0.0211	**52.2**	79.587	-23.800	-24.100	83.156	-16.847	0.00348523	55.47	1.703
3.40	-0.1282	**38.6**	57.753	-15.100	-15.400	59.771	-14.931	0.00431062	68.61	1.839
4.09	-0.2512	**29.9**	43.129	-10.000	-10.300	44.342	-13.432	0.00523853	83.37	1.931
4.90	-0.3706	**23.0**	31.398	-6.300	-6.600	32.084	-11.871	0.00641154	102.04	1.968
5.71	-0.4747	**17.8**	23.429	-4.000	-4.300	23.820	-10.400	0.00757832	120.61	1.924
6.58	-0.5644	**13.9**	17.582	-2.400	-2.700	17.788	-8.730	0.00853305	135.81	1.767
8.00	-0.6598	**10.2**	12.335	-1.100	-1.400	12.414	-6.475	0.00908429	144.58	1.431
10.10	-0.7281	**7.9**	9.261	-0.404	-0.704	9.288	-4.347	0.00816121	129.89	1.015
13.10	-0.7756	**6.3**	7.550	-0.128	-0.428	7.562	-3.245	0.00748439	119.12	0.781
18.20	-0.8159	**5.1**	6.176	0.058	-0.242	6.181	-2.244	0.00633482	100.82	0.554
25.00	-0.8514	**4.0**	5.098	0.165	-0.135	5.100	-1.517	0.00519074	82.61	0.382
33.00	-0.8766	**3.3**	4.330	0.215	-0.085	4.331	-1.125	0.00453185	72.13	0.287
40.20	-0.8844	**3.1**	4.107	0.249	-0.051	4.107	-0.711	0.00302311	48.11	0.183
51.50	-0.8878	**3.0**	3.967	0.255	-0.045	3.967	-0.650	0.00285912	45.50	0.167
63.10	-0.8915	**2.9**	3.896	0.213	-0.087	3.897	-1.279	0.00572882	91.18	0.330
75.40	-0.8948	**2.8**	3.805	0.223	-0.077	3.806	-1.159	0.00531623	84.61	0.299
88.20	-0.8979	**2.7**	3.725	0.143	-0.157	3.728	-2.413	0.01129474	179.76	0.623
100.00	-0.8999	**2.6**	3.699	0.157	-0.143	3.702	-2.214	0.01043563	166.09	0.572
115.00	-0.9013	**2.6**	3.634	0.089	-0.211	3.640	-3.323	0.01592396	253.44	0.859

Gain - Reverse Bias	Time Domain Data		Frequency Domain Data							
DC_Bias (μA)	Gamma (V/V)	Dyn_R (Ω)	Resistance (Ω)	Reactance (Ω)	Xc (Ω)	Magnitude (Ω)	Phase (Degrees)	Susceptance (1/Ω)	Capacitance (pF)	Tau (ns)
-5	0.9661	**2899.9**	47.312	-1045.0	-1045.3	1046.370	-87.408	0.00095471	15.19	0.369
-10	0.9676	**3036.4**	25.892	-1064.0	-1064.3	1064.615	-88.606	0.00093903	14.95	0.255
-15	0.9673	**3008.1**	33.608	-1072.0	-1072.3	1072.827	-88.205	0.00093166	14.83	0.298
-20	0.9670	**2980.3**	43.005	-1088.0	-1088.3	1089.149	-87.737	0.00091743	14.60	0.338
-25	0.9672	**2998.8**	21.387	-1089.0	-1089.3	1089.510	-88.875	0.00091767	14.61	0.219
-30	0.9672	**2998.8**	43.803	-1091.0	-1091.3	1092.179	-87.701	0.00091486	14.56	0.340
-35	0.9674	**3017.5**	48.164	-1085.0	-1085.3	1086.368	-87.459	0.00091959	14.64	0.359
-45	0.9674	**3017.5**	12.372	-1144.0	-1144.3	1144.367	-89.381	0.00087379	13.91	0.138
-55	0.9677	**3046.0**	8.064	-1151.0	-1151.3	1151.328	-89.599	0.00086854	13.82	0.096
-65	0.9677	**3046.0**	1.704	-1180.0	-1180.3	1180.301	-89.917	0.00084724	13.48	0.022
										Max Tau (ns)
										1.97

SOA - Forward Bias	Time Domain Data		Frequency Domain Data		* Lead inductance estimated to be 16 **nH** based on highest reactance measurement from this PUT.					
DC_Bias (mA)	Gamma (V/V)	Dyn_R (Ω)	Resistance (Ω)	Reactance (Ω)	Xc (Ω)	Magnitude (Ω)	Phase (Degrees)	Susceptance (1/Ω)	Capacitance (pF)	Tau (ns)
0.00	0.8811	**791.0**	122.652	-1367.000	-1367.100	1372.591	-84.873	0.00072563	11.55	0.41
0.39	0.6082	**205.2**	431.538	-367.100	-367.200	566.622	-40.395	0.00114371	18.20	0.82
0.72	0.4784	**141.7**	310.438	-175.900	-176.000	356.858	-29.551	0.00138204	22.00	0.95
1.02	0.3643	**107.3**	236.271	-107.900	-108.000	259.784	-24.565	0.00160028	25.47	1.05
1.43	0.2354	**80.8**	172.398	-65.890	-65.990	184.596	-20.946	0.00193657	30.82	1.19
2.13	0.0440	**54.6**	111.378	-34.580	-34.680	116.652	-17.295	0.00254855	40.56	1.40
2.72	-0.0957	**41.3**	81.552	-22.630	-22.730	84.660	-15.574	0.00317131	50.47	1.56
3.42	-0.2419	**30.5**	59.051	-14.610	-14.710	60.856	-13.988	0.00397202	63.22	1.71
4.04	-0.3526	**23.9**	45.337	-10.280	-10.380	46.510	-12.896	0.00479847	76.37	1.82
4.92	-0.4781	**17.7**	31.933	-6.307	-6.407	32.569	-11.345	0.00603997	96.13	1.87
5.73	-0.5745	**13.5**	23.733	-4.076	-4.176	24.098	-9.979	0.00719139	114.45	1.84
6.53	-0.6505	**10.6**	18.283	-2.665	-2.765	18.491	-8.600	0.00808685	128.71	1.72
8.03	-0.7403	**7.5**	12.504	-1.280	-1.380	12.580	-6.298	0.00872014	138.79	1.39
10.10	-0.8038	**5.4**	9.478	-0.607	-0.707	9.504	-4.266	0.00782665	124.57	0.99
13.10	-0.8477	**4.1**	7.760	-0.296	-0.396	7.770	-2.921	0.00655907	104.39	0.70
18.20	-0.8851	**3.0**	6.454	-0.148	-0.248	6.459	-2.201	0.00594502	94.62	0.54
25.00	-0.9110	**2.3**	5.631	-0.085	-0.185	5.634	-1.882	0.00582817	92.76	0.47
33.00	-0.9296	**1.8**	5.013	0.007	-0.093	5.014	-1.063	0.00369946	58.88	0.27
40.20	-0.9402	**1.5**	4.685	-0.022	-0.122	4.687	-1.492	0.00555452	88.40	0.38
51.50	-0.9552	**1.1**	4.255	0.037	-0.063	4.255	-0.848	0.00347893	55.37	0.22
63.20	-0.9668	**0.8**	3.946	0.060	-0.040	3.946	-0.581	0.00256863	40.88	0.15
75.40	-0.9771	**0.6**	3.694	-0.003	-0.103	3.695	-1.597	0.00754234	120.04	0.41
88.20	-0.9844	**0.4**	3.432	0.017	-0.083	3.433	-1.385	0.00704254	112.09	0.36
100.00	-0.9911	**0.2**	3.268	0.021	-0.079	3.269	-1.385	0.00739281	117.66	0.36
115.00	-0.9971	**0.1**	3.046	0.023	-0.077	3.047	-1.448	0.00829380	132.00	0.38
130.00	-1.0000	**0.0**	2.960	0.004	-0.096	2.962	-1.858	0.01094539	174.20	0.49
145.00	-1.0000	**0.0**	2.845	-0.036	-0.136	2.848	-2.737	0.01676421	266.81	0.72
160.00	-1.0000	**0.0**	2.710	-0.054	-0.154	2.714	-3.252	0.02090172	332.66	0.86

SOA - Reverse Bias	Time Domain Data		Frequency Domain Data							
DC_Bias (μA)	Gamma (V/V)	Dyn_R (Ω)	Resistance (Ω)	Reactance (Ω)	Xc (Ω)	Magnitude (Ω)	Phase (Degrees)	Susceptance (1/Ω)	Capacitance (pF)	Tau (ns)
-5	0.8826	**801.8**	43.452	-1357.0	-1357.1	1357.795	-88.166	0.00073611	11.72	0.27
-10	0.8825	**801.1**	39.433	-1410.0	-1410.1	1410.651	-88.398	0.00070862	11.28	0.25
-15	0.8833	**806.9**	40.250	-1407.0	-1407.1	1407.676	-88.362	0.00071010	11.30	0.25
-20	0.8832	**806.2**	39.116	-1432.0	-1432.1	1432.634	-88.435	0.00069775	11.11	0.24
-25	0.8840	**812.1**	27.718	-1464.0	-1464.1	1464.362	-88.915	0.00068277	10.87	0.19
-30	0.8838	**810.6**	59.374	-1444.0	-1444.1	1445.320	-87.646	0.00069130	11.00	0.30
-35	0.8835	**808.4**	28.301	-1458.0	-1458.1	1458.375	-88.888	0.00068557	10.91	0.20
-45	0.8834	**807.6**	37.049	-1461.0	-1461.1	1461.570	-88.547	0.00068398	10.89	0.23
-55	0.8838	**810.6**	17.530	-1497.0	-1497.1	1497.203	-89.329	0.00066787	10.63	0.14
-65	0.8837	**809.8**	26.463	-1484.0	-1484.1	1484.336	-88.978	0.00067359	10.72	0.19
-75	0.8843	**814.3**	11.115	-1486.0	-1486.1	1486.142	-89.571	0.00067286	10.71	0.10
-85	0.8834	**807.6**	48.749	-1536.0	-1536.1	1536.873	-88.182	0.00065034	10.35	0.26
										Max Tau (ns)
										1.87

Appendix C: Tabulated RLC Data for the 1060nm VTL-2 Laser

FM - Forward Bias		Time Domain Data		Frequency Domain Data		* Lead inductance estimated to be **30 nH** based on highest reactance measurement from this PUT.					
DC_Bias (mA)	Port Voltage (V)	Gamma (V/V)	Dyn_R (Ω)	Resistance (Ω)	Reactance (Ω)	Xc (Ω)	Magnitude (Ω)	Phase (Degrees)	Susceptance (1/Ω)	Capacitance (pF)	Tau (ns)
0.0	0.00	0.9828	**5764.0**	195.771	-822.479	-824.379	847.306	-76.641	0.00114828	18.28	0.73
0.6	1.42	0.7223	**310.1**	247.418	-144.491	-146.391	287.482	-30.612	0.00177130	28.19	1.17
0.9	1.48	0.6514	**236.9**	207.136	-90.431	-92.331	226.783	-24.025	0.00179526	28.57	1.15
1.2	1.53	0.5923	**195.3**	177.342	-62.149	-64.049	188.554	-19.858	0.00180154	28.67	1.12
1.6	1.57	0.5200	**158.3**	147.346	-39.993	-41.893	153.186	-15.871	0.00178527	28.41	1.06
2.1	1.63	0.4373	**127.7**	121.573	-25.476	-27.376	124.617	-12.690	0.00176285	28.06	0.99
2.4	1.67	0.3576	**105.7**	101.579	-16.360	-18.260	103.207	-10.191	0.00171428	27.28	0.91
3.7	1.74	0.2370	**81.1**	78.875	-8.819	-10.719	79.600	-7.739	0.00169172	26.92	0.82
5.1	1.82	0.0918	**60.1**	58.949	-4.014	-5.914	59.245	-5.729	0.00168492	26.82	0.73
6.6	1.89	-0.0202	**48.0**	47.374	-1.786	-3.686	47.517	-4.449	0.00163250	25.98	0.63
9.6	2.00	-0.1621	**36.1**	35.739	-0.029	-1.929	35.791	-3.089	0.00150578	23.97	0.50
12.5	2.09	-0.2475	**30.2**	29.972	0.645	-1.255	29.998	-2.398	0.00139450	22.19	0.42
16.5	2.19	-0.3262	**25.4**	25.333	1.112	-0.788	25.345	-1.782	0.00122668	19.52	0.33
21.5	2.31	-0.3924	**21.8**	21.809	1.408	-0.492	21.815	-1.292	0.00103389	16.45	0.25
27.5	2.43	-0.4447	**19.2**	19.247	1.528	-0.372	19.251	-1.107	0.00100382	15.98	0.22
33.5	2.53	-0.4816	**17.5**	17.541	1.647	-0.253	17.543	-0.826	0.00082209	13.08	0.17
40.4	2.65	-0.5124	**16.1**	16.192	1.741	-0.159	16.193	-0.563	0.00060639	9.65	0.12
48.5	2.77	-0.5398	**14.9**	15.059	1.740	-0.160	15.060	-0.609	0.00070547	11.23	0.13
56.5	2.88	-0.5591	**14.1**	14.210	1.785	-0.115	14.210	-0.464	0.00056948	9.06	0.10
65.4	3.00	-0.5783	**13.4**	13.451	1.818	-0.082	13.451	-0.349	0.00045320	7.21	0.08
74.4	3.11	-0.5941	**12.7**	12.856	1.841	-0.059	12.856	-0.263	0.00035697	5.68	0.06
83.4	3.21	-0.6077	**12.2**	12.323	1.824	-0.076	12.323	-0.353	0.00050045	7.96	0.08
92.4	3.31	-0.6206	**11.7**	11.870	1.851	-0.049	11.870	-0.237	0.00034777	5.53	0.05
100.4	3.39	-0.6300	**11.3**	11.541	1.840	-0.060	11.541	-0.298	0.00045046	7.17	0.07

Max Tau (ns)
1.17

BM - Forward Bias		Time Domain Data		Frequency Domain Data		* Lead inductance assumed to be **16 nH** based on highest reactance measurement.					
DC_Bias (mA)	Port Voltage (V)	Gamma (V/V)	Dyn_R (Ω)	Resistance (Ω)	Reactance (Ω)	Xc (Ω)	Magnitude (Ω)	Phase (Degrees)	Susceptance (1/Ω)	Capacitance (pF)	Tau (ns)
0.0	0.00	0.9303	**1384.7**	193.718	-596.523	-597.523	628.140	-72.037	0.00151440	24.10	0.96
0.5	1.29	0.6080	**205.1**	189.260	-149.661	-150.661	241.905	-38.522	0.00257461	40.98	1.62
0.7	1.35	0.5048	**151.9**	160.620	-96.244	-97.244	187.764	-31.192	0.00275829	43.90	1.67
1.1	1.39	0.4289	**125.1**	137.677	-66.760	-67.760	153.448	-26.205	0.00287773	45.80	1.68
1.5	1.43	0.3473	**103.2**	114.610	-43.795	-44.795	123.053	-21.348	0.00295832	47.08	1.64
1.9	1.46	0.2825	**89.4**	98.137	-30.823	-31.823	103.168	-17.966	0.00298988	47.59	1.58
2.3	1.49	0.2266	**79.3**	85.678	-22.681	-23.681	88.890	-15.451	0.00299702	47.70	1.51
3.0	1.53	0.1428	**66.7**	70.332	-14.421	-15.421	72.003	-12.367	0.00297450	47.34	1.38
3.7	1.57	0.0740	**58.0**	59.881	-9.734	-10.734	60.835	-10.163	0.00290033	46.16	1.26
4.5	1.60	-0.0004	**50.0**	51.189	-6.561	-7.561	51.744	-8.402	0.00282392	44.94	1.14
5.5	1.64	-0.0800	**42.6**	43.259	-4.327	-5.327	43.586	-7.020	0.00280410	44.63	1.04
7.0	1.69	-0.1846	**34.4**	34.970	-2.407	-3.407	35.136	-5.565	0.00275980	43.92	0.90
10.1	1.78	-0.3220	**25.6**	25.985	-0.808	-1.808	26.048	-3.981	0.00266518	42.42	0.73
15.0	1.88	-0.4403	**19.4**	19.650	0.039	-0.961	19.673	-2.800	0.00248291	39.52	0.56
20.1	1.97	-0.5116	**16.2**	16.356	0.388	-0.612	16.367	-2.143	0.00228449	36.36	0.45
30.0	2.10	-0.5918	**12.8**	12.983	0.642	-0.358	12.988	-1.578	0.00211991	33.74	0.35
45.0	2.27	-0.6555	**10.4**	10.467	0.784	-0.216	10.469	-1.182	0.00197072	31.36	0.27
60.0	2.41	-0.6924	**9.1**	9.188	0.879	-0.121	9.189	-0.755	0.00143307	22.81	0.18
75.1	2.53	-0.7155	**8.3**	8.343	0.917	-0.083	8.343	-0.570	0.00119231	18.98	0.14
90.1	2.65	-0.7338	**7.7**	7.769	0.922	-0.078	7.769	-0.573	0.00128720	20.49	0.14
110.4	2.79	-0.7505	**7.1**	7.198	0.915	-0.085	7.198	-0.673	0.00163263	25.98	0.16
130.6	2.92	-0.7686	**6.5**	6.613	0.891	-0.109	6.614	-0.943	0.00248722	39.59	0.23
151.0	3.04	-0.7766	**6.3**	6.422	0.913	-0.087	6.423	-0.779	0.00211638	33.68	0.19
175.0	3.17	-0.7873	**6.0**	6.184	0.883	-0.117	6.185	-1.084	0.00305838	48.68	0.27
200.0	3.30	-0.7883	**5.9**	6.025	0.847	-0.153	6.027	-1.455	0.00421209	67.04	0.36
											Max Tau (ns)
											1.68

PM - Forward Bias		Time Domain Data		Frequency Domain Data		* Lead inductance assumed to be **29 nH** based on highest reactance measurement.					
DC_Bias (mA)	Port Voltage (V)	Gamma (V/V)	Dyn_R (Ω)	Resistance (Ω)	Reactance (Ω)	Reactance (Ω)	Magnitude (Ω)	Phase (Degrees)	Susceptance (1/Ω)	Capacitance (pF)	Tau (ns)
0.0	0.00	0.9799	**4925.1**	138.235	-651.523	-653.323	667.787	-78.053	0.00146505	23.32	0.86
0.6	1.35	0.6623	**246.1**	188.146	-133.414	-135.214	231.693	-35.703	0.00251881	40.09	1.58
0.9	1.40	0.5780	**187.0**	159.442	-85.322	-87.122	181.692	-28.653	0.00263910	42.00	1.60
1.3	1.45	0.4870	**144.9**	132.260	-53.862	-55.662	143.496	-22.824	0.00270322	43.02	1.56
1.8	1.49	0.3944	**115.1**	108.990	-34.145	-35.945	114.764	-18.253	0.00272913	43.44	1.49
2.4	1.54	0.2921	**91.3**	88.108	-20.576	-22.376	90.905	-14.250	0.00270774	43.10	1.37
3.4	1.60	0.1612	**69.2**	67.663	-10.469	-12.269	68.766	-10.277	0.00259452	41.29	1.19
4.8	1.66	0.0162	**51.6**	51.160	-4.905	-6.705	51.598	-7.467	0.00251850	40.08	1.01
6.3	1.72	-0.1022	**40.7**	40.323	-2.273	-4.073	40.528	-5.768	0.00247971	39.47	0.88
9.3	1.81	-0.2601	**29.4**	29.394	-0.224	-2.024	29.464	-3.939	0.00233152	37.11	0.69
12.2	1.88	-0.3516	**24.0**	24.144	0.550	-1.250	24.176	-2.963	0.00213809	34.03	0.55
16.2	1.96	-0.4305	**19.9**	20.094	0.989	-0.811	20.110	-2.312	0.00200629	31.93	0.46
21.3	2.05	-0.4943	**16.9**	17.132	1.256	-0.544	17.141	-1.819	0.00185159	29.47	0.38
27.3	2.14	-0.5451	**14.7**	14.995	1.439	-0.361	14.999	-1.379	0.00160458	25.54	0.29
33.3	2.23	-0.5804	**13.3**	13.589	1.576	-0.224	13.591	-0.944	0.00121270	19.30	0.21
40.2	2.32	-0.6083	**12.2**	12.443	1.632	-0.168	12.444	-0.774	0.00108488	17.27	0.17
48.2	2.41	-0.6324	**11.3**	11.593	1.696	-0.104	11.593	-0.514	0.00077376	12.31	0.12
56.2	2.50	-0.6441	**10.8**	10.920	1.724	-0.076	10.920	-0.399	0.00063730	10.14	0.09
65.2	2.61	-0.6625	**10.2**	10.494	1.724	-0.076	10.494	-0.415	0.00069009	10.98	0.10
74.2	2.70	-0.6733	**9.8**	9.954	1.741	-0.059	9.954	-0.340	0.00059544	9.48	0.08
83.2	2.79	-0.6856	**9.3**	9.596	1.790	-0.010	9.596	-0.060	0.00010860	1.73	0.01
92.2	2.87	-0.6933	**9.1**	9.268	1.763	-0.037	9.268	-0.229	0.00043075	6.86	0.05
100.2	2.94	-0.7012	**8.8**	9.056	1.764	-0.036	9.056	-0.228	0.00043896	6.99	0.05

Max Tau (ns)
1.60

Gain - Forward Bias		Time Domain Data		Frequency Domain Data		* Lead inductance assumed to be **30 nH** based on highest reactance measurement.					
DC_Bias (mA)	Port Voltage (V)	Gamma (V/V)	Dyn_R (Ω)	Resistance (Ω)	Reactance (Ω)	Xc (Ω)	Magnitude (Ω)	Phase (Degrees)	Susceptance (1/Ω)	Capacitance (pF)	Tau (ns)
0.0	0.00	0.9382	**1568.1**	83.860	-279.754	-281.654	293.873	-73.420	0.00326134	51.91	1.63
0.3	1.02	0.7921	**431.0**	124.110	-178.449	-180.349	218.927	-55.466	0.00376283	59.89	2.13
0.6	1.06	0.7122	**297.5**	127.638	-137.247	-139.147	188.821	-47.470	0.00390278	62.11	2.23
0.9	1.09	0.6319	**221.7**	122.409	-103.932	-105.832	161.816	-40.846	0.00404180	64.33	2.28
1.2	1.11	0.5589	**176.7**	114.197	-80.994	-82.894	141.111	-35.975	0.00416294	66.26	2.30
1.5	1.13	0.4911	**146.5**	104.703	-63.340	-65.240	123.365	-31.927	0.00428675	68.23	2.31
1.8	1.15	0.4226	**123.2**	95.475	-50.053	-51.953	108.695	-28.553	0.00439736	69.99	2.30
2.1	1.16	0.3502	**103.9**	85.622	-38.934	-40.834	94.861	-25.497	0.00453785	72.22	2.28
3.1	1.20	0.1509	**67.8**	62.654	-19.257	-21.157	66.130	-18.659	0.00483794	77.00	2.14
4.1	1.23	-0.0208	**48.0**	46.518	-9.747	-11.647	47.954	-14.057	0.00506484	80.61	1.94
5.1	1.26	-0.1442	**37.4**	35.722	-4.815	-6.715	36.348	-10.646	0.00508268	80.89	1.69
6.1	1.29	-0.2609	**29.3**	28.448	-2.145	-4.045	28.734	-8.093	0.00489917	77.97	1.41
7.1	1.31	-0.3435	**24.4**	23.933	-0.763	-2.663	24.081	-6.350	0.00459263	73.09	1.18
10.3	1.36	-0.5028	**16.5**	16.473	-0.841	-2.741	16.700	-9.448	0.00982955	156.44	1.94
15.3	1.42	-0.6349	**11.2**	11.292	1.524	-0.376	11.298	-1.907	0.00294554	46.88	0.43
20.3	1.47	-0.6878	**9.2**	9.320	1.726	-0.174	9.322	-1.070	0.00200247	31.87	0.25
30.2	1.55	-0.7412	**7.4**	7.461	1.782	-0.118	7.462	-0.906	0.00211924	33.73	0.22
40.2	1.61	-0.7745	**6.4**	6.453	1.807	-0.093	6.454	-0.826	0.00223290	35.54	0.20
55.2	1.70	-0.8030	**5.5**	5.549	1.833	-0.067	5.549	-0.692	0.00217561	34.63	0.17
70.2	1.78	-0.8190	**5.0**	4.993	1.793	-0.107	4.994	-1.228	0.00429004	68.28	0.31
85.2	1.84	-0.8330	**4.6**	4.613	1.809	-0.091	4.614	-1.130	0.00427470	68.03	0.29
105.2	1.93	-0.8470	**4.1**	4.265	1.834	-0.066	4.266	-0.887	0.00362745	57.73	0.23
125.2	2.00	-0.8541	**3.9**	3.979	1.848	-0.052	3.979	-0.749	0.00328383	52.26	0.19
145.2	2.07	-0.8601	**3.8**	3.832	1.866	-0.034	3.832	-0.508	0.00231523	36.85	0.13
165.1	2.14	-0.8647	**3.6**	3.704	1.812	-0.088	3.705	-1.361	0.00641056	102.03	0.35
195.1	2.23	-0.8680	**3.5**	3.542	1.809	-0.091	3.543	-1.472	0.00724866	115.37	0.38
225.1	2.32	-0.8710	**3.4**	3.483	1.777	-0.123	3.485	-2.023	0.01012644	161.17	0.52
255.1	2.41	-0.8724	**3.4**	3.481	1.690	-0.210	3.487	-3.452	0.01726766	274.82	0.89
285.1	2.49	-0.8691	**3.5**	3.500	1.620	-0.280	3.511	-4.574	0.02271179	361.47	1.18
300.1	2.53	-0.8686	**3.5**	3.536	1.565	-0.335	3.552	-5.412	0.02655459	422.63	1.40

Max Tau (ns)
2.31

SOA - Forward Bias		Time Domain Data		Frequency Domain Data		* Lead inductance assumed to be **32 nH** based on highest reactance measurement.					
DC_Bias (mA)	Port Voltage (V)	Gamma (V/V)	Dyn_R (Ω)	Resistance (Ω)	Reactance (Ω)	Xc (Ω)	Magnitude (Ω)	Phase (Degrees)	Susceptance (1/Ω)	Capacitance (pF)	Tau (ns)
0.0	0.00	0.9407	**1636.3**	85.648	-289.252	-291.252	303.584	-73.613	0.00316017	50.30	1.59
0.3	1.01	0.7838	**412.5**	135.429	-176.919	-178.919	224.395	-52.877	0.00355329	56.55	2.07
0.6	1.05	0.7237	**311.9**	136.919	-140.305	-142.305	197.478	-46.105	0.00364908	58.08	2.13
0.9	1.08	0.6439	**230.8**	131.103	-105.411	-107.411	169.485	-39.327	0.00373927	59.51	2.15
1.2	1.10	0.5761	**185.9**	121.752	-81.668	-83.668	147.729	-34.497	0.00383378	61.02	2.16
1.5	1.12	0.5077	**153.1**	111.173	-63.077	-65.077	128.819	-30.343	0.00392161	62.41	2.15
1.8	1.14	0.4426	**129.4**	101.262	-49.706	-51.706	113.699	-27.050	0.00399969	63.66	2.13
2.1	1.16	0.3722	**109.3**	90.875	-38.390	-40.390	99.447	-23.963	0.00408408	65.00	2.10
2.4	1.17	0.3122	**95.4**	82.684	-30.786	-32.786	88.947	-21.629	0.00414406	65.95	2.06
3.4	1.22	0.1246	**64.2**	60.988	-15.251	-17.251	63.381	-15.794	0.00429436	68.35	1.88
4.4	1.25	-0.0232	**47.7**	46.608	-7.787	-9.787	47.624	-11.859	0.00431508	68.68	1.66
5.4	1.28	-0.1300	**38.5**	37.215	-3.957	-5.957	37.689	-9.094	0.00419376	66.75	1.42
6.4	1.31	-0.2251	**31.6**	31.008	-1.854	-3.854	31.247	-7.085	0.00394736	62.82	1.20
7.4	1.33	-0.2914	**27.4**	27.046	-0.784	-2.784	27.189	-5.877	0.00376618	59.94	1.05
10.5	1.40	-0.4272	**20.1**	20.022	0.609	-1.391	20.070	-3.974	0.00345295	54.96	0.79
15.6	1.48	-0.5400	**14.9**	15.001	1.261	-0.739	15.019	-2.820	0.00327606	52.14	0.60
20.6	1.54	-0.6076	**12.2**	12.289	1.570	-0.430	12.297	-2.004	0.00284383	45.26	0.45
30.4	1.64	-0.6847	**9.4**	9.535	1.719	-0.281	9.539	-1.688	0.00308808	49.15	0.39
40.4	1.73	-0.7271	**7.9**	8.037	1.857	-0.143	8.038	-1.019	0.00221315	35.22	0.24
55.4	1.82	-0.7671	**6.6**	6.765	1.882	-0.118	6.766	-0.999	0.00257759	41.02	0.24
70.4	1.93	-0.7904	**5.9**	5.972	1.878	-0.122	5.973	-1.170	0.00341931	54.42	0.29
85.4	2.01	-0.8069	**5.3**	5.482	1.904	-0.096	5.483	-1.003	0.00319345	50.83	0.25
105.4	2.11	-0.8203	**4.9**	5.027	1.909	-0.091	5.028	-1.037	0.00359982	57.29	0.26
125.4	2.20	-0.8311	**4.6**	4.733	1.882	-0.118	4.734	-1.428	0.00526428	83.78	0.36
145.4	2.28	-0.8391	**4.4**	4.501	1.901	-0.099	4.502	-1.260	0.00488435	77.74	0.32
165.2	2.36	-0.8425	**4.3**	4.371	1.818	-0.182	4.375	-2.384	0.00950950	151.35	0.61
195.2	2.48	-0.8478	**4.1**	4.227	1.800	-0.200	4.232	-2.709	0.01116849	177.75	0.69

Max Tau (ns)
2.16

Appendix D: TDR Validation Measurements

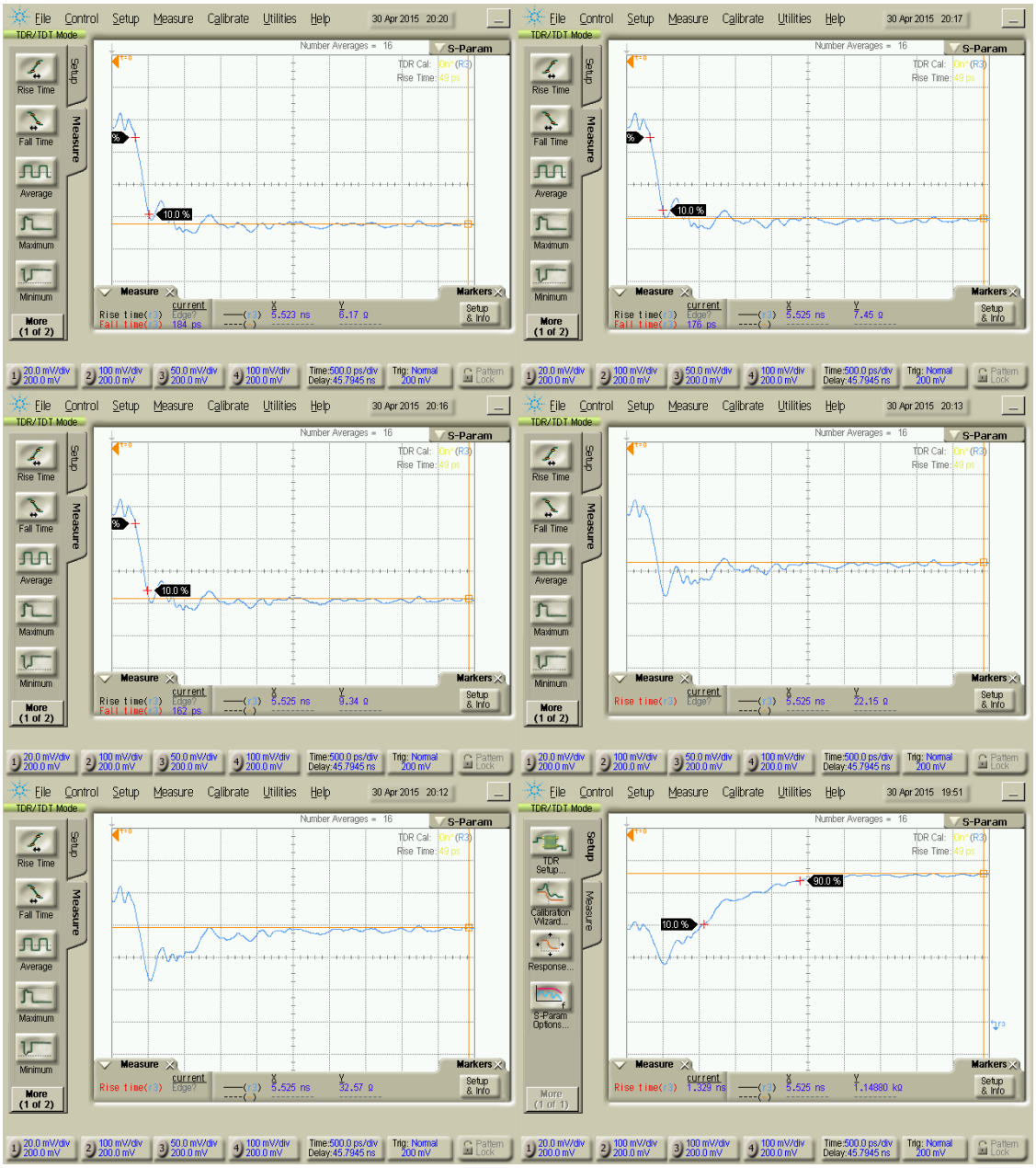

BM Section Response Time		
DC_Bias (mA)	**Dyn_R (Ω)**	**Tau (ns)**
200.0	**6.2**	0.300
130.6	**7.5**	0.30
75.1	**9.3**	0.25
10.1	**22.5**	0.50
4.5	**32.0**	0.70
0.0	**1148.0**	1.30

Appendix E: Tuning Map Matlab Functions

LASERMEASUREMENT()

```
% LASERMEASUREMENT() function summary:
% This function automates the collection of a tunable VT-DBR laser's
% wavelength, power, and spectral content as a function of control port
% bias current. The sample point resolution is user defined by inputing
the
% desired start, stop, and step of the bias current for the front and
back
% mirrors. This data can then be used to generate the laser's tuning
map.

function [ ] =
LaserMeasurement(FMstart,FMstop,FMstep,BMstart,BMstop,...
    BMstep,startsample)
% Determine FMspan and BMspan
    FMspan = FMstop-FMstart;
    BMspan = BMstop-BMstart;
% Condition variables to avoid erronious operation.
    floor(startsample);
% Configure FM and BM current drivers.
    %Find a GPIB object.
    BM = instrfind('Type', 'gpib', 'BoardIndex', 32,
'PrimaryAddress',...
        2, 'Tag', '');
    FM = instrfind('Type', 'gpib', 'BoardIndex', 32,
'PrimaryAddress',...
        1, 'Tag', '');

    % Create the GPIB object if it does not exist otherwise use the
object
    % that was found.
    if isempty(BM)
        BM = gpib('AGILENT', 32, 2);
    else
        fclose(BM);
        BM = BM(1);
    end

    if isempty(FM)
        FM = gpib('AGILENT', 32, 1);
    else
        fclose(FM);
        FM = FM(1);
    end
    %Connect to the FM and BM instruments.
    fopen(BM);
    fopen(FM);

    %Communicating with instruments BM and FM current drivers.
    fprintf(BM, '*RST');
    fprintf(BM, 'LAS:RAN 1');
    fprintf(BM, 'LAS:LIM:I1 101');
```

```
    fprintf(BM, 'LAS:MOD:ILBW');

    fprintf(FM, '*RST');
    fprintf(FM, 'LAS:RAN 1');
    fprintf(FM, 'LAS:LIM:I1 101');
    fprintf(FM, 'LAS:MOD:ILBW');

    % Increments along each axis determined by user input current range
and
    % step.
    FMnum = floor(FMspan/FMstep);
        if rem(FMspan,FMstep)>0.3*FMstep
            FMnum = FMnum+1;
        end
    BMnum = floor(BMspan/BMstep);
        if rem(BMspan,BMstep)>0.3*BMstep
            BMnum = BMnum+1;
        end
% If startsample < 2, create new excel data-file called
'TuningMap.xlsx'
% unless one already exist. Add new sheet to 'TuningMap.xlsx'.
warning off;
if startsample < 2;
    % Display number of samples to be taken
    fprintf([ num2str((FMnum+1)*(BMnum+1)) ' samples will be taken.']);
    % Create header object.
    parameters = {'Sample (#)', 'FM current bias (mA)',...
        'BM current bias (mA)', 'Wavelength (nm)', 'Amplitude (dBm)'};
    % Check to see if 'TuningMap.xls' already exists, if not create it.
Add
    % new sheet to 'TuningMap.xls'.
    if exist('TuningMap.xls', 'file') == 0
        time = fix(clock);
        sheetname = [num2str(time(2)) '.' num2str(time(3)) '.'...
            num2str(time(1)) '_@_' num2str(time(4)) '.'
num2str(time(5))...
            '.' num2str(time(6))];
        xlswrite('TuningMap', parameters(1), sheetname, 'a1:a1');
        xlswrite('TuningMap', parameters(2), sheetname, 'b1:b1');
        xlswrite('TuningMap', parameters(3), sheetname, 'c1:c1');
        xlswrite('TuningMap', parameters(4), sheetname, 'd1:d1');
        xlswrite('TuningMap', parameters(5), sheetname, 'e1:e1');
        %Delete extra blank sheets
        xls_sheet_delete();
    else
        %Ensure new sheetname is used and old data is not overwritten.
        time = fix(clock);
        sheetname = [num2str(time(2)) '.' num2str(time(3)) '.'...
            num2str(time(1)) '_@_' num2str(time(4)) '.'
num2str(time(5))...
            '.' num2str(time(6))];
        xlswrite('TuningMap', parameters(1), sheetname, 'a1:a1');
        xlswrite('TuningMap', parameters(2), sheetname, 'b1:b1');
        xlswrite('TuningMap', parameters(3), sheetname, 'c1:c1');
        xlswrite('TuningMap', parameters(4), sheetname, 'd1:d1');
        xlswrite('TuningMap', parameters(5), sheetname, 'e1:e1');
```

```
    end
    % Creat unique folder for OSA screen images to be collected; folder
    % name corresponds to sheet name in excel data document.
        mkdir(pwd, ['OSAimages_' sheetname]);
    % If startsample > 1, active sheet is the last sheet created in
    % 'TuningMap.xls'
    FMstartpos = 0;
    BMstartpos = 0;
else
    % Display number of samples to be taken.
    fprintf([ num2str((FMnum+1)*(BMnum+1)-(startsample-1))...
        ' samples will be taken.']);
    % Have user select sheet to append data to 'TuningMap.xls'; for
case
    % where data collection starts at startsample > 1.
        [~, sheets] = xlsfinfo('TuningMap.xls');
        for i = 1:length(sheets)
            disp([num2str(i) ' - ' char(sheets(i))]);
        end
    sheetname = char(sheets(input('Select the number corresponding to
the\nsheet you would like append data to: ')));
    % Determine current offset for FM and BM.
    FMstartpos = floor((startsample-1)/(BMnum+1));
    BMstartpos = rem((startsample-1),(BMnum+1));
warning on;
end
% Display how long it should take.
    duration = 1.08333*((FMnum+1)*(BMnum+1)-(startsample-1));
    days = floor(duration/1440);
    hours = floor(duration/60)-days*24;
    minutes = duration-days*1440-hours*60;
    fprintf(['\nThis should take approximately: ' num2str(days)...
        ' days, ' num2str(hours) ' hours, and '
num2str(floor(minutes))...
        ' minutes.\n\n']);
% Write current limits and increments to 'TuningMap.xls'.
    xlswrite('TuningMap', {'Current Limits:'}, sheetname, 'g1:g1');
    xlswrite('TuningMap', {'FM min (mA):'}, sheetname, 'g2:g2');
    xlswrite('TuningMap', {'FM max (mA):'}, sheetname, 'g3:g3');
    xlswrite('TuningMap', {'FM step (mA):'}, sheetname, 'g4:g4');
    xlswrite('TuningMap', {'BM min (mA):'}, sheetname, 'g5:g5');
    xlswrite('TuningMap', {'BM max (mA):'}, sheetname, 'g6:g6');
    xlswrite('TuningMap', {'BM step (mA):'}, sheetname, 'g7:g7');
    xlswrite('TuningMap', FMstart, sheetname, 'h2:h2');
    xlswrite('TuningMap', FMstop, sheetname, 'h3:h3');
    xlswrite('TuningMap', FMstep, sheetname, 'h4:h4');
    xlswrite('TuningMap', BMstart, sheetname, 'h5:h5');
    xlswrite('TuningMap', BMstop, sheetname, 'h6:h6');
    xlswrite('TuningMap', BMstep, sheetname, 'h7:h7');
% Turn current driver outputs on
    fprintf(FM, 'LAS:OUT 1');
    fprintf(BM, 'LAS:OUT 1');
% Loop through bias currents and run 'OSAdatafetch.m' at each bias
point.
    %FM control code (outer loop)
    for FMpos = FMstartpos:1:(FMnum)
    % Ensure current drivers are limited to the max current defined by
```

```
    % user's current settings.
    if FMpos*FMstep<(FMspan)
        FMsetpoint = ['LAS:LDI ' num2str(FMpos*FMstep + FMstart)];
        fprintf(FM, FMsetpoint);
    else
        FMsetpoint = ['LAS:LDI ' num2str(FMspan + FMstart)];
        fprintf(FM, FMsetpoint);
    end
        %BM control code (inner loop)
        for BMpos = BMstartpos:1:(BMnum)
            if BMpos*BMstep<(BMspan)
                BMsetpoint = ['LAS:LDI ' num2str(BMpos*BMstep +
BMstart)];
                fprintf(BM, BMsetpoint);
            else
                BMsetpoint = ['LAS:LDI ' num2str(BMspan + BMstart)];
                fprintf(BM, BMsetpoint);
            end

        %Determine 'sample_num', call OSAdatafetch and write data
        %to the 'TuningMap.xls' excel file.
            pause(1)
            sample_num = (BMnum+1)*FMpos + (BMpos+1);
            fprintf(['\nsample# ' num2str(sample_num) '/'...
                num2str((FMnum+1)*(BMnum+1))]);
            %Command OSA to find optical signal, take screen-shot,
            %and return wavelength and amplitude information.
            [wavelength, amp] = OSAdatafetch(sample_num, sheetname);
            %Determine bias currents and write to excel file
            fprintf(FM, 'LAS:LDI?');
            FMcurrent = str2double(fscanf(FM));
            xlswrite('TuningMap', FMcurrent, sheetname,...
                ['B' num2str(sample_num+1) ':B'
num2str(sample_num+1)]);
            fprintf(BM, 'LAS:LDI?');
            BMcurrent = str2double(fscanf(BM));
            xlswrite('TuningMap', BMcurrent, sheetname,...
                ['C' num2str(sample_num+1) ':C'
num2str(sample_num+1)]);
            BMstartpos = 0;
            % Write sample number, wavelength, and amplitude data
            % to the 'TuningMap.xls'.
            xlswrite('TuningMap', sample_num, sheetname,...
                ['A' num2str(sample_num+1) ':A'
num2str(sample_num+1)]);
            xlswrite('TuningMap', wavelength, sheetname,...
                ['D' num2str(sample_num+1) ':D'
num2str(sample_num+1)]);
            xlswrite('TuningMap', amp, sheetname,...
                ['E' num2str(sample_num+1) ':E'
num2str(sample_num+1)]);
        end
    end
% Turn instrument outputs 'off'.
fprintf(FM, 'LAS:OUT 0');
fprintf(BM, 'LAS:OUT 0');
```

```
fprintf(FM, 'LAS:LDI 0');
fprintf(BM, 'LAS:LDI 0');

% Format excel document (i.e. - autofit column width) and close it.
%=========================================================================
===
        % Selects all cells in the current worksheet and
        % auto-sizes all the columns and vertically and
        % horizontally aligns all the cell contents. Leaves
        % with cell A1 selected.

        try
        excelObject = actxserver('Excel.Application');
        excelWorkbook = excelObject.workbooks.Open([pwd
'\TuningMap.xls']);
        worksheets = excelObject.sheets;
        numSheets = worksheets.Count;



        % Loop over all sheets
        for currentSheet = 1 : numSheets
            thisSheet = get(worksheets, 'Item', currentSheet);
            invoke(thisSheet, 'Activate');
            % Center data in cells, and auto-size all
            % columns.
            try
                % Select the entire
                % spreadsheet.
                excelObject.Cells.Select;
                % Auto fit all the columns.
                excelObject.Cells.EntireColumn.AutoFit;
                % Center align the cell
                % contents.
                excelObject.Selection.HorizontalAlignment = 3;
                excelObject.Selection.VerticalAlignment = 2;
                % Put "cursor" or active cell
                % at A1, the upper left cell.
                excelObject.Range('A1').Select;
            catch ME
                errorMessage = sprintf(...
                    'Error in function.\n\nError Message:\n%s',
ME.message);
                fprintf('%s\n', errorMessage);
            end
        end
        catch ME
            errorMessage = sprintf(...
                'Error in function AutoSizeAllSheets.\n\nError
Message:\n%s', ME.message);
            fprintf('%s\n', errorMessage);
        end

        %Save and quit
        excelWorkbook.Save;
        excelObject.Quit;
```

```
        fclose('all');

% Close and clear all objects from memory.
 close all;
 clear all;
 disp('Data collected successfully!')

end



% This function is for communicating with the OSA instrument. Instument
is
%directed to acquire the optical signal with the largest power
magnitude;
%then the wavelength, power magnitude, and screen capture of the signal
are
%returned to the computer.
function [wavelength, amp] = OSAdatafetch(sample_num, sheetname)

% Find a GPIB object.
OSA = instrfind('Type', 'gpib', 'BoardIndex', 32, 'PrimaryAddress',
4,...
    'Tag', '');

% Create the GPIB object if it does not exist otherwise use the object
that
% was found.
if isempty(OSA)
    OSA = gpib('AGILENT', 32, 4);
else
    fclose(OSA);
    OSA = OSA(1);
end

% Configure OSA instrument.
set(OSA, 'EOIMode', 'on');
set(OSA, 'EOSMode', 'none');
set(OSA, 'InputBufferSize', 500000);
set(OSA, 'OutputBufferSize', 500000);
set(OSA, 'Timeout', 30.0);

% Connect to OSA instrument.
fopen(OSA);

% Initializing OSA instrument: remove write warnings, reset, adjust the
% verticle scale to 6.4 dB/div, and perform auto-measure.
warning('off','instrument:fread:unsuccessfulRead')
fprintf(OSA, '*rst');
fprintf(OSA, 'disp:trac:Y:scal:auto:pdiv 6.4 dB');
fprintf(OSA, 'disp:wind:trac:all:scal:auto; *wai');

% Continually sweep, set span to 2 nm, and set averaging to 20 sweeps.
```

```
fprintf(OSA, 'init:cont on');
fprintf(OSA, 'sens:wav:span 2 nm');
fprintf(OSA, 'calc1:aver:coun 20');
fprintf(OSA, 'calc1:aver:stat on');
pause(2)

% Move marker to peak, center trace data, adjust reference level to
peak.
fprintf(OSA, 'calc:mark1:max');
fprintf(OSA, 'calc:mark1:scen');
fprintf(OSA, 'calc:mark1:srl');
pause(6)

% Query wavelength (nm), query power level (dBm), record to excel file.
fprintf(OSA, 'calc:mark1:x?');
wavelength = str2double(fscanf(OSA))*10^9;
fprintf(['\nWavelength: ' num2str(wavelength,8) '(nm)']);
fprintf(OSA, 'calc:mark1:y?');
amp = str2double(fscanf(OSA));
fprintf(['\nPower: ' num2str(amp,6) '(dBm)\n']);

% Set OSA image data language to 'gif' format, ask for image data, and
% suppress data transfer warnings while reading data from OSA.
fprintf(OSA, 'HCOP:DEV:LANG ''GIF''');
fprintf(OSA, 'HCOP:DATA?');
raw = fread(OSA);



% Remove initial '#0' characters and EOI character from image data.
gooddata = raw(3:(length(raw)-1));

% Creating 'gif' image file containing screen capture
sample_num = num2str(sample_num);
filename = [ pwd '\OSAimages_' sheetname '\Num' sample_num
'_OSAcap.gif'];
fid = fopen(filename, 'w');
fwrite(fid, gooddata);
% disp([num2str(length(raw)) ' bytes of image-data transferred to '
% filename]);

% Disconnect all objects.
fclose(fid);
fclose(OSA);

% Clean up all objects.
delete(OSA);
clear OSA;

end



% This function deletes the first three excel sheets from a newly
created
% 'TuningMap.xls' file.
```

```
function [] = xls_sheet_delete()

XL_file = [pwd '\TuningMap.xls'];
xlsfinfo(XL_file);
% First open Excel as a COM Automation server
Excel = actxserver('Excel.Application');
% Make the application invisible
set(Excel, 'Visible', 0);
% Make excel not display alerts
set(Excel,'DisplayAlerts',0);
% Get a handle to Excel's Workbooks
Workbooks = Excel.Workbooks;
% Open an Excel Workbook and activate it
Workbook=Workbooks.Open(XL_file);
% Get the sheets in the active Workbook
Sheets = Excel.ActiveWorkBook.Sheets;
% Cycle through the sheets and delete them.
index_adjust = 0;
for i = 1:3
      current_sheet = get(Sheets, 'Item', 1);
      invoke(current_sheet, 'Delete')
      index_adjust = index_adjust +1;
end
% Now save the workbook
Workbook.Save;
% Close the workbook
Workbooks.Close;
% Quit Excel
invoke(Excel, 'Quit');
% Delete the handle to the ActiveX Object
delete(Excel);

end
```

TUNINGMAPPER()

```
% TUNINGMAPPER() function summary: This function takes the data
collected
% using LaserMeasurement() and maps the wavelength and power data into
% surface plots. The data is extracted from the 'TuningMap.xls' file in
the
% parent directory. Each data-set collected by LaserMeasurement()
generates
% a new sheet in the .xls file; the user is prompted to select the
data-set
% to process based on the .xls sheet name.

function [] =  TuningMapper()
% Close any open objects and clear memory.
    clear('all')
    close all
% Removes warning from lack of microsoft excel
    warning off;
```

```
% Find available sheets in 'TuningMap.xls' and prompt user to select
one.
    [~, sheets] = xlsfinfo('TuningMap.xls');
        for i = 1:length(sheets)
            disp([num2str(i) ' - ' char(sheets(i))]);
        end
    sheetname = char(sheets(input('Select the number corresponding
to\nthe sheet you would like to process: ')));
    map = str2double(input('\n1 - Wavelength tuning-map.\n2 - Power
tuning-map.\n3 - Wave & Pwr tuning-map.\nInput number corresponding
to\ndesired tuning-map generation: ', 's'));
% Read in current bias and wavelength data from 'TuningMap.xls' excel
file.
    [wavedata, ~ ]=xlsread('TuningMap.xls',sheetname);
    FMcurrent = wavedata(2:end,2);
    BMcurrent = wavedata(2:end,3);
    wavelength = wavedata(2:end,4);
    pwr = wavedata(2:end,5);
            % Give user option to import color-map range from another
            % tuning-map sheet.
            a = input('\nWould you like to import the colormap\nscale
from another sheet? (y/n) : ', 's');
            switch a
                case 'y'
                    fprintf('\n')
                    [~, sheets] = xlsfinfo('TuningMap.xls');
                    for i = 1:length(sheets)
                        disp([num2str(i) ' - ' char(sheets(i))]);
                    end
                    % Have user select sheet
                    crange_sheet = char(sheets(input('Select the sheet
containing the colormap\nscale you''d like to import: ')));
                    % Import colormap range from selected sheet
                    [wavedata, ~
]=xlsread('TuningMap.xls',crange_sheet);
                    cwavelength = wavedata(2:end,4);
                    cpwr =  wavedata(2:end,5);
                    % Filter caxis_pwr to remove outliers.
                            cpwrave = sum(cpwr)/length(cpwr);
                            for i = 1:length(cpwr)
                                if cpwr(i)<(cpwrave-5)
                                    cpwr(i) = cpwrave-5;
                                end
                            end
                    caxis_wave = [min(cwavelength) max(cwavelength)];
                    caxis_pwr = [min(cpwr) max(cpwr)];
                    fprintf('Colormap imported. Generating
figure(s).\n\n')
                case 'n'
                    fprintf('Default colormap range will be used.\n\n')
            end
            warning on;
% Determine wavelength and power ranges.
%     global deltawave global deltapwr
    deltawave = (max(wavelength)-min(wavelength));
    deltapwr = (max(pwr)-min(pwr));
```

```
        % Filter power data outliers due to multi-mode operation from
power
        % data.
            pwrave = sum(pwr)/length(pwr);
            for i = 1:length(pwr)
                if pwr(i)<(pwrave-.25*deltapwr)
                    pwr(i) = pwrave-.25*deltapwr;
                end
            end
            pwrave = sum(pwr)/length(pwr);
        % Redefine deltapwr with filtered data.
            deltapwr = (max(pwr)-min(pwr));
% Interpolate non-uniform map-data to generate surface plot.
    % Create uniform grid with linespace()
        xlin = linspace(min(FMcurrent),max(FMcurrent),...
            2*floor((max(BMcurrent)-min(BMcurrent))/...
            (BMcurrent(2)-BMcurrent(1))));
        ylin = linspace(min(BMcurrent),max(BMcurrent),...
            2*floor((max(BMcurrent)-min(BMcurrent))/...
            (BMcurrent(2)-BMcurrent(1))));
        % Now use these points to generate a uniformly spaced grid:
        [X,Y] = meshgrid(xlin,ylin);

    switch map
    % Code for wavelength figure generation.
        case 1 % case 1 = Wavelength tuning-map.
            % Wavelength figure: Create interpolated object 'f' from
            % wavelength data.
                f = scatteredInterpolant(FMcurrent, BMcurrent,
wavelength);
            % Evaluate 'f' at uniform vertices and save into 'Z'.
                Zw = f(X,Y);
            % Create surface plot for wavelength.
                F1 = figure(1);
                surf(X,Y,Zw, 'EdgeAlpha', 0.2); % Interpolated data Zw
used.
                axis tight;
                hold on
            % Plot nonuniform data points.

plot3(FMcurrent,BMcurrent,wavelength+deltawave/370,'.',...
                    'MarkerSize',4, 'MarkerEdgeColor', 'w');
            % Set DataCursor function
                dcm_obj = datacursormode(F1);
                set(dcm_obj, 'UpdateFcn', @DataCursorCallback)
            % Set caxis limits if importing colormap
                if a == 'y'
                    caxis(caxis_wave)
                end
            % Edit title and axis labels.
                title ('Wavelength Tuning Map');
                ylabel('BM (mA)');
                xlabel('FM (mA)');
                zlabel('\lambda (nm)');
            % Set background color
                whitebg('black')
```

```
            % Set viewpoint to default position
                set(gca,'CameraPosition', [307*((max(FMcurrent)-...
                    min(FMcurrent))/100), 392*((max(BMcurrent)-...
                    min(BMcurrent))/100), max(wavelength)+250*...
                    (max(wavelength)-min(wavelength))/36])
                set(gca,'CameraViewAngleMode', 'auto')
            % Print wavelength range to console.
                fprintf(['Wavelength range: ' num2str(min(wavelength))
...
                    ' (nm) - ' num2str(max(wavelength)) ' (nm).\n\n'])
    % Code for power-map figure generation.
        case 2 % case 2 = Power tuning-map.
            % Create interpolated object 'g' from power data.
                g = scatteredInterpolant(FMcurrent, BMcurrent, pwr);
            % Evaluate 'g' at uniform vertices and save into 'Z'
                Za = g(X,Y);
            % Create surface plot for power.
                F2 = figure(2);
                surf(X,Y,Za, 'EdgeAlpha', 0.2) %interpolated
                axis tight;
                hold on
            % Plot nonuniform data points.
                plot3(FMcurrent,BMcurrent,pwr+deltapwr/1150,'.',...
                    'MarkerSize',4, 'MarkerEdgeColor', 'w');
            % Set DataCursor function
                dcm_obj = datacursormode(F2);
                set(dcm_obj, 'UpdateFcn', @DataCursorCallback)
            % Set caxis limits if importing colormap
                if a == 'y'
                    caxis(caxis_pwr)
                end
            % Edit title and axis labels
                title ('Power Tuning Map');
                ylabel('BM (mA)');
                xlabel('FM (mA)');
                zlabel('Power (dBm)');
            % Set background color
                whitebg('black')
            % Set viewpoint to default position
                set(gca,'CameraPosition', [307*((max(FMcurrent)-...
                    min(FMcurrent))/100), 392*((max(BMcurrent)-...
                    min(BMcurrent))/100), pwrave + 5 + 55*...
                    (max(max(FMcurrent)-min(FMcurrent),...
                    max(BMcurrent)-min(BMcurrent))/100)])
                set(gca,'CameraViewAngleMode', 'auto')
            % Print power range to console.
                fprintf(['Average power: ' num2str(pwrave) ...
                    ' (dBm).\nMaximum power: ' num2str(max(pwr))...
                    ' (dBm).\n\n'])
    % Code for wavelength and power figure generation
        case 3 % case 3 = Wavelength and Power tuning-map
           % Wavelength figure:
            % Create interpolated object 'f' from wavelength data.
                f = scatteredInterpolant(FMcurrent, BMcurrent,
wavelength);
            % Evaluate 'f' at uniform vertices and save into 'Z'.
                Zw = f(X,Y);
```

```
            % Create surface plot for wavelength.
                F1 = figure(1);
                surf(X,Y,Zw, 'EdgeAlpha', 0.2);
                axis tight;
                hold on
            % Plot nonuniform data points.

plot3(FMcurrent,BMcurrent,wavelength+deltawave/370,'.',...
                    'MarkerSize',4, 'MarkerEdgeColor', 'w');
            % Set DataCursor function
                dcm_obj = datacursormode(F1);
                set(dcm_obj, 'UpdateFcn', @DataCursorCallback)
                assetData =
struct('WaveRange',deltawave,'PowerRange',...
                    deltapwr);
                setappdata(gca,'AssetData',assetData);
            % Set caxis limits if importing colormap
                if a == 'y'
                    caxis(caxis_wave)
                end
            % Edit title and axis labels.
                title ('Wavelength Tuning Map');
                ylabel('BM (mA)');
                xlabel('FM (mA)');
                zlabel('\lambda (nm)');
            % Set background color
                whitebg('black')
            % Set viewpoint to default position
                set(gca,'CameraPosition', [307*((max(FMcurrent)-...
                    min(FMcurrent))/100), 392*((max(BMcurrent)-...
                    min(BMcurrent))/100), max(wavelength)+250*...
                    (max(wavelength)-min(wavelength))/36])
                set(gca,'CameraViewAngleMode', 'auto')
            % Create interpolated object 'g' from power data.
                g = scatteredInterpolant(FMcurrent, BMcurrent, pwr);
            % Evaluate 'g' at uniform vertices and save into 'Z'
                Za = g(X,Y);
            % Create interplated surface plot of power.
                F2 = figure(2);
                surf(X,Y,Za, 'EdgeAlpha', 0.2);
                axis tight;
                hold on
            % Plot nonuniform data points.
                plot3(FMcurrent,BMcurrent,pwr+deltapwr/1150,'.',...
                    'MarkerSize',4, 'MarkerEdgeColor', 'w');
            % Set DataCursor function
                dcm_obj = datacursormode(F2);
                set(dcm_obj, 'UpdateFcn', @DataCursorCallback)
            % Set caxis limits if importing colormap
                if a == 'y'
                    caxis(caxis_pwr)
                end
            % Edit title and axis labels.
                title ('Power Tuning Map');
                ylabel('BM (mA)');
                xlabel('FM (mA)');
                zlabel('Power (dBm)');
```

```
            % Set background color
                whitebg('black')
            % Set viewpoint to default position
                set(gca,'CameraPosition', [307*((max(FMcurrent)-...
                    min(FMcurrent))/100), 392*((max(BMcurrent)-...
                    min(BMcurrent))/100), pwrave + 5 + 55*...
                    (max(max(FMcurrent)-
min(FMcurrent),max(BMcurrent)...
                    -min(BMcurrent))/100)])
                set(gca,'CameraViewAngleMode', 'auto')
            % Print wavelength range to console.
                fprintf(['Wavelength range: '
num2str(min(wavelength))...
                    ' (nm) to ' num2str(max(wavelength)) ' (nm).\n'])
            % Print power range to console.
                fprintf(['Average power: ' num2str(pwrave)...
                    ' (dBm).\nMaximum power: ' num2str(max(pwr))...
                    ' (dBm).\n\n'])
    end

% Save deltawave and deltapwr to memory for the 'DataCursorCallback'
% function.
    assetData = struct('WaveRange',deltawave,'PowerRange', deltapwr);
    setappdata(gca,'AssetData',assetData);
% Clean-up
    clear all;
    fclose('all');
    fprintf('Processing complete!\n\n')
end


function output_txt = DataCursorCallback(~,event_obj)
% Display the position of the data cursor obj          Currently not
used
% (empty) event_obj    Handle to event object output_txt   Data cursor
text
% string (string or cell array of strings).


% Get the parent of the target object (i.e. the axes):
    hAxes = get(get(event_obj,'Target'),'Parent');
    % Get the data stored with the axes object:
    assetData = getappdata(hAxes,'AssetData');


    pos = get(event_obj,'Position');

    output_txt = {['FM current (mA): ',num2str(pos(1),5)],...
        ['BM current (mA): ',num2str(pos(2),5)]};

    % If there is a Z-coordinate in the position, display it as well
    if gcf == 1
        output_txt{end+1} = ['Wavelength (nm): ',...
            num2str(pos(3)-assetData.WaveRange/370,8)];
    elseif gcf == 2
```

```
        output_txt{end+1} = ['Power (dBm): ',...
            num2str(pos(3)-assetData.PowerRange/1150,8)];
    end

end
```

TUNINGMAPVID()

```
% TUNINGMAPVID() function summary: This function creates a video using
a surface
% plot of the laser's tuning-map by rotating the the selected figure's
viewpoint
% and appending the resulting frame sequence to a video object which is
% then saved to the parent directory with the corresponding sheet name
% included in the file name.

function [] = TuningMapVid()

% Close any open objects and clear memory.
    clear('all')
    close all
% Set video format and file destination-path. Format options include:
% 'Motion JPEG AVI', 'Motion JPEG 2000','Uncompressed AVI',
and'Archival'.
    format = 'Uncompressed AVI';
    path = 'C:\Users\Greg\Desktop\';
% Determine sheet-names available in the 'TuningMap.xls' file. Prompt
user
% to select sheet and ask which map-videos to generate.
    warning off; % Removes warning from lack of microsoft excel.
    [~, sheets] = xlsfinfo('TuningMap.xls');
        for i = 1:length(sheets)
            disp([num2str(i) ' - ' char(sheets(i))]);
        end
    sheetname = char(sheets(input('Select the number corresponding
to\nthe sheet you would like to process: ')));
    map = str2double(input('\n1 - Wavelength tuning-map video.\n2 -
Power tuning-map video.\n3 - Wave & Pwr tuning-map videos.\nInput
number corresponding to\ndesired tuning map generation: ', 's'));
    precision = input('\nWhat is the desired number of\nviewpoint
incriments? (i.e. - any number > 0): ');
% Adjust framerate based on user input precision.
    if precision<=300
        framerate = floor(precision/25)+1;
    elseif precision>300
        framerate = 26;
    end
% Read in current bias and wavelength data from 'TuningMap.xls' excel
file.
    [wavedata,~] = xlsread('TuningMap.xls',sheetname);
    FMcurrent = wavedata(2:end,2);
    BMcurrent = wavedata(2:end,3);
    wavelength = wavedata(2:end,4);
    pwr = wavedata(2:end,5);
```

```
            % Give user option to import colormap range from another
            % tuning-map sheet.
            a = input('\nWould you like to import the colormap\nscale
from another sheet? (y/n) : ', 's');
            switch a
                case 'y'
                    [~, sheets] = xlsfinfo('TuningMap.xls');
                    fprintf('\n')
                    for i = 1:length(sheets)
                        disp([num2str(i) ' - ' char(sheets(i))]);
                    end
                    % Have user select sheet
                    crange_sheet = char(sheets(input('Select the sheet
containing the colormap\nscale you''d like to import: ')));
                    % Import colormap range from selected sheet
                    [wavedata, ~
]=xlsread('TuningMap.xls',crange_sheet);
                    cwavelength = wavedata(2:end,4);
                    cpwr =  wavedata(2:end,5);
                    % Filter caxis_pwr to remove outliers.
                            cpwrave = sum(cpwr)/length(cpwr);
                            for i = 1:length(cpwr)
                                if cpwr(i)<(cpwrave-5)
                                    cpwr(i) = cpwrave-5;
                                end
                            end
                    caxis_wave = [min(cwavelength) max(cwavelength)];
                    caxis_pwr = [min(cpwr) max(cpwr)];
                    disp('Colormap imported. Beginning data
collection...')
                case 'n'
                    disp('Default colormap range will be used.')
            end
    warning on;
% Set video's change in the following: field of view, viewpoint
elevation
% for wavelength-map, viewpoint elevation for power-map.
    % Set initial value and change in field of view.
        fov = 30+.35*(max(FMcurrent)-min(FMcurrent));
        deltafov = 5+.30*(max(FMcurrent)-min(FMcurrent));
    % Determine wavelength and power ranges.
    global deltawave
    global deltapwr
    deltawave = (max(wavelength)-min(wavelength));
    deltapwr = (max(pwr)-min(pwr));
        % Filter power data outliers due to multi-mode operation from
power
        % data.
            pwrave = sum(pwr)/length(pwr);
            for i = 1:length(pwr)
                if pwr(i)<(pwrave-.25*deltapwr)
                    pwr(i) = pwrave-.25*deltapwr;
                end
            end
            pwrave = sum(pwr)/length(pwr);
        % Redefine deltapwr with filtered data.
            deltapwr = (max(pwr)-min(pwr));
```

```
% Interpolate non-uniform map-data to generate surface plot.
    % Create uniform grid with linespace()
        xlin = linspace(min(FMcurrent),max(FMcurrent),floor((...
            max(BMcurrent)-min(BMcurrent))/(BMcurrent(2)-
BMcurrent(1))));
        ylin = linspace(min(BMcurrent),max(BMcurrent),floor((...
            max(BMcurrent)-min(BMcurrent))/(BMcurrent(2)-
BMcurrent(1))));
        % Now use these points to generate a uniformly spaced grid:
        [X,Y] = meshgrid(xlin,ylin);
% Beginning of conditional code selected by the user defined string
'map'.
    switch map
    % Code for wavelength-map video generation
        case 1 % Case 1 = Wavelength tuning-map video.
            % Create interpolated object 'f' from wavelength data.
                f = scatteredInterpolant(FMcurrent, BMcurrent,
wavelength);
            % Evaluate 'f' at uniform vertices and save into 'Z'.
                Zw = f(X,Y);
            % Create figure and generate surface plot.
                F1 = figure(1);
                surf(X,Y,Zw);
            % Edit figure properties
                axis tight;
                hold on
            % Plot nonuniform data points.

plot3(FMcurrent,BMcurrent,wavelength+deltawave/370,'.',...
                    'MarkerSize',4, 'MarkerEdgeColor', 'w');
            % Set DataCursor function
                dcm_obj = datacursormode(F1);
                set(dcm_obj, 'UpdateFcn', @DataCursorCallback,...
                    'DisplayStyle', 'window')
            % Set caxis limits if importing colormap
                if a == 'y'
                    caxis(caxis_wave)
                end
            % Edit title and axis labels.
                title ('Wavelength Tuning Map');
                ylabel('BM (mA)');
                xlabel('FM (mA)');
                zlabel('\lambda (nm)');
            % Make an animation of the tuning-map's wavelength data.
                % Set background color
                    whitebg('black')
            % Create video object
                animation = VideoWriter(['TuningMap_Wave_'
sheetname],...
                    format);
                animation.FrameRate = framerate;
                open(animation);
            % Manipulate plot view
                set(gca, 'CameraPositionMode', 'manual')
                set(gca,'CameraViewAngleMode','manual')
                set(gca,'CameraViewAngle', fov)
                set(gca, 'CameraTargetMode', 'manual')
```

```
                set(gca, 'CameraTarget', [(max(FMcurrent)+min(...
                    FMcurrent))/2, (max(BMcurrent)+min(BMcurrent))/2,
...
                    (sum(wavelength)/length(wavelength))])
                set(gca,'Box', 'on')
            % Camera position iteration
                for j=0:precision
                  % Camera position follows a downward spiral in space
                    x = (max(FMcurrent)+min(FMcurrent))/2+(max(...
                        FMcurrent)-min(FMcurrent))*cos(-
2*pi*j/precision);
                    y = (max(BMcurrent)+min(BMcurrent))/2+(max(...
                        BMcurrent)-min(BMcurrent))*sin(-
2*pi*j/precision);
                    z = max(wavelength)+(deltawave+1)-...
                        (j*(deltawave+1))/precision;
                    set(gca,'CameraPosition', [x,y,z])
                    set(gca,'CameraViewAngle', (fov -
j*deltafov/precision))
                  % Capture frame
                    M(j+1) = getframe(gcf);
                    writeVideo(animation,M(j+1));
                end
            % Free up memory, change field of view for next iteration
                close(animation);
                clear M
            % Set viewpoint to default position
                set(gca,'CameraPosition', [307*((max(FMcurrent)-...
                    min(FMcurrent))/100), 392*((max(BMcurrent)-...
                    min(BMcurrent))/100), max(wavelength)+250*...
                    (max(wavelength)-min(wavelength))/36])
                set(gca,'CameraViewAngleMode', 'auto')
            % Moves video files to the directory specified by the sting
            % 'path' on line 11.
                switch format
                    case {'Archival', 'Motion JPEG 2000'}
                        movefile(['TuningMap_Wave_' sheetname
'.mj2'],...
                            path, 'f');
                    case {'Motion JPEG AVI', 'Uncompressed AVI'}
                        movefile(['TuningMap_Wave_' sheetname
'.avi'],...
                            path, 'f');
                end

    % Code for power-map video generation
        case 2 % case 2 = Power tuning-map video.
            % Create interpolated object 'g' from power data.
                g = scatteredInterpolant(FMcurrent, BMcurrent, pwr);
            % Evaluate 'g' at uniform vertices and save into 'Z'
                Za = g(X,Y);
            % Create figure and generate surface plot.
                F2 = figure(2);
                surf(X,Y,Za);
            % Edit figure properties
                axis tight;
```

```
                hold on
            % Plot nonuniform data points.
                plot3(FMcurrent,BMcurrent,pwr+deltapwr/1150,'.',...
                    'MarkerSize',4, 'MarkerEdgeColor', 'w');
            % Set DataCursor function
                dcm_obj = datacursormode(F2);
                set(dcm_obj, 'UpdateFcn', @DataCursorCallback,...
                    'DisplayStyle', 'window')
            % Set caxis limits if importing colormap
                if a == 'y'
                    caxis(caxis_pwr)
                end
            % Edit title and axis labels.
                title ('Power Tuning Map');
                ylabel('BM (mA)');
                xlabel('FM (mA)');
                zlabel('Power (dBm)');
            % Make an animation of the tuning-map's power power data.
                % Set background color
                    whitebg('black')
            % Create video object
                animation = VideoWriter(['TuningMap_Pwr_'
sheetname],...
                    format);
                animation.FrameRate = framerate;
                open(animation);
            % Manipulate plot view
                set(gca, 'CameraPositionMode', 'manual')
                set(gca,'CameraViewAngleMode','manual')
                set(gca,'CameraViewAngle', fov)
                set(gca, 'CameraTargetMode', 'manual')
                set(gca, 'CameraTarget', [(max(FMcurrent)+min(...
                    FMcurrent))/2,
(max(BMcurrent)+min(BMcurrent))/2,...
                    (sum(pwr)/length(pwr))])
                set(gca,'Box', 'on')
            % Camera position iteration
                for j=0:precision
                  % Camera position follows a downward spiral in space
                      x = (max(FMcurrent)+min(FMcurrent))/2+(max(...
                          FMcurrent)-min(FMcurrent))*cos(-
2*pi*j/precision);
                      y = (max(BMcurrent)+min(BMcurrent))/2+(max(...
                          BMcurrent)-min(BMcurrent))*sin(-
2*pi*j/precision);
                      z = max(pwr)+deltapwr-(j*deltapwr)/precision;
                      set(gca,'CameraPosition', [x,y,z])
                      set(gca,'CameraViewAngle',...
                          (fov - j*deltafov/precision))
                  % Capture frame
                      M(j+1) = getframe(gcf);
                      writeVideo(animation,M(j+1));
                end
            % Free up memory, change field of view for next iteration
                close(animation);
                clear M
            % Set viewpoint to default position
```

```
                set(gca,'CameraPosition', [307*((max(FMcurrent)-...
                    min(FMcurrent))/100), 392*((max(BMcurrent)-...
                    min(BMcurrent))/100), pwrave + 5 + 55*(max(max(...
                    FMcurrent)-min(FMcurrent),max(BMcurrent)-...
                    min(BMcurrent))/100)])
                set(gca,'CameraViewAngleMode', 'auto')
            % Moves video files to the directory specified by the sting
            % 'path' on line 11.
                switch format
                    case {'Archival', 'Motion JPEG 2000'}
                        movefile(['TuningMap_Pwr_' sheetname
'.mj2'],...
                            path, 'f', 'f');
                    case {'Motion JPEG AVI', 'Uncompressed AVI'}
                        movefile(['TuningMap_Pwr_' sheetname
'.avi'],...
                            path, 'f');
                end

    % Code for wavelength and power tuning-map video generation.
        case 3 % case 3 = Wave and Pwr tuning-map videos are
generated.
            % Code for wavelength-map video generation Create
interpolated
            % object 'f' from wavelength data.
                f = scatteredInterpolant(FMcurrent, BMcurrent,
wavelength);
            % Evaluate 'f' at uniform vertices and save into 'Z'.
                Zw = f(X,Y);
            % Create figure, generate surface plot, and edit figure
properties.
                F1 = figure(1);
                surf(X,Y,Zw);
                axis tight;
                hold on
            % Plot nonuniform data points.

plot3(FMcurrent,BMcurrent,wavelength+deltawave/370,'.',...
                    'MarkerSize',4, 'MarkerEdgeColor', 'w');
            % Set DataCursor function
                dcm_obj = datacursormode(F1);
                set(dcm_obj, 'UpdateFcn', @DataCursorCallback,...
                    'DisplayStyle', 'window')
            % Set caxis limits if importing colormap
                if a == 'y'
                    caxis(caxis_wave)
                end
            % Edit title and axis labels.
                title ('Wavelength Tuning Map');
                ylabel('BM (mA)');
                xlabel('FM (mA)');
                zlabel('\lambda (nm)');
            % Make an animation of the tuning-map's wavelength data.
                % Set background color
                    whitebg('black')
            % Create video object
```

```
                animation = VideoWriter(['TuningMap_Wave_'
sheetname],...
                    format);
                animation.FrameRate = framerate;
                open(animation);
            % Manipulate plot view
                set(gca, 'CameraPositionMode', 'manual')
                set(gca,'CameraViewAngleMode','manual')
                set(gca,'CameraViewAngle', fov)
                set(gca, 'CameraTargetMode', 'manual')
                set(gca, 'CameraTarget', [(max(FMcurrent)+min(...
                    FMcurrent))/2, (max(BMcurrent)+min(BMcurrent))/2,
...
                    (sum(wavelength)/length(wavelength))])
                set(gca,'Box', 'on')
            % Camera position iteration
                for j=0:precision
                  % Camera position follows a downward spiral in space
                      x = (max(FMcurrent)+min(FMcurrent))/2+(max(...
                          FMcurrent)-min(FMcurrent))*cos(-
2*pi*j/precision);
                      y = (max(BMcurrent)+min(BMcurrent))/2+(max(...
                          BMcurrent)-min(BMcurrent))*sin(-
2*pi*j/precision);
                      z = max(wavelength)+(deltawave+1)-...
                          (j*(deltawave+1))/precision;
                      set(gca,'CameraPosition', [x,y,z])
                      set(gca,'CameraViewAngle', (fov -
j*deltafov/precision))
                    % Capture frame
                      M(j+1) = getframe(gcf);
                      writeVideo(animation,M(j+1));
                end
            % Free up memory, change field of view for next iteration
                close(animation);
                clear M
            % Set viewpoint to default position
                set(gca,'CameraPosition', [307*((max(FMcurrent)-min(...
                    FMcurrent))/100), 392*((max(BMcurrent)-min(...
                    BMcurrent))/100), max(wavelength)+250*(max(...
                    wavelength)-min(wavelength))/36])
                set(gca,'CameraViewAngleMode', 'auto')
            % Moves video files to the directory specified by the sting
            % 'path' on line 11.
                switch format
                    case {'Archival', 'Motion JPEG 2000'}
                        movefile( ['TuningMap_Wave_' sheetname
'.mj2'],...
                            path, 'f');
                    case {'Motion JPEG AVI', 'Uncompressed AVI'}
                        movefile( ['TuningMap_Wave_' sheetname
'.avi'],...
                            path, 'f');
                end
            % Create interpolated object 'g' from power data.
                g = scatteredInterpolant(FMcurrent, BMcurrent, pwr);
            % Evaluate 'g' at uniform vertices and save into 'Z'
```

```
                Za = g(X,Y);
            % Create figure, initialize viewpoint, and generate surface
            % plot.
                F2 = figure(2);
            % Generate surface with uniform vertices from interpolated
            % data.
                surf(X,Y,Za);
            % Edit figure properties
                axis tight;
                hold on
            % Plot nonuniform data points.
                plot3(FMcurrent,BMcurrent,pwr+deltapwr/1150,'.',...
                    'MarkerSize',4, 'MarkerEdgeColor', 'w');
            % Set DataCursor function
                dcm_obj = datacursormode(F2);
                set(dcm_obj, 'UpdateFcn', @DataCursorCallback,...
                    'DisplayStyle', 'window')
            % Set caxis limits if importing colormap
                if a == 'y'
                    caxis(caxis_pwr)
                end
            % Edit title and axis labels.
                title ('Power Tuning Map');
                ylabel('BM (mA)');
                xlabel('FM (mA)');
                zlabel('Power (dBm)');
            % Make an animation of the tuning-map's power power data.
                whitebg('black')
            % Create video object
                animation = VideoWriter(['TuningMap_Pwr_' sheetname],
format);
                animation.FrameRate = framerate;
                open(animation);
            % Manipulate plot view
                set(gca, 'CameraPositionMode', 'manual')
                set(gca,'CameraViewAngleMode','manual')
                set(gca,'CameraViewAngle', fov)
                set(gca, 'CameraTargetMode', 'manual')
                set(gca, 'CameraTarget', [(max(FMcurrent)+min(...
                    FMcurrent))/2,
(max(BMcurrent)+min(BMcurrent))/2,...
                    (sum(pwr)/length(pwr))])
                set(gca,'Box', 'on')
            % Camera position iteration
                for j=0:precision
                  % Camera position follows a downward spiral in space
                      x = (max(FMcurrent)+min(FMcurrent))/2+(max(...
                          FMcurrent)-min(FMcurrent))*cos(-
2*pi*j/precision);
                      y = (max(BMcurrent)+min(BMcurrent))/2+(max(...
                          BMcurrent)-min(BMcurrent))*sin(-
2*pi*j/precision);
                      z = max(pwr)+deltapwr-(j*deltapwr)/precision;
                      set(gca,'CameraPosition', [x,y,z])
                      set(gca,'CameraViewAngle',...
                          (fov - j*deltafov/precision))
                  % Capture frame
```

```
                    M(j+1) = getframe(gcf);
                    writeVideo(animation,M(j+1));
                end
                close(animation);
                clear M
            % Set viewpoint to default position
                set(gca,'CameraPosition', [307*((max(FMcurrent)-min(...
                    FMcurrent))/100), 392*((max(BMcurrent)-min(...
                    BMcurrent))/100), pwrave + 5 + 55*(max(max(...
                    FMcurrent)-min(FMcurrent),max(BMcurrent)-min(...
                    BMcurrent))/100)])
                set(gca,'CameraViewAngleMode', 'auto')
            % Moves video files to the directory specified by the sting
            % 'path' on line 11.
                switch format
                    case {'Archival', 'Motion JPEG 2000'}
                        movefile(['TuningMap_Pwr_' sheetname
'.mj2'],...
                            path, 'f');
                    case {'Motion JPEG AVI', 'Uncompressed AVI'}
                        movefile(['TuningMap_Pwr_' sheetname
'.avi'],...
                            path, 'f');
                end
    end
    fprintf('\nProcessing complete!\n\n')
end

function output_txt = DataCursorCallback(~,event_obj)
% This function displays the position of the data cursor object.
global deltawave
global deltapwr
pos = get(event_obj,'Position');

output_txt = {['FM current (mA): ',num2str(pos(1),5)],...
    ['BM current (mA): ',num2str(pos(2),5)]};
% If there is a Z-coordinate in the position, display it as well
if gcf == 1
    output_txt{end+1} = ['Wavelength (nm): ',...
        num2str(pos(3)-deltawave/370,8)];
elseif gcf == 2
    output_txt{end+1} = ['Power (dBm): ',...
        num2str(pos(3)-deltapwr/1150,8)];
end
end
```

Appendix F: Neptune - Tuning Map Collection and Data

The following file icon links to the embedded “TuningMap.xls” file which contains all the tabulated tuning map data collected from the Neptune laser. To access the data, ensure excel is installed on your computer and double click the file below.

To analyze the data, have MatLab installed on your computer and use the “TuningMapper()” function below. The “TuningMap.xls” file must be copied to the same directory as the function.

To create a novel video of a tuning map, use the “TuningMapVid()” MatLab function below. Again, the “TuningMap.xls” file must be in the same directory as the function.

The MatLab function “LaserMeasurement()” below is a useful tool for future VT-DBR tuning map collection.

Appendix G: Neptune - SMSR Screen Captures

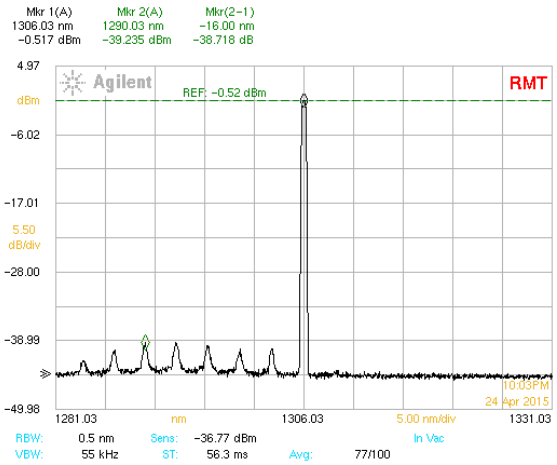

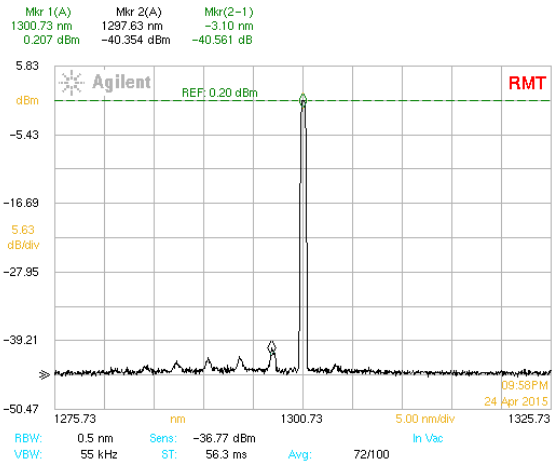

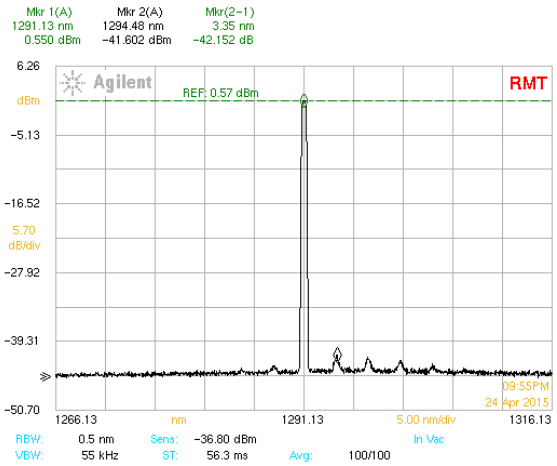

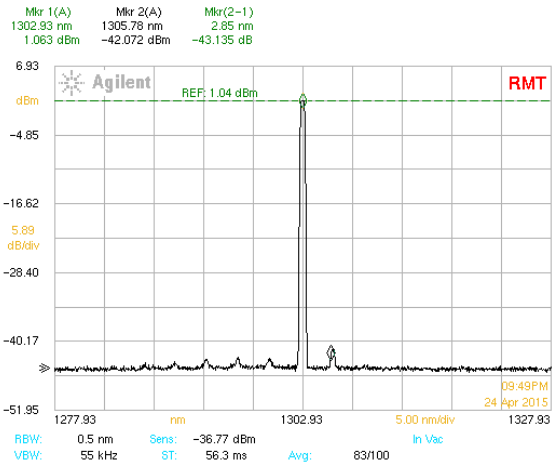

Measurement	FM Bias (mA)	BM Bias (mA)	Wavelength (nm)	SMSR (dB)
1	0	0	1302.93	43.1
2	0	41.72	1291.13	42.2
3	38.42	41.72	1300.73	40.6
4	68.71	0	1306.03	38.7

Appendix H: Neptune - Additional OSA and Linewidth Measurements

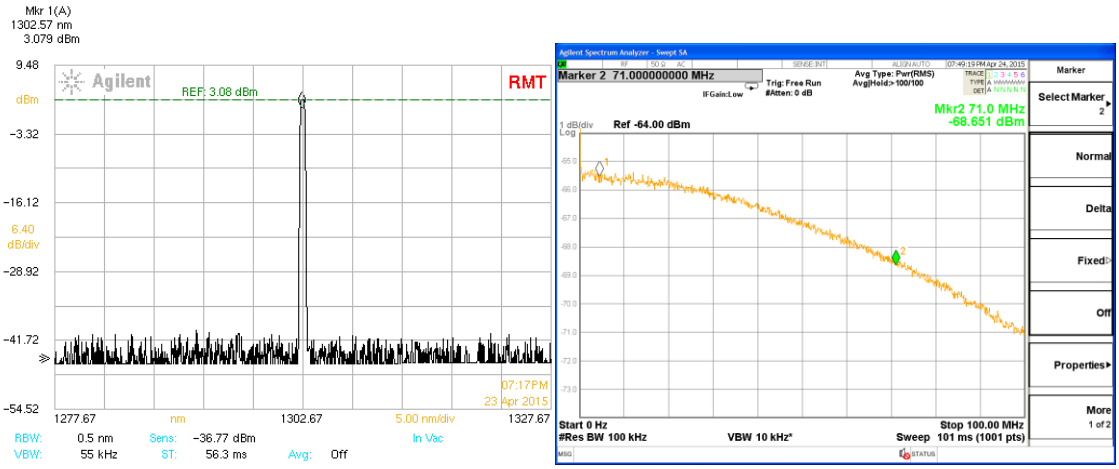

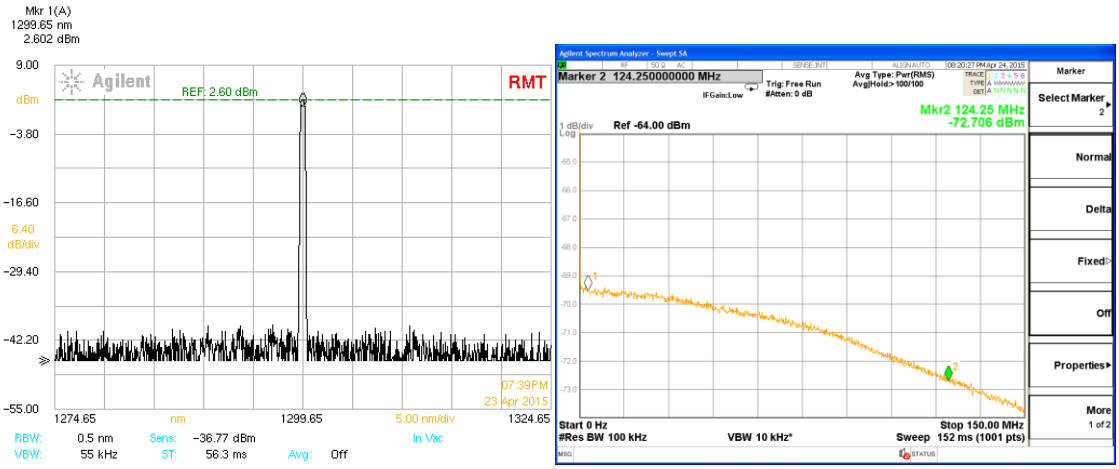

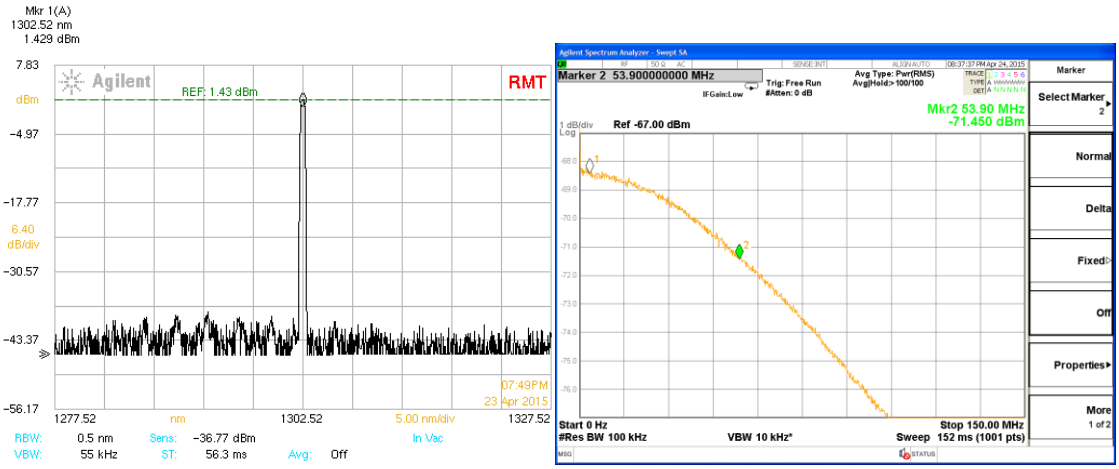

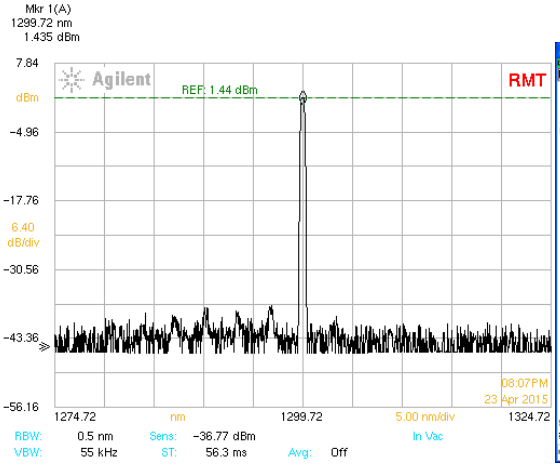
Mkr 1(A)
1299.72 nm
1.435 dBm
Agilent
REF: 1.44 dBm
RMT
7.84
dBm
-4.96
-17.76
6.40
dB/div
-30.56
-43.36
-56.16
08:07 PM
23 Apr 2015
1274.72
nm
1299.72
5.00 nm/div
1324.72
RBW: 0.5 nm
Sens: -36.77 dBm
In Vac
VBW: 55 kHz
ST: 56.3 ms
Avg: Off

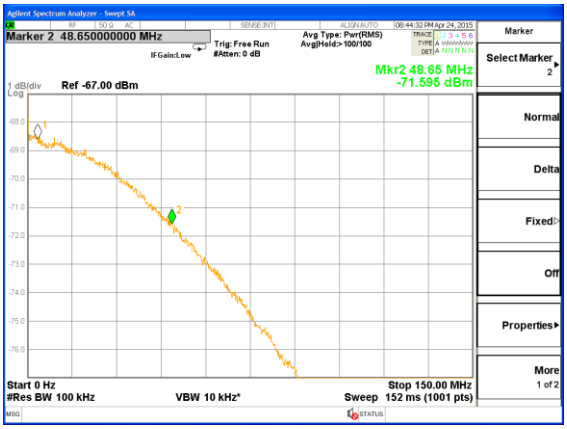
Agilent Spectrum Analyzer - Swept SA
Marker 2 48.650000000 MHz
Trig: Free Run
#Atten: 0 dB
Avg Type: Pwr(RMS)
Avg|Hold:>100/100
Mkr2 48.65 MHz
-71.595 dBm
1 dB/div
Ref -67.00 dBm
Start 0 Hz
#Res BW 100 kHz
VBW 10 kHz*
Stop 150.00 MHz
Sweep 152 ms (1001 pts)
Marker
Select Marker
Normal
Delta
Fixed
Off
Properties
More
1 of 2

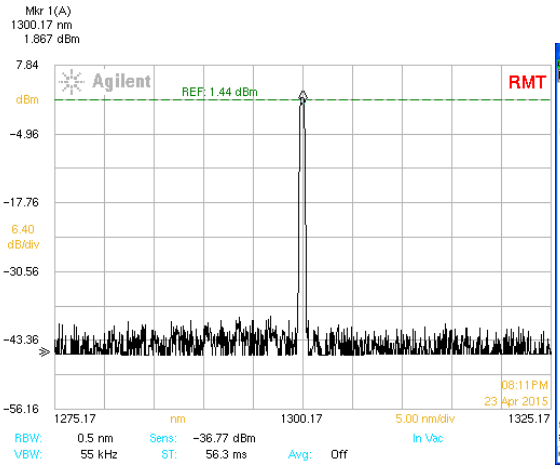
Mkr 1(A)
1300.17 nm
1.867 dBm
Agilent
REF: 1.44 dBm
RMT
7.84
dBm
-4.96
-17.76
6.40
dB/div
-30.56
-43.36
-56.16
08:11 PM
23 Apr 2015
1275.17
nm
1300.17
5.00 nm/div
1325.17
RBW: 0.5 nm
Sens: -36.77 dBm
In Vac
VBW: 55 kHz
ST: 56.3 ms
Avg: Off

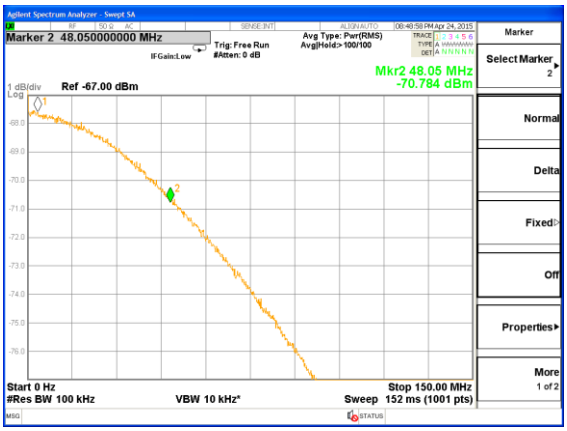
Agilent Spectrum Analyzer - Swept SA
Marker 2 48.050000000 MHz
Trig: Free Run
#Atten: 0 dB
Avg Type: Pwr(RMS)
Avg|Hold:>100/100
Mkr2 48.05 MHz
-70.784 dBm
1 dB/div
Ref -67.00 dBm
Start 0 Hz
#Res BW 100 kHz
VBW 10 kHz*
Stop 150.00 MHz
Sweep 152 ms (1001 pts)
Marker
Select Marker
Normal
Delta
Fixed
Off
Properties
More
1 of 2

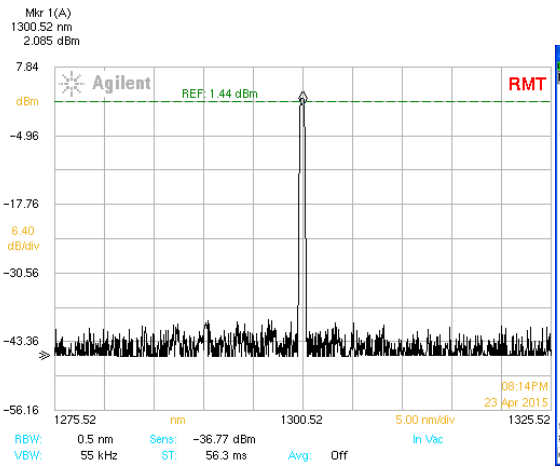
Mkr 1(A)
1300.52 nm
2.085 dBm
Agilent
REF: 1.44 dBm
RMT
7.84
dBm
-4.96
-17.76
6.40
dB/div
-30.56
-43.36
-56.16
08:14 PM
23 Apr 2015
1275.52
nm
1300.52
5.00 nm/div
1325.52
RBW: 0.5 nm
Sens: -36.77 dBm
In Vac
VBW: 55 kHz
ST: 56.3 ms
Avg: Off

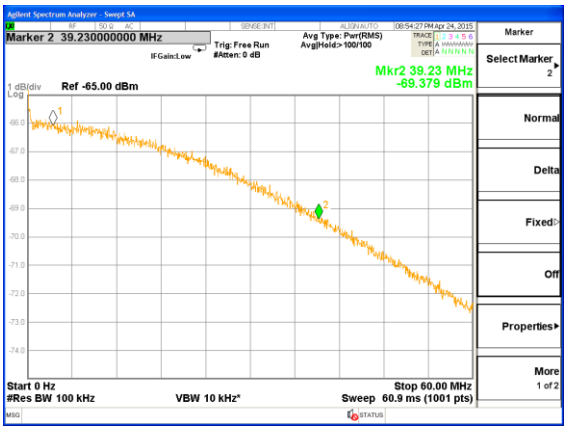
Agilent Spectrum Analyzer - Swept SA
Marker 2 39.230000000 MHz
Trig: Free Run
#Atten: 0 dB
Avg Type: Pwr(RMS)
Avg|Hold:>100/100
Mkr2 39.23 MHz
-69.379 dBm
1 dB/div
Ref -65.00 dBm
Start 0 Hz
#Res BW 100 kHz
VBW 10 kHz*
Stop 60.00 MHz
Sweep 60.9 ms (1001 pts)
Marker
Select Marker
Normal
Delta
Fixed
Off
Properties
More
1 of 2

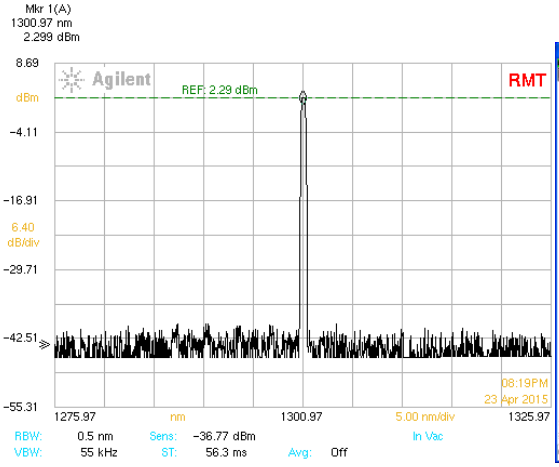
Mkr 1(A)
1300.97 nm
2.299 dBm
8.69
dBm
-4.11
-16.91
6.40
dB/div
-29.71
-42.51
-55.31
Agilent
REF: 2.29 dBm
RMT
08:19PM
23 Apr 2015
1275.97
nm
1300.97
5.00 nm/div
1325.97
RBW: 0.5 nm
Sens: -36.77 dBm
In Vac
VBW: 55 kHz
ST: 56.3 ms
Avg: Off

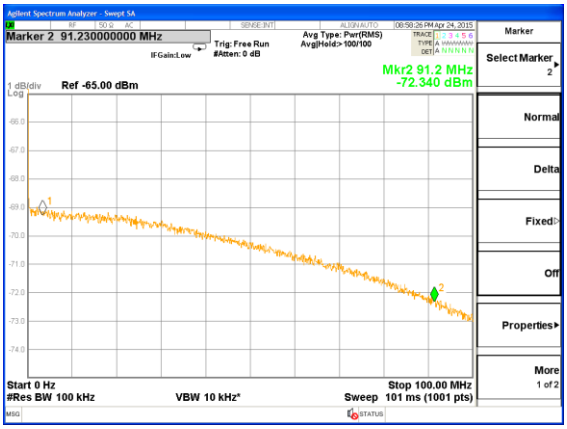
Agilent Spectrum Analyzer - Swept SA
Marker 2 91.230000000 MHz
Trig: Free Run
#Atten: 0 dB
Avg Type: Pwr(RMS)
Avg|Hold:>100/100
Mkr2 91.2 MHz
-72.340 dBm
1 dB/div
Ref -65.00 dBm
Start 0 Hz
#Res BW 100 kHz
VBW 10 kHz*
Stop 100.00 MHz
Sweep 101 ms (1001 pts)
Marker
Select Marker
Normal
Delta
Fixed
Off
Properties
More
1 of 2

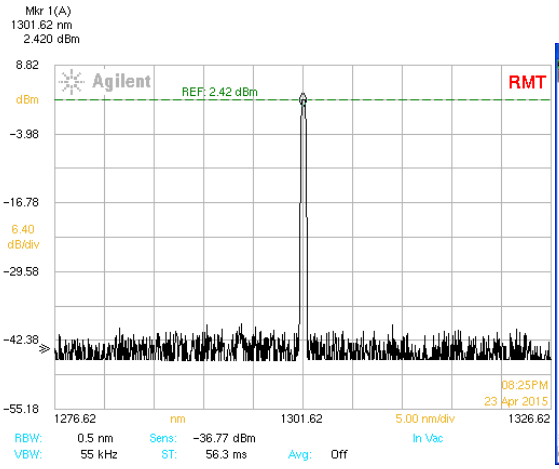
Mkr 1(A)
1301.62 nm
2.420 dBm
8.82
dBm
-3.98
-16.78
6.40
dB/div
-29.58
-42.38
-55.18
Agilent
REF: 2.42 dBm
RMT
08:25PM
23 Apr 2015
1276.62
nm
1301.62
5.00 nm/div
1326.62
RBW: 0.5 nm
Sens: -36.77 dBm
In Vac
VBW: 55 kHz
ST: 56.3 ms
Avg: Off

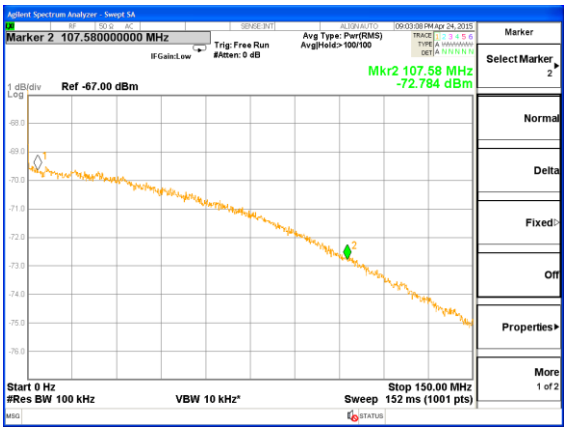
Agilent Spectrum Analyzer - Swept SA
Marker 2 107.580000000 MHz
Trig: Free Run
#Atten: 0 dB
Avg Type: Pwr(RMS)
Avg|Hold:>100/100
Mkr2 107.58 MHz
-72.784 dBm
1 dB/div
Ref -67.00 dBm
Start 0 Hz
#Res BW 100 kHz
VBW 10 kHz*
Stop 150.00 MHz
Sweep 152 ms (1001 pts)
Marker
Select Marker
Normal
Delta
Fixed
Off
Properties
More
1 of 2

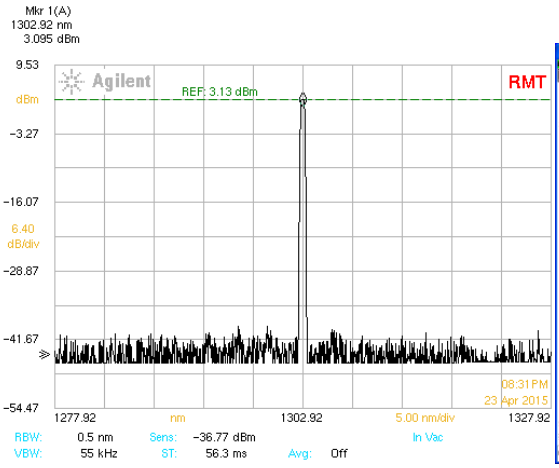
Mkr 1(A)
1302.92 nm
3.095 dBm
9.53
dBm
-3.27
-16.07
6.40
dB/div
-28.87
-41.67
-54.47
Agilent
REF: 3.13 dBm
RMT
08:31PM
23 Apr 2015
1277.92
nm
1302.92
5.00 nm/div
1327.92
RBW: 0.5 nm
Sens: -36.77 dBm
In Vac
VBW: 55 kHz
ST: 56.3 ms
Avg: Off

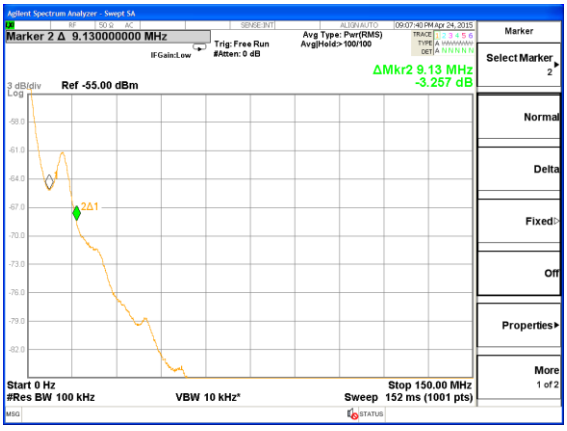
Agilent Spectrum Analyzer - Swept SA
Marker 2 Δ 9.130000000 MHz
Trig: Free Run
#Atten: 0 dB
Avg Type: Pwr(RMS)
Avg|Hold:>100/100
ΔMkr2 9.13 MHz
-3.257 dB
3 dB/div
Ref -55.00 dBm
2Δ1
Start 0 Hz
#Res BW 100 kHz
VBW 10 kHz*
Stop 150.00 MHz
Sweep 152 ms (1001 pts)
Marker
Select Marker
Normal
Delta
Fixed
Off
Properties
More
1 of 2

Appendix I: VTL-2 - SMSR Screen Captures

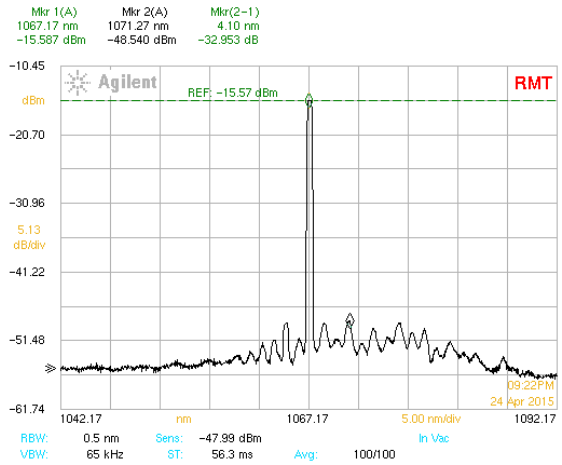

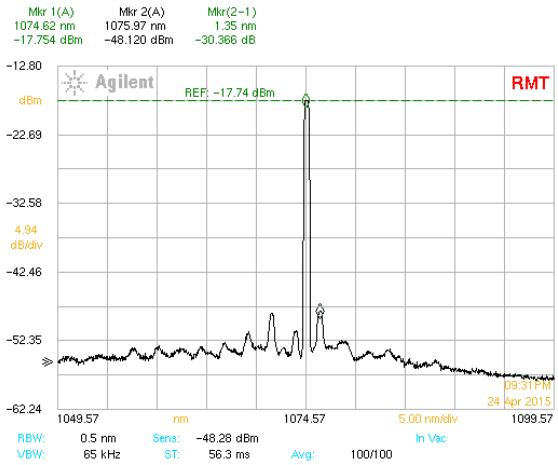

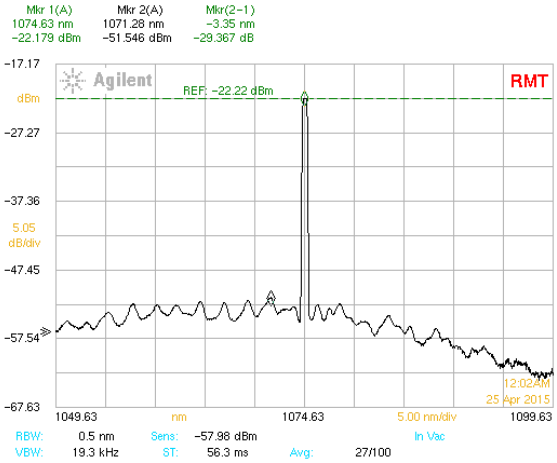

Measurement	FM Bias (mA)	BM Bias (mA)	Wavelength (nm)	SMSR (dB)
1	0	0	1302.93	43.1
2	0	41.72	1291.13	42.2
3	38.42	41.72	1300.73	40.6

Appendix J: VTL-2 - Linewidth Measurement Screen Captures

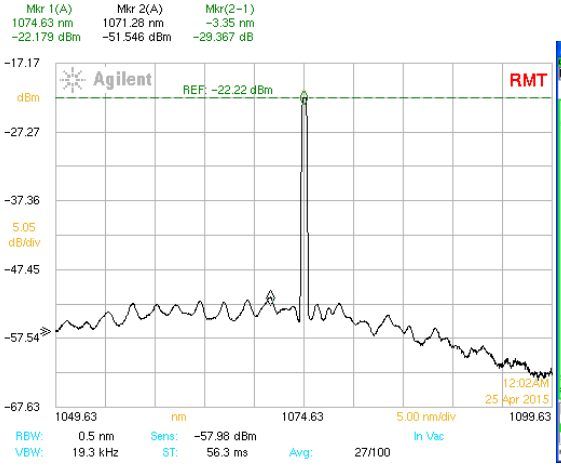

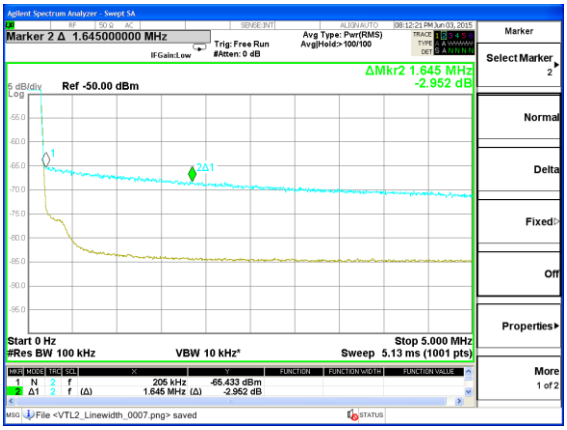

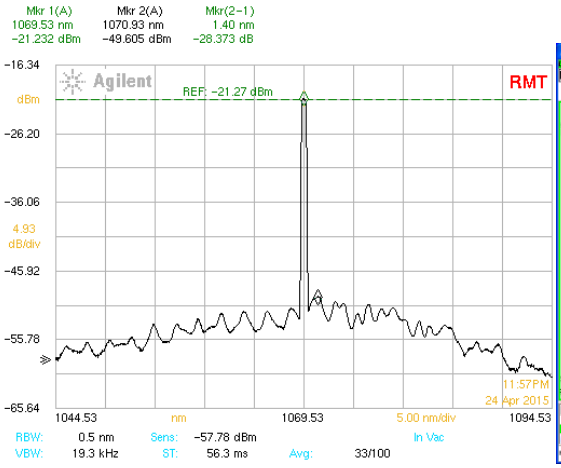

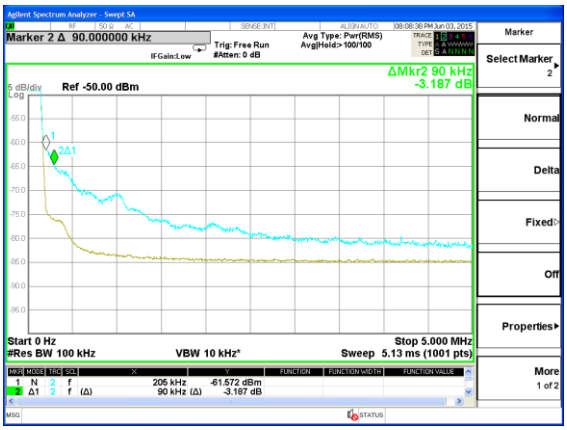

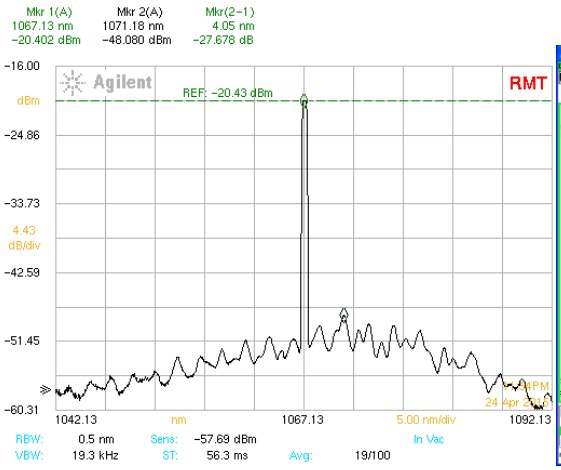

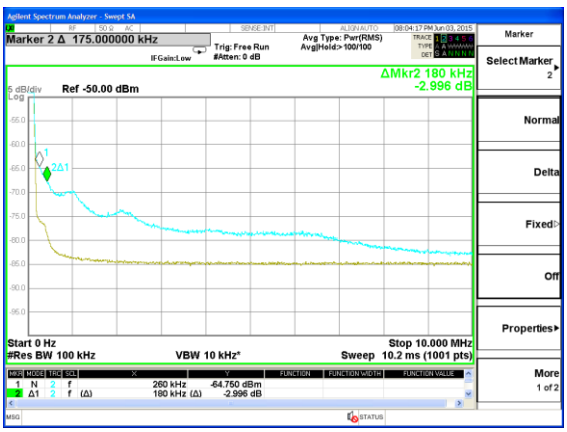

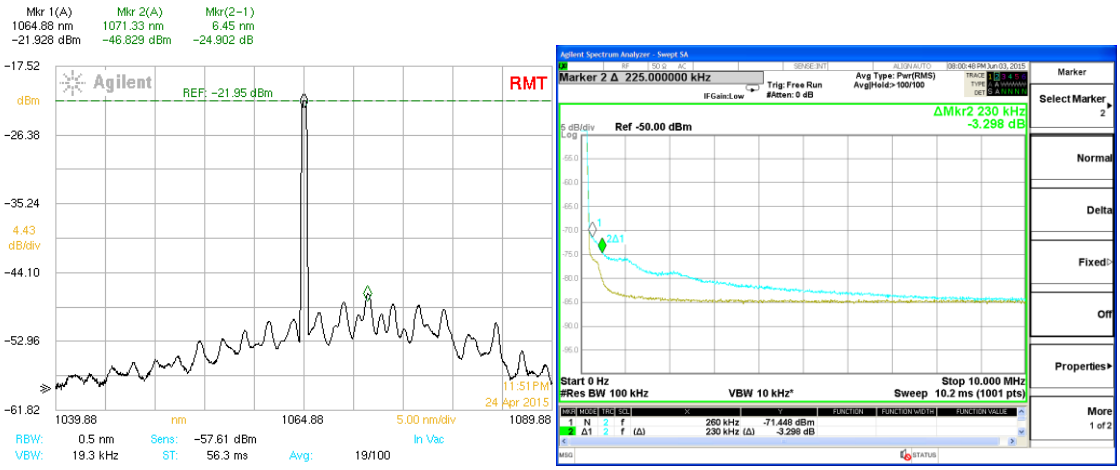
Mkr 1(A) 1064.88 nm −21.928 dBm
Mkr 2(A) 1071.33 nm −46.829 dBm
Mkr(2−1) 6.45 nm −24.902 dB
Agilent
REF: −21.95 dBm
RMT
−17.52
dBm
−26.38
−35.24
4.43 dB/div
−44.10
−52.96
−61.82
11:51 PM 24 Apr 2015
1039.88 nm 1064.88 5.00 nm/div 1089.88
RBW: 0.5 nm Sens: −57.61 dBm In Vac
VBW: 19.3 kHz ST: 56.3 ms Avg: 19/100
Agilent Spectrum Analyzer - Swept SA
Marker 2 Δ 225.000000 kHz
Trig: Free Run #Atten: 0 dB
Avg Type: Pwr(RMS) Avg|Hold:>100/100
ΔMkr2 230 kHz -3.298 dB
5 dB/div Ref -50.00 dBm
Start 0 Hz #Res BW 100 kHz
VBW 10 kHz* Stop 10.000 MHz Sweep 10.2 ms (1001 pts)
1 N 2 f 260 kHz -71.448 dBm
2 Δ1 2 f (Δ) 230 kHz (Δ) -3.298 dB
Marker
Select Marker
Normal
Delta
Fixed
Off
Properties
More 1 of 2

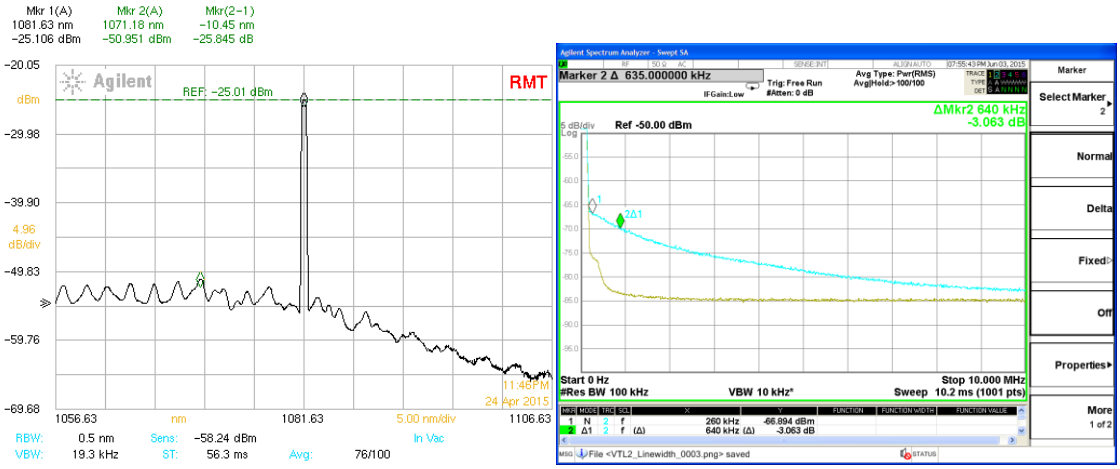
Mkr 1(A) 1081.63 nm −25.106 dBm
Mkr 2(A) 1071.18 nm −50.951 dBm
Mkr(2−1) −10.45 nm −25.845 dB
Agilent
REF: −25.01 dBm
RMT
−20.05
dBm
−29.98
−39.90
4.96 dB/div
−49.83
−59.76
−69.68
11:48 PM 24 Apr 2015
1056.63 nm 1081.63 5.00 nm/div 1106.63
RBW: 0.5 nm Sens: −58.24 dBm In Vac
VBW: 19.3 kHz ST: 56.3 ms Avg: 76/100
Agilent Spectrum Analyzer - Swept SA
Marker 2 Δ 635.000000 kHz
Trig: Free Run #Atten: 0 dB
Avg Type: Pwr(RMS) Avg|Hold:>100/100
ΔMkr2 640 kHz -3.063 dB
5 dB/div Ref -50.00 dBm
Start 0 Hz #Res BW 100 kHz
VBW 10 kHz* Stop 10.000 MHz Sweep 10.2 ms (1001 pts)
1 N 2 f 260 kHz -66.894 dBm
2 Δ1 2 f (Δ) 640 kHz (Δ) -3.063 dB
File <VTL2_Linewidth_0003.png> saved
Marker
Select Marker
Normal
Delta
Fixed
Off
Properties
More 1 of 2

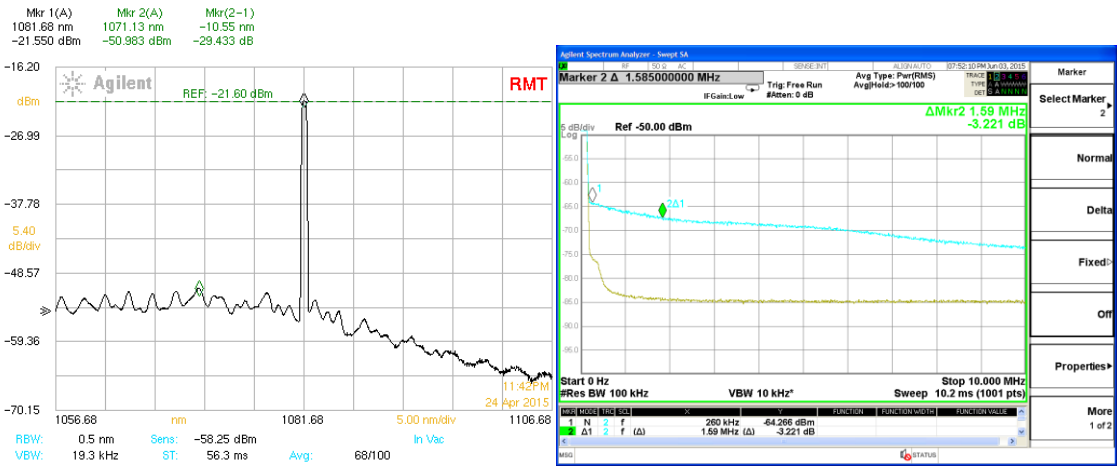
Mkr 1(A) 1081.68 nm −21.550 dBm
Mkr 2(A) 1071.13 nm −50.983 dBm
Mkr(2−1) −10.55 nm −29.433 dB
Agilent
REF: −21.60 dBm
RMT
−16.20
dBm
−26.99
−37.78
5.40 dB/div
−48.57
−59.36
−70.15
11:42 PM 24 Apr 2015
1056.68 nm 1081.68 5.00 nm/div 1106.68
RBW: 0.5 nm Sens: −58.25 dBm In Vac
VBW: 19.3 kHz ST: 56.3 ms Avg: 68/100
Agilent Spectrum Analyzer - Swept SA
Marker 2 Δ 1.585000000 MHz
Trig: Free Run #Atten: 0 dB
Avg Type: Pwr(RMS) Avg|Hold:>100/100
ΔMkr2 1.59 MHz -3.221 dB
5 dB/div Ref -50.00 dBm
Start 0 Hz #Res BW 100 kHz
VBW 10 kHz* Stop 10.000 MHz Sweep 10.2 ms (1001 pts)
1 N 2 f 260 kHz -64.266 dBm
2 Δ1 2 f (Δ) 1.59 MHz (Δ) -3.221 dB
Marker
Select Marker
Normal
Delta
Fixed
Off
Properties
More 1 of 2

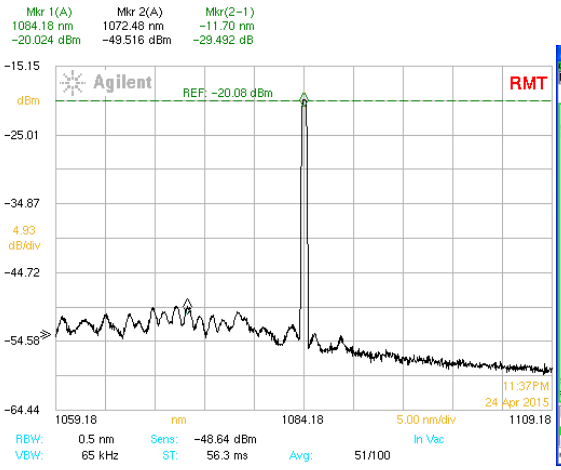
Mkr 1(A)
1084.18 nm
-20.024 dBm
Mkr 2(A)
1072.48 nm
-49.516 dBm
Mkr(2-1)
-11.70 nm
-29.492 dB
Agilent
REF: -20.08 dBm
RMT
-15.15
dBm
-25.01
-34.87
4.93
dB/div
-44.72
-54.58
-64.44
11:37PM
24 Apr 2015
1059.18
nm
1084.18
5.00 nm/div
1109.18
RBW: 0.5 nm
Sens: -48.64 dBm
In Vac
VBW: 65 kHz
ST: 56.3 ms
Avg: 51/100

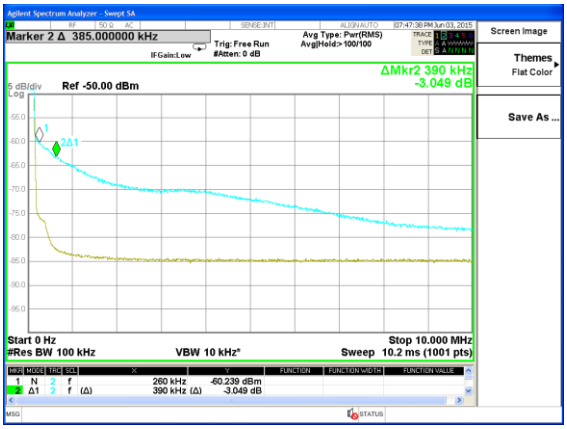
Agilent Spectrum Analyzer - Swept SA
Marker 2 Δ 385.000000 kHz
Trig: Free Run
#Atten: 0 dB
Avg Type: Pwr(RMS)
Avg|Hold:>100/100
ΔMkr2 390 kHz
-3.049 dB
5 dB/div
Ref -50.00 dBm
Start 0 Hz
#Res BW 100 kHz
VBW 10 kHz*
Stop 10.000 MHz
Sweep 10.2 ms (1001 pts)
1 N 2 f 260 kHz -60.239 dBm
2 Δ1 2 f (Δ) 390 kHz (Δ) -3.049 dB
Screen Image
Themes
Flat Color
Save As ...

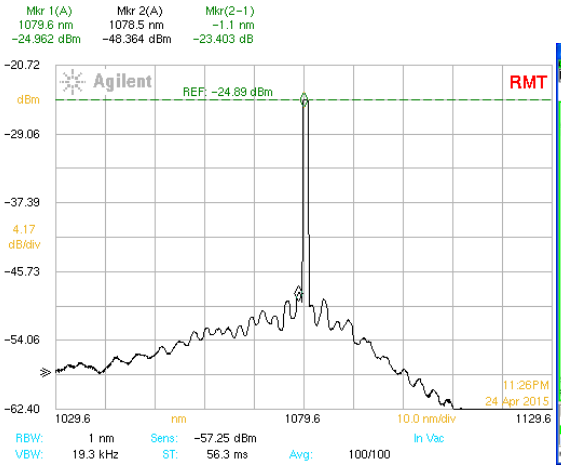
Mkr 1(A)
1079.6 nm
-24.962 dBm
Mkr 2(A)
1078.5 nm
-48.364 dBm
Mkr(2-1)
-1.1 nm
-23.403 dB
Agilent
REF: -24.89 dBm
RMT
-20.72
dBm
-29.06
-37.39
4.17
dB/div
-45.73
-54.06
-62.40
11:26PM
24 Apr 2015
1029.6
nm
1079.6
10.0 nm/div
1129.6
RBW: 1 nm
Sens: -57.25 dBm
In Vac
VBW: 19.3 kHz
ST: 56.3 ms
Avg: 100/100

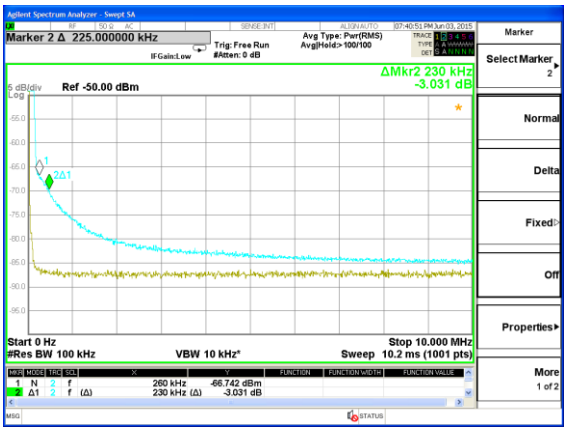
Agilent Spectrum Analyzer - Swept SA
Marker 2 Δ 225.000000 kHz
Trig: Free Run
#Atten: 0 dB
Avg Type: Pwr(RMS)
Avg|Hold:>100/100
ΔMkr2 230 kHz
-3.031 dB
5 dB/div
Ref -50.00 dBm
Start 0 Hz
#Res BW 100 kHz
VBW 10 kHz*
Stop 10.000 MHz
Sweep 10.2 ms (1001 pts)
1 N 2 f 260 kHz -66.742 dBm
2 Δ1 2 f (Δ) 230 kHz (Δ) -3.031 dB
Marker
Select Marker
Normal
Delta
Fixed
Off
Properties
More
1 of 2

Appendix K: TDR, FDR, and RLC Data of Neptune Laser

The following icon links to a ".zip" file that contains all the FDR, TDR, and RLC measurements of the Neptune laser. To open the file, ensure a software decompression program like WinRar or 7zip is installed on your computer; then, click the icon below.

Neptune TDR, FDR, and RLC Data.zip

Appendix L: TDR, FDR, and RLC Data of VTL-2 Laser

The following icon links to a ".zip" file that contains all the FDR, TDR, and RLC measurements of the VTL-2 laser. To open the file, ensure a software decompression program like WinRar or 7zip is installed on your computer; then, click the icon below.

VTL2 TDR, FDR, and RLC Data.zip

Appendix M: Photograph of Automated Tuning Map Collection

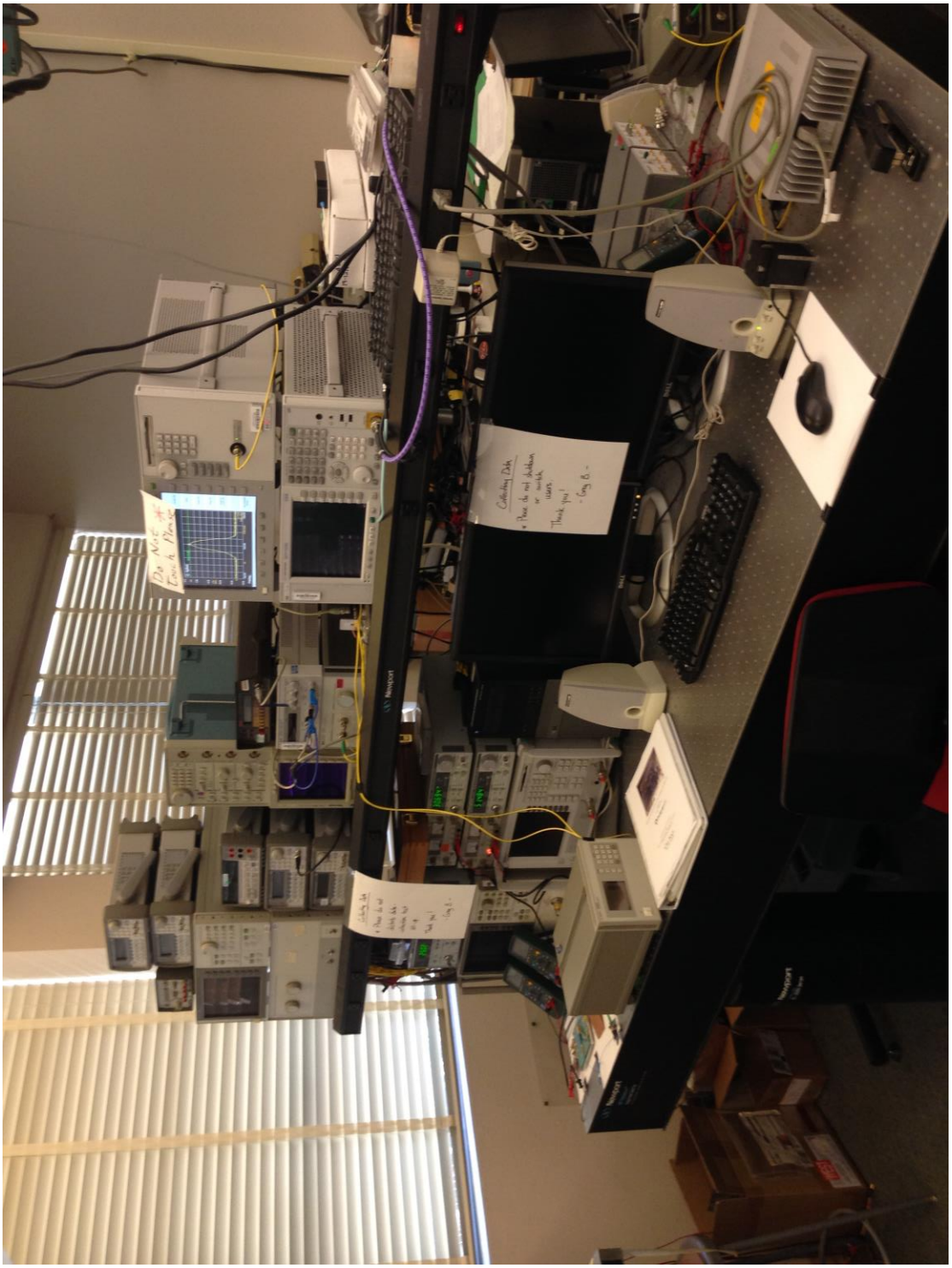

Appendix N: Photograph of Photonics Lab Workstation